PETROLEUM RESEARCH JOURNAL

TECHNICAL PAPERS

ENGINEERING

Evaluation of Itabirite as a Barite Substitute for Weighting Material in Water-based Muds .....
Mohamed Bizanti 1

Implementations of Enhanced Oil Recovery Techniques in the Arab World are Questioned? .....
Al-Khafaji, Ali H. 9

EXPLORATION

Seismic Interpretation of Gargaf Group Palaeostructures, NW of Concession 6, Sirt Basin, Libya .....
Senusi M. Harsha and Falah H. Owaina 19

Estimated Generation Time and Migration Trends of Upper Cretaceous Source Rocks, Sirt Basin .....
A. M. Ben-Ashour 25

Groundwater Recharge in Jabal al Haruj and Vicinity, Central Libya .....
M.T. Busrewil 39

CHEMISTRY

The Effect of Hydrogen, some Hydrocarbons, Carbon monoxide and Sulphur Treatments on the Structure of Platinum Supported Catalysts .....
Ezziddin A. Arafa 47

SHORT COMMUNICATION

The Influence of Edge Surface Finishing on the Fatigue Life of Low Carbon Steel Sheet .....
Muhsin M. Hamdoon 57

VOLUME 12 – (1430) / (2000)

Petroleum Research Centre
P.O. Box 6431, Tripoli
Great Socialist People's Libyan Arab Jamahiriya

Petroleum Res. J. Vol. 12 (2000); P. 1–8, 5 Figs.

Evaluation of Itabirite as a Barite Substitute for Weighting Material in Water-based Muds

Mohamed Bizanti*

تقييم إمكانية استخدام إيتابرايت كمادة سائل حفر بديلة عن البارايت في سوائل الحفر المائية

محمد البزنطي

يُستَغَلّ أكثر من 90% من خام البارايت المعروف حالياً كمادة إضافة تزيد من كثافة سوائل الحفر أثناء عمليات التنقيب عن النفط والغاز، ونظراً لزيادة الطلب على هذا الخام ولوجود شوائب به، في بعض الأحيان، تؤثر على كفاءته كسائل حفر فإن الحاجة أصبحت ملحة للبحث عن مادة بديلة تزيد من كثافة سائل الحفر.

يتناول هذا البحث الفوائد والمشاكل الناجمة عن استخدام خام الإيتابرايت (الهيماتيت الغني بمعدن الميكا) كمادة بديلة تضاف إلى سائل الحفر. ولإيجاد كمية التآكل الناجمة عن استخدام هذه المادة تم اختيار ثلاثة أحجام تتراوح مجالاتها ما بين 74 إلى 125 و44 إلى 74 وأقل من 44 مايكرون. أجريت التجارب المعملية بواسطة جهاز خلط ولمدة 30 دقيقة وعند سرعات 9800 و11200 و12570 و14350 دورة في الدقيقة وتم تحليل ودراسة خواص اللزوجة والمرونة واللدونة والترشيح والتآكل الناتج عن استعمال هذه الأحجام المختلفة من مادة الإيتابرايت.

وللتغلب على مشاكل التآكل ونقص في الترشيح فإن هذه الدراسة تشير بأنه بالإمكان استخدام خام الإيتابرايت كمادة سائل حفر بديلة عندما تكون أحجام جزئياته 44 مايكرون وفي حالة إضافة البوليجير كمادة إضافية محسنة.

Abstract: *A laboratory investigation evaluates the benefits and problems associated with the use of itabirite (micaceous hematite) as a weighting material in water-based mud.*

Three different ranges of particle sizes itabirite were selected for the test: (1) particle sizes between 74 and 125 microns, (2) particle sizes between 44 and 74 microns, (3) particle sizes smaller than 44 microns. Thirty-minute abrasion tests were conducted with a modified Hamilton Beach Blender at 9,800, 11,200, 12,570, and 14,350 rpm. Rheological properties, filtration properties, and abrasiveness were studied and analyzed.

Itabirite exhibited better rheological characteristics than barite and could increase the penetration rate since a lower solids content can be used to obtain proper weight. However, it did not exhibit good filtration properties and was found to be more abrasive. The feasibility of using itabirite as a weighting material was enhanced with a finer particle size distribution and by using a determined amount of Drispac Superlo polymer, which controlled filtration and acted as a coating agent to lower abrasiveness.

* Petroleum Engineering Dept. Chairman , Al Fateh University, Tripoli Libya. E-mail: mbizanti@yahoo.com

INTRODUCTION

Over the past few years, increases in the cost of drilling fluids, a shortage of high-quality barite, and growing dissatisfaction with using barite as a weighting material have forced the petroleum industry to seek a new weighting material which will meet the standards set for barite. The alternative weighting material can be found among the iron oxide materials. Ilmenite and itabirite (a mixture of iron oxide and silica) have been reported to be superior barite alternatives. Itabirite is micaceous hematite (Fe0) and has a hardness of 5.0 to 6.0 Mohs and a specific gravity of 5.1.

This study describes laboratory tests and measurements on itabirite and barite in water-based muds. Comparison of the rheological and filtration properties and abrasiveness provides a basis for evaluating itabirite for use as a weighting material in drilling fluids[1].

The deeper the hole, the greater the amount of barite, as a percentage of the total mud mix, is needed to suppress high formation pressures and prevent blowouts. Recent discoveries in frontier areas have generally been deeper than the discovery depths in existing oil and gas producing areas. The trend is expected to continue, resulting in more barite being consumed[2].

Previous field and laboratory studies have concluded that improved rheological properties and a lower attrition rate are attained with fine particles of ilmenite[3]. However, excessive wear will occur in high-velocity parts of the mud system, such as the mud mixer, storage system, and centrifuge pumps. Little abrasion occurs at low velocity because of elastic impacts, whereas plastic deformation causes severe abrasion at a higher velocity. It is suggested that the dilemma of ilmenite hardness can be resolved by processing the ilmenite to a particle size of no more than 3 wt percent larger than 45 microns as compared to API barite, which has 3 wt percent larger than 74 microns.

Drispac Superlo

Drispac Superlo is a chain polymer, shorter than regular Drispac, which is a polyionic cellulose derivative. This polymer is manufactured and marketed by the Drilling Specialties Company.

Drispac Superlo is dispersible in water-based mud and functions in both fresh and salt-water muds. It controls water loss with only a small viscosity increase, compared to regular Drispac. In addition, it works with all of the thinners now in use in water-based muds and performs well with inhibiting salts such as NaC1, KC1, and $CaSO_4$. It also mixes with unweighted muds and weighted muds. Drispac Superlo is resistant to microorganism, (Drilling Specialties Company, 1985) and is an effective coating agent that protects hydratable solids from disintegration and does not alter mud viscosity appreciably[4,5].

Equipment

Test equipment used includes the following:

1- Aroid Mud Balance
2- Standard Filter Press
3- Hamilton Beach 14 Speed Blender

Presently, there is no API approved method for determining the abrasiveness of a fluid or oil field material. A modified Hamilton Beach 14 speed blender was used to conduct the abrasion tests. It consists of: (1) a two-piece cover, (2) an open container, (3) a cutting unit assembly, (4) a high/low selector switch, (5) a control panel, and (6) a blender base.

Other Equipment

A portable sieve shaker, thermometer, mixer, Mettler macro balance, and a Beckman Zeromatic IV pH Meter were also used[6].

Abrasion Test

The abrasion test was conducted as follows:

1- The blade to be tested was weighed to 0.0001 gram.
2- After the blade was installed in the blender, 500 cc of the mud sample was poured into the blender.
3- The mud with test material was stirred for 30 minutes at 9800 rpm.
4- The blade was removed, cleaned, dried, and reweighed to 0.0001 gram.

5- Steps 1 through 4 were repeated for speeds of 11,200, 12,750, and 14,350 rpm.
6- The weight loss of the blade in grams and percent weight loss at each rpm was determined.

Interpretation and Discussion of Experimental Results

Sixteen mud types were investigated during this research (Table 1). The nomenclature for this study is listed at the end of this paper. All the mud types contained the same amount of bentonite 14 lbm/bbl. (14 g/350 ml). This is 1.54 percent of bentonite by total volume for each mud type. Using a small amount of bentonite in high weight water-based muds was essential for proper suspension of weighting materials in the continuous phase.

It was determined that in the itabirite mud system, 16 percent inert solids by total volume were required to obtain the desired mud density of 14 ppg. Table 2 lists the properties of itabirite used in this study. In the barite mud system, 20.5 percent inert solids by total volume were required to obtain the same mud density. The difference in the solid percent of these two muds was due mainly to the difference in specific gravities.

With the exception of mud types B, IL, IM, and IS (untreated muds, Table 1) 0.5 lbm. (0.5 g./350 ml) Desco thinner was used to (a): minimize the effect of viscosity (the selected polymer Drispac Superlo was used in concentrations of 0.25, 0.5, and 0.75 lbm/bbl. as a coating agent to lower mud abrasiveness), and (b) to reduce the yield point, because Desco thinner has a tendency to decrease the attraction of the active clay particles through adsorption on the clay surfaces.

Analysis of the Abrasion Tests

Abrasion is measured as weight loss (in grams) of a modified Hamilton Beach 14-speed blender blade. It was assumed that the greater the weight loss, the greater the abrasiveness of the mud.

It is believed that in a drilling system, shear rate varies from 170-10,000 $sec.^{-1}$ at the solids removal equipment and drill pipe, and from 10,000 to 1,000,000 $sec.^{-1}$ at the bit and bit nozzle[7]. Thirty-minute abrasion tests were conducted at 9800, 11,200, 12,750, and 14,350 rpm. Spanning the rpm range of the Hamilton Beach 14-speed blender. Four different speeds were selected to investigate the correlation between shear rate, abrasion, and polymer concentration.

Table 1. Drilling mud types

Mud type	Mud composition	Size distribution
B	(1.54% Ben + 20.5 % Bar + 77.96% Dis W	API
B1	(Type B) + .5 ppb D + .25 ppb NaOH + .25 ppb DS Pol	API
B2	(Type B) + .5 ppb D + .25 ppb NaOH + .5 ppb DS Pol	API
B3	(Type B) + .5 ppb D + .25 ppb NaOH + .75 ppb DS Pol	API
IL	(1.54 % Ben + 16.0 % Itab + 82.46% Dis W	74-125 microns
IL1	(Type IL) + .5 ppb D + .25 ppb NaOH + .25 ppb DS Pol	74-125 microns
IL2	(Type IL) + .5 ppb D + .25 ppb NaOH + .5 ppb DS Pol	74-125 microns
IL3	(Type IL) + .5 ppb D + .25 ppb NaOH + .75 ppb DS Pol	74-125 microns
IM	(1.54% Ben + 16.0% Itab + 2.46% Dis W	44-74 microns
IM1	(Type IM) + .5 ppb D + .25 ppb NaOH + .25 ppb DS Pol	44-74 microns
IM2	(Type IM) + .5 ppb D + .25 ppb NaOH + .5 ppb DS Pol	44-74 microns
IM3	(Type IM) + .5 ppb D + .25 ppb NaOH + .75 ppb DS Pol	44-74 microns
IS	(1.54% Ben + 16.0% Itab + 2.46% Dis W	37-44 microns
IS1	(Type IS) + .5 ppb D + .25 ppb NaOH + .25 ppb DS Pol	37-44 microns
IS2	(Type IS) + .5 ppb D + .25 ppb NaOH + .5 ppb DS Pol	37-44 microns
IS3	(Type IS) + .5 ppb D + .25 ppb NaOH + .75 ppb DS Pol	37-44 microns

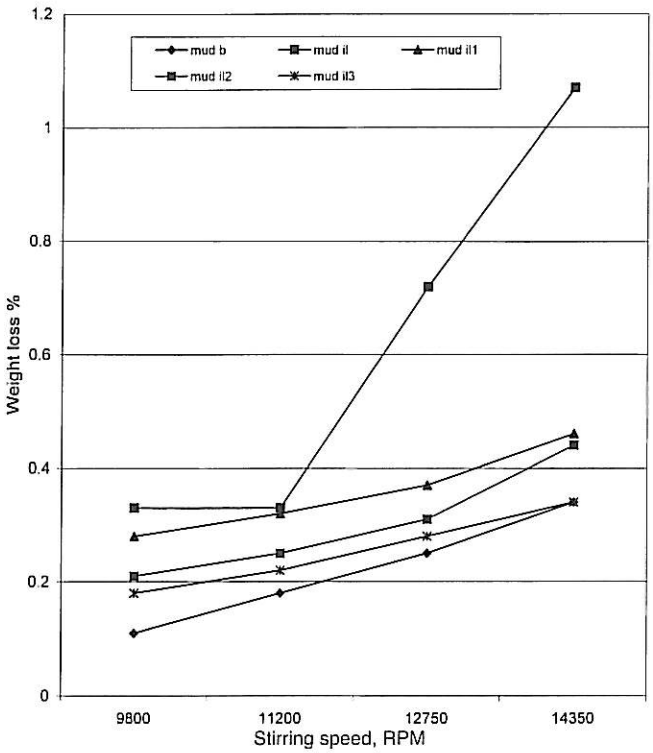


Fig. 1. Weight loss % *vs* rpm.

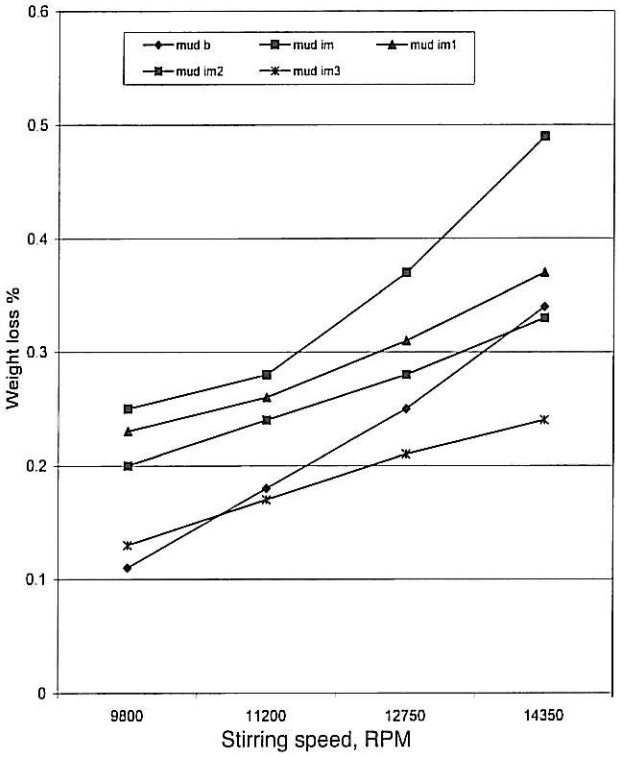


Fig. 2. Weight loss % *vs* rpm.

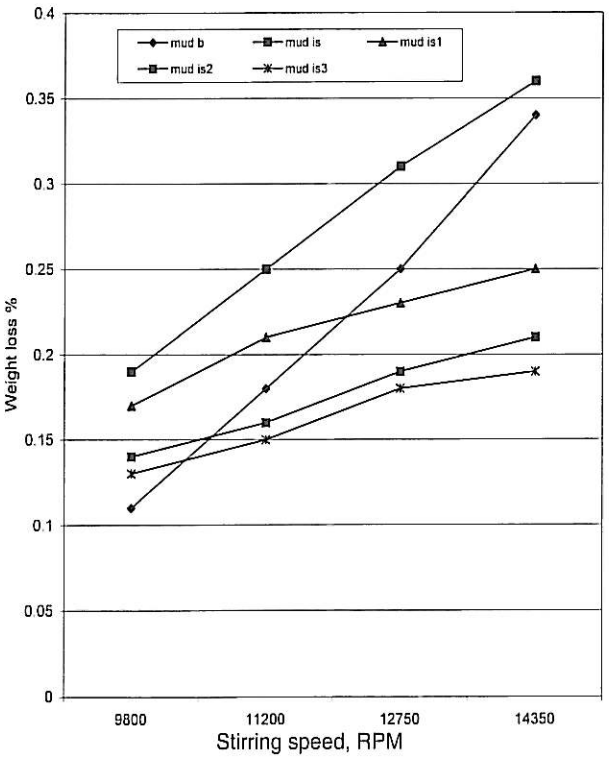


Fig. 3. Weight loss % *vs* rpm.

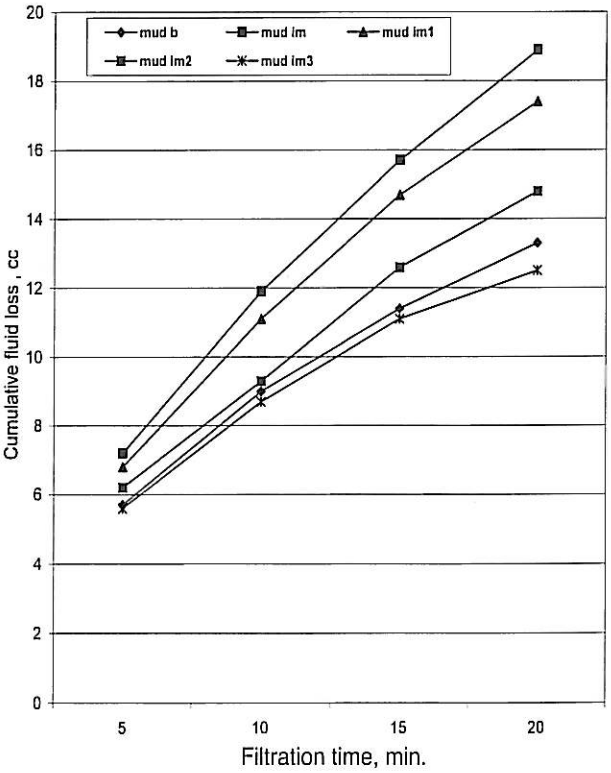


Fig. 4. Cumulative fluid loss *vs* time.

Resulting weight losses (percentage) as a function of stirring speed are plotted (Figs. 1-4). The figures show the relation between the relative abrasiveness of barite and itabirite with varying ranges of particle size at each polymer concentration of Drispac Superlo (DS).

In this paper, Drispac Superlo polymer concentrations of 0.25, 0.5, and 0.75 lbm/bbl were used as coating agents for the purpose of lowering the abrasiveness. It was experimentally verified that the use of polymers greatly reduced the abrasivity of the mud system and rendered it more efficient.

It can be seen in figures 1 through 3 that 0.75 lbm/bbl. concentration of DS for large particle sizes (between 74-125 microns) and 0.5 lbm/bbl. for small particle sizes (between 37-44) were adequate for lowering the abrasivity of the itabirite mud system to the barite level.

Table 2. Properties of itabirite used in the study (Densimix Technical Data, 1983)

Typical itabirite physical analysis	
Minus 100 mesh	100%
Minus 200 mesh	98.5% - 99.8%
Minus 325 mesh	92.0% - 96.0%
Free moisture @ 105° C	Less than 0.15%
Colour	Brown to red brown
Specific gravity	5.1
Magnetite content	Trace
pH	6.5-7.5
Plaine surface area	1900 – 2100 cm^{-2}/gm
Typical itabirite chemical analysis	
Fe	68.0–68.5% (97.2–97.9% Fe_2O_3)
SiO_2	0.5–1.0%
Al_2O_3	0.5–1.0%
CaO + MgO	0.15%
S	0.01%
P	0.03%
Cu	0.01%
Na_2O	0.02%
K_2O	0.005%
Ca^{++}	10.0–15.0 ppm
Mg^{++}	0.5–2.0 ppm

It was postulated in this study that abrasion in a mud system could be demonstrated as a function of mud density, shear rate (in the lab, stirring speed of the blender blade in rpm; in the field, velocity of the mud circulation, $sec.^{-1}$), polymer concentration (PC, lbm/bbl), stirring time (in the field, time of mud circulation), and particle size (S) associated within the mud system. In this study, some of the independent variables were constant for the itabirite mud system, such as the mud density (14 ppg) and stirring time for the abrasion tests (30 minutes).

To further assess the abrasion tests for the itabirite mud system, regression analyses were used to study the predictive models that exist between abrasion (AB) as the dependent variable and regressor independent variables chosen from the set (S. PC, rpm) studied in this paper. The results of the regression analyses of three different models: linear, semi-log, and log-log are presented in Table 3. It is believed that the log-log model is best suited for describing the laboratory data.

It was observed that 0.75 lbm/bbl concentration of Drispac Superlo for large particles of itabirite (between 74 and 125 microns), and 0.5 lbm/bbl for small particle sizes of itabirite (between 37 and 44 microns) was adequate to improve the filtration properties. Figure 4 shows that there is an increase in cumulative fluid loss as the itabirite weighting material is introduced in the base mud (bentonite plus water). This was a result of the inert solid particles changing and disturbing the texture of the filter cake. These particles would not allow the bentonite clay particles to lie on top of each other, therefore, preventing the formation of an impermeable filter cake. This increase in cumulative fluid is improved by the addition of Drispac Superlo.

Polymer concentration-plastic viscosity relationships for barite and itabirite mud types are presented graphically in figure 5 for the Drispac Superlo polymer.. This figure shows that with the addition of polymer at each concentration, lower plastic viscosity can be obtained with the itabirite mud system than with barite. Therefore, the use of polymers was more beneficial in the itabirite mud system. Because of this advantage, the abrasion problem in the mud system could be overcome by increasing the polymer concentration.

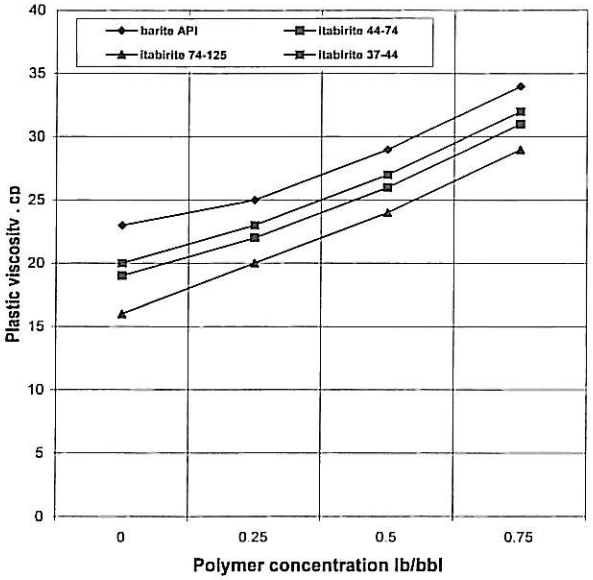


Fig. 5. Polymer concentration *vs* plastic viscosity.

Impact of the Study

Previous work[8,9], using drilling mud weighted with itabirite has reduced the cost of oil mud to three hundred and fifty thousand dollars a saving of 70 to 100 thousand dollars compared to other offset wells using mud weighted with barite.

The rate of penetration in the test well should almost twice the ROP obtained using itabirite mud system compared to barite mud system.

CONCLUSIONS

In this study the feasibility of using itabirite has been demonstrated. Based on the results obtained in this study, the following conclusions can be drawn:

1- Itabirite can be an acceptable weighting material as a barite substitute in water base muds.
2- Abrasion is dependent on the particle size distribution in a mud system. The smaller the solid particle sizes contained within the mud of the same density, the less abrasive it is.
3- Itabirite is more abrasive than barite.
4- The feasibility of using itabirite as a weighting material in water-base mud can be improved by selecting the particle size distribution between 37 and 44 microns and by using Drispac Superlo or Kelzan XCD polymer as a coating agent to lower the abrasivity of the itabirite mud to the barite level. The use of a polymer also helps control the filtration properties while maintaining reasonable rheological properties.
5- Regression analysis was applied to the experimental results to predict the abrasion equations for the mud system. Results indicate that there is a good predictive linear regression existing between abrasion (AB) as a dependent variable and regressors chosen from the set {S,PC,rpm} studied in this research. The log-log model was found to be the best in predicting abrasion.
6- From regression analysis, abrasion rates were found to be dependent on particle size and polymer concentration, and they were strongly dependent on shear rate.

Recommendations for Future Research

The feasibility of using itabirite, as an alternative weighting material in water-base muds can be best determined through laboratory testing. The following additional laboratory research is required before selecting itabirite for actual applications:

1- Effect of high pressure & temperature on rheological and filtration properties.
2- Effect of dynamic filtration properties.
3- Effect of additional particle sizes and shapes.

Table3. Prediction of abrasion equations (AB=f(S, PC,rpm))

Model	Polymer	Prediction equation	R^2-value	F	standard error
Linear	DS	AB=0.32304979+2.94808731(S)-0.27266667(PC)+0.000043049(rpm)	0.6727	30.157	0.0343
Semi-log	DS	$AB=0.04059807e^{8.80979373(S)}e^{-0.83701060(PC)}e^{0.00013234(rpm)}$	0.9027	136.059	0.0942
Log-log	DS	$AB=0.00000249(S)^{0.53060128}(PC)^{-0.31992027}(rpm)^{1.35026810}$	0.9350	153.323	0.0362

REFERENCES

[1] El Bokle, F.M., 1982. *Technique for Evaluation and Improving the Performance of the Iron Oxides Used as Barite Substitutes in Oil Well Drilling Fluids*. Ph.D. dissertation, University of Oklahoma, Norman, Oklahoma.

[2] Sarkis, G. Amapin, 1985. Barite, mineral facts and problems. *Bureau Mines, Bull.* **675**, 56–73.

[3] Blomberg, N.E., *et al.*, 1984 (June). Evaluation of ilmenite as weight material in drilling fluids. *J. Petrol. Tech*, 969–974.

[4] Drilling Specialties Company,1985. Product Literature, "Drispac Superlo Additive," "Desco,",Technical Services Division, Drilling specialties company, Bartlesville, Oklahoma, P. 7.

[5] Densimix Technical Data, June 1983. Houston, Texas.

[6] Moonesan, A., 1987 (March). *Itabirite Evaluation*. M.Sc. thesis, Louisiana Tech. University, Ruston, Louisiana.

[7] Chilingarian, G.V., and Vorabutr, 1981. *Drilling and Drilling Fluids*, Elsevier Scientific Publishing Co.

[8] Binder, G.G., Jr. *et al.*, 1981 (Dec.). Evaluating barite as a source of soluble carbonate and sulfide contamination in drilling fluids. *J. Petrol. Tech.* 2371–2375.

[9] Scharf , A.D. and Watts, R. D., 1988. Itabirite : an alternative weighted material for heavy oil – base muds. Paper *SPE* 13159, Exhibition, Houston.

NOMENCLATURE

AB	=	Abrasion
B = BAR	=	Barite
Ben	=	Bentonite
Conc	=	Concentration
cp	=	Centipoise
Cumu	=	Cumulative
Dis W	=	Distilled water
D	=	Desco
DS	=	Drispac superlo
IL	=	Itabirite large particle sizes (between 74 and 125 microns)
IM	=	Itabirite medium particle sizes (between 44 and 74 microns)
IS	=	Itabirite small particle sizes (between 37 and 44 microns)
Itab	=	Itabirite
ml	=	Milliliters
PC	=	Polymer concentration
Pol	=	Polymer
lbm/bbl	=	Pound mass per barrel
ppg	=	Pounds per gallon
PV	=	Plastic viscosity
rpm	=	Revolution per minute
S	=	Particle size
Yp	=	Yield point

Petroleum Res. J. Vol. 12 (2000); P. 9–18, 13 Figs.

Implementations of Enhanced Oil Recovery Techniques in the Arab World are Questioned?

Al-Khafaji, Ali H.*

التساؤل عن تطبيقات تقنيات الإسترداد الإضافي للنفط في الوطن العربي؟

علي حبيب الخفاجي

في العام 1998، قُدر الاحتياطي النفطي العالمي بحوالي 1051,74 مليار برميل وقُدر الاحتياطي العالمي للغاز الطبيعي بحوالي 152,5 تريلين متر مكعب. وتتواجد كميات كبيرة جدا من هذه المواد الهيدروكربونية الطبيعية المولدة للطاقة في الوطن العربي وخاصة في منطقة الخليج، قدرت بحوالي 61% (643,41 مليار برميل) من الاحتياطي العالمي للنفط و21% (32,6 تريليون متر مكعب) من الاحتياطي العالمي للغاز الطبيعي. وعلى العموم، فإن حوالي 70% من هذه المواد الهيدروكربونية المكتشفة تبقى في المكامن حيث تتخلف في باطن الأرض وذلك بعد عمليات الإنتاج التي تعتمد بالدرجة الأولى على طرق الاستخراج الاعتيادية الشائعة. وهناك عوامل رئيسة متعددة تسبب بقاء المواد الهيدروكربونية في باطن الأرض ومنها الاختلاف الطبقي، قوى الضغط الشعري، طريقة إكمال الآبار، انخفاض الضغط في المكامن وغيرها من العوامل التي تؤثر على كفاءة استخلاص البترول من باطن الأرض.

إن الهدف الرئيسي لهذا البحث هو إبراز أهمية تطبيق طرق الاسترداد الإضافي للنفط والدور المهم الذي تلعبه في زيادة نسبة الاستخلاص للنفط والذي يؤدي بالتالي إلى إيرادات إضافية وإلى إطالة عمر الإنتاج. وتم توضيح ذلك بأمثلة أخذت من الاختبارات المعملية والميدانية بهذا الخصوص. وعلى سبيل المثال عند زيادة نسبة الاستخلاص بمقدار 1% من الاحتياطي النفطي الأصلي في الوطن العربي سيؤدي إلى إيرادات إضافية تقدر بـ 536 ألف مليون دولار حسب الأسعار السائدة 25 دولاراً للبرميل بالإضافة إلى الزيادة في عمر الإنتاج بحوالي ثلاث سنوات إستناداً إلى معدلات الإنتاج السائدة حالياً (20 مليون برميل/اليوم). وعليه بات من الضروري القيام بالبحوث والدراسات المتطورة والواعدة وتطوير مناهج الدراسات والتطبيقات العملية لتقنيات الإسترداد الإضافي في وطننا العربي لتحقيق الزيادة في نسبة الاسترداد الإضافي من هذه الثروة الهيدروكربونية الناضبة.

Abstract: *At the end of 1998, the proven world oil reserve is estimated as1051.74 milliard barrels and the natural gas reserve as 152.5 trillion cubic meters. A tremendous amount of these natural resources of energy is deposited in the Arab World, especially in the Arabian Gulf. About 61% (643.41 milliard barrels) of the world oil reserve and 21% (32.613 trillion cubic meters) of the world natural gas reserve are allocated in the Arabian countries. In general, about 70% of the hydrocarbon resources remain in the underground petroleum reservoirs after conventional recovery methods of production. Several factors, such as reservoir heterogeneity, capillary forces, well completion and pressure decline, are affect the hydrocarbon recovery efficiency.*

*Petroleum Research Centre, P.O. Box 6431, Tripoli, Libya.
E-mail: alihalk@hotmail.com

The main objective of this research is to emphasize the importance of Enhanced Oil Recovery (EOR) techniques and their role to increase the percentage of oil recovery. Some examples of experimental work done in this aspect are demonstrated. Indeed, an increament of only 1.0% of the Original Oil in Place (OOIP), in the Arab World for example, results an additional income of about 536 milliard US dollars at a current oil price of $25 per barrel. Also, on the bases of 20 million barrels/day oil production rate, an additional production life of about three years will be achieved. Therefore, It becomes increasingly necessary to establish sophisticated research and development programs for study and implementation of the enhanced oil recovery techniques.

INTRODUCTION

Proven oil reserve in the Arab World is approximately equal to 643.41 milliard barrels. This forms about 61.18 % of the total oil reserve in the world as shown in Fig. 1[1,2,3]. The Arab natural gas reserve is 32.613 trillion cubic meters, which forms 21.38% of the total world gas reserve[1,2,3] as illustrated in figure 2. However, about 30% of the original hydrocarbons in place could be recovered using the conventional production methods. Therefore, about 1500 milliard barrels of oil and 76.1 trillion cubic meters of the natural gas will be left unrecoverable. Enhanced Oil Recovery Techniques (EOR) should be thoroughly investigated and implemented to achieve an ultimate hydrocarbon recovery. Also, the production life of reservoirs will be prolonged. This is a strategic target to support the national income to develop Arab countries. If the oil recovery in the Arab World is increased, for example, by 1% of the OOIP, the additional amount of oil that will be produced is equal to 21447 million barrels. Life of production will be prolonged by about three years at a daily rate oil production of 20 million barrels. An additional income at the current oil price of $25/barrel will be about $536 milliards (Fig. 3). In order to produce as much as possible of the remaining hydrocarbon in the petroleum reservoir, one should enable hydrocarbon to flow toward the production wells by improving the volumetric

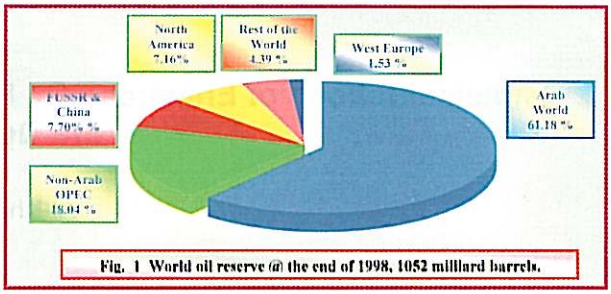


Fig. 1 World oil reserve @ the end of 1998, 1052 milliard barrels.

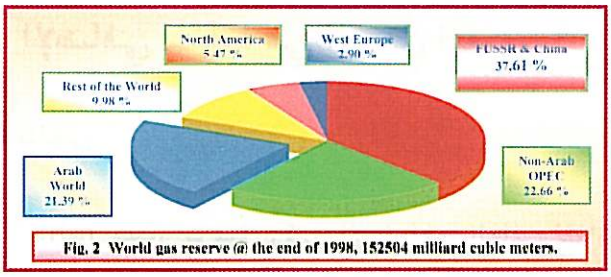


Fig. 2 World gas reserve @ the end of 1998, 152504 milliard cubic meters.

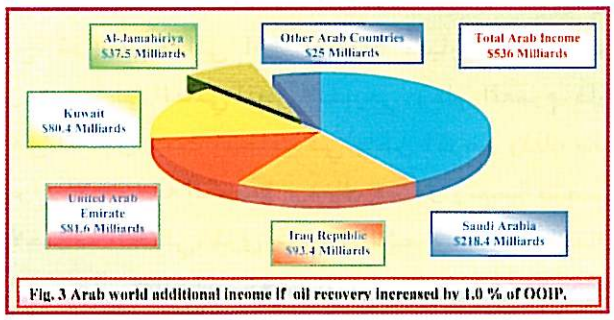


Fig. 3 Arab world additional income if oil recovery increased by 1.0 % of OOIP.

sweep and the displacing efficiencies utilizing a proper EOR method. Accordingly, it becomes urgently demanded to give a high priority for (EOR) research and development programs.

HYDROCARBON RECOVERY METHODS

Petroleum recovery may be classified as Primary Recovery Methods, Pressure Maintenance Methods (Secondary) and Enhanced Oil recovery Methods (Tertiary). When the reservoir is producing by its natural energy, this stage of production is referred to as Primary Recovery Methods. Pressures Maintenance Methods are usually applied by injection of either water, gas or both into the reservoir to maintain the reservoir pressure at a desirable level. The primary and pressure maintenance methods of production may be categorized as the Conventional Recovery Methods. Applying the conventional methods, the ultimate recovery is estimated as 30% of the OOIP. However, the most promising methods to increase the recovery are the Enhanced Oil Recovery Methods.

Primary Recovery Methods

These methods depend upon the natural energy prevailing in the petroleum reservoir that provides a drive mechanism for hydrocarbon production. These drive mechanisms fall in three categories; dissolved gas drive, gas cap drive, and natural water drive. Dissolved gas drive reservoirs exhibits: a rapid pressure decline, a low produced gas oil ratio (GOR) at the early life of production. (GOR) increases to a maximum value then declines at later production stages. Water cut is small, and the expected oil recovery is 5-10% of the OOIP. In the gas cap drive reservoirs, pressure declines gradually and continuously, (GOR) is higher in the wells produced near the gas-oil contact, water production is negligible and the expected recovery is 15-30% of the OOIP. Characterization of the water drive reservoirs is that the reservoir pressure declines at a low rate, (GOR) remains close to the initial value, water production increases with time and the expected oil recovery is from 30-50% of the OOIP. From the practical experience, only 30% of the OOIP can be recovered during the primary methods of production[4]. Hence, about 70% of the OOIP remains unrecoverable.

Pressure Maintenance Methods

Either water or gas is injected into the petroleum reservoirs to maintain the pressure at a required level. Water flood is applied worldwide since the dawn of the oil industry due to economic considerations and simple technical application. In spite of the worldwide application of water flood, a great amount of oil remains unrecoverable because of the areal sweep efficiency, the contact factor, and displacement efficiency.

Areal Sweep Efficiency

Areal sweep efficiency is defined as the area of the reservoir portion that is flooded by the injected water for a given production pattern[5]. This efficiency depends upon the well pattern, well spacing and the mobility ratio (M). Mobility is the ratio of the relative permeability of the flowing fluid to its viscosity. Hence, the mobility ratio is the mobility of the displacing fluid (water) to the mobility of the displaced fluid (oil). When the mobility ratio is one or less, water will push against the oil in a piston like manner. This mobility is referred to as favorable mobility ratio. When the mobility ratio is ten and greater (unfavorable), the water will traverse the oil leaving a large amount behind the flooding front and in turn reduces the recovery factor. Unfavorable mobility ratio occurs at a low viscosity and a high permeability of the displacing fluid and also at a high viscosity and a low permeability of the displaced fluid. Reduction of the oil viscosity and elevation of water viscosity will improve mobility ratio toward the favorable value and thus increase the oil recovery.

Contact Factor

It is defined as the portion of the reservoir that is swept and contacted by the water in the flooded zone[5]. It was evident that not all of the rock in the flooded area is contacted by water due to the reservoir rock heterogeneity, which in turn reduces the oil recovery.

Displacement Efficiency

Although the injection water contacts the reservoir rock, a high percentage of oil remains in the reservoir due to inefficient pore-to-pore displacement (Fig. 4). Consider a doublet model composed of two different capillaries previously filled with oil[5]. At the beginning of water injection, the water evenly displaces the oil at the inlet of doublet, (Fig. 4-A). Further water injection results in a complete oil displacement in the small capillary and part of the oil in the large one, (Fig. 4-B). At the end of the flood, the injected water locks the back door of the large capillary and traps the oil under equilibrium capillary pressures exerted at both ends of the doublet, (Fig. 4-C). The pressure gradient needed to unlock the trapped oil is usually very large due to the interfacial tension at the water-oil interface.

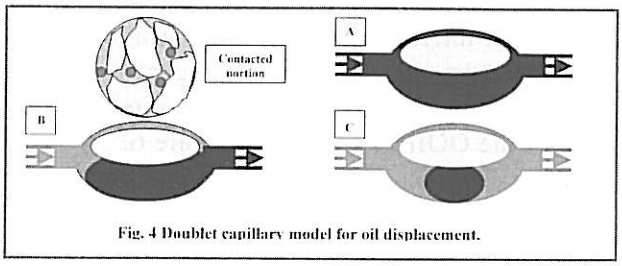


Fig. 4 Doublet capillary model for oil displacement.

ENHANCED OIL RECOVERY TECHNIQUES

The remaining oil after the conventional oil recovery methods (primary and pressure maintenance) is the target for the Enhanced Oil Recovery Techniques (EOR). Two main factors affect improvement of oil recovery. Firstly, the reduction of the interfacial tension at the interface of the injected fluid and the reservoir oil and secondly, reduction of the mobility ratio of the flowing fluids in the flooded portion and the oil zone of the reservoir. Essentially, there are three major EOR methods to achieve the above objectives. These methods are chemical flooding, miscible flooding and thermal recovery method, which are implemented worldwide to improve oil recovery.

Chemical Flooding Method

Chemical flooding is comprised of two mechanisms: either, by reducing the interfacial tension at the water-oil interface using surfactants or reducing mobility ratio by adding low concentration of polymer (synthetic polymers-polyacrylamide or biologically produced polymers -polysaccharide) into the injected water to increase its viscosity and in turn improve oil recovery. A surfactant (surface-active agent) has a dual function, the hydrophilic and the lipophilic properties that enable it to reduce the interfacial tension into an ultra-low value at the water-oil interface. Surfactants may be mixed with the injected water at the surface, or may be generated in-situ in an alkaline flooding. In-situ surfactant generation occurs when alkaline chemicals such as sodium hydroxide and/or sodium orthosilicate react with petroleum acids, provided sufficient amount of these acids are available in the reservoir oil. Also, surfactants improve oil recovery by oil emulsification and wettability alteration mechanisms. Addition of a surfactant aqueous solution composed of 50% anionic and 50% nonionic with 0.6% by weight concentration reduces the interfacial tension to an ultra-low value of 0.035 dynes/cm as shown in figure 5, hence, increases the oil recovery to a great extent (about 70% of the OOIP) as shown in figure 6.

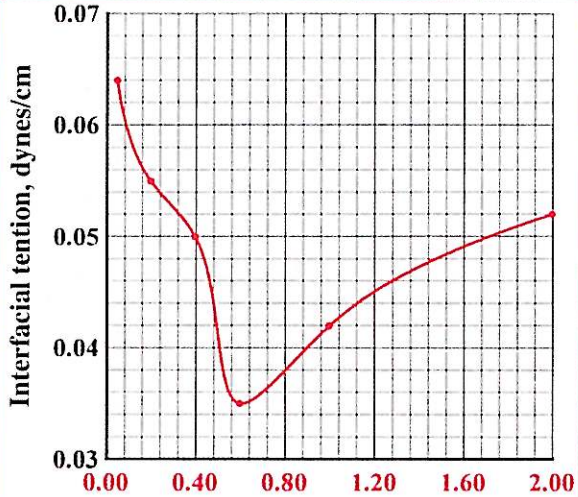


Fig. 5. Interfacial tention as a function of the surfactant concentration.

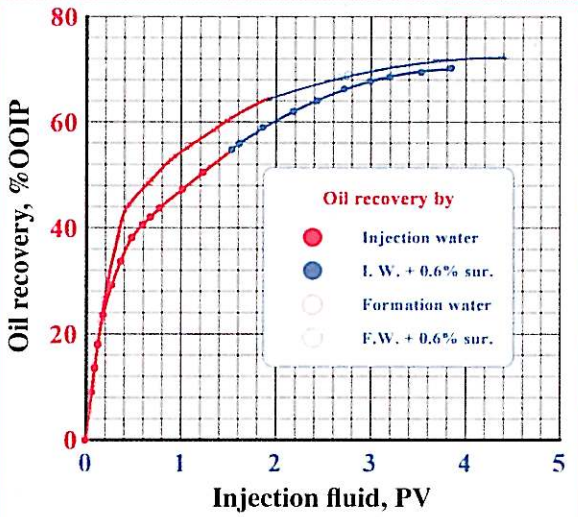


Fig. 6. Oil recovery as a function of injected water and formation water with and without sufactant.

Miscible Flooding Method

This method depends on injection of hydrocarbon and non-hydrocarbon fluids into the reservoir, in which the injected fluids will be mixed at all proportions with the reservoir oil at the prevailing reservoir conditions. As a result, the interfacial tension between the injected fluid and the reservoir oil will be eliminated. When this occurs, about 100% of the oil contacted by the injection fluid will be displaced and recovered. Miscibility is achieved at certain conditions of pressure and temperature depending on the composition of both the reservoir oil and the injected gases or solvents.

There are generally two types of miscible processes, the first contact miscible (FCM), and the multiple-contact miscible (MCM) process (dynamic miscibility processes). In the first contact miscible process, solvents of liquefied petroleum gas (LPG) mix directly with reservoir oil in all proportions and their mixtures always remain in a single phase. In the multiple-contact miscible process, gases or solvents are not directly miscible with reservoir oil, but under appropriate conditions of pressure, temperature and oil-gas or oil-solvent compositions, in-situ miscibility could be achieved through repeated contacts of the injected material with reservoir oil. MCM is of three kinds: the condensing, the vaporising and the condensing/vaporising miscible processes.

In a multiple contact condensing drive mechanism, the hydrocarbon intermediate compounds (C_2-C_6) in the injected solvent condense into the reservoir oil until a sufficient quantity of this solvent exists at the displacement front to cause miscibility with the oil. Minimum miscibility composition (MMC), for example, of LPG/Dry Gas mixture was determined experimentally using the slim tube displacement technique[6,7]. Results graphed (Fig. 7) indicate that about 100% of the OOIP is recovered.

In the vaporising drive, for example (CO_2), the injected fluid will extract hydrocarbon compounds (C_2-C_{30}) from the reservoir oil until a sufficient quantity of these hydrocarbons exists at the displacement front to cause miscibility with the oil. The minimum miscibility pressure (MMP) is experimentally determined[6,7] and illustrated on figure 8. Again, about 90% of the OOIP is recovered by CO_2 injection. In the above investigation, Peng-Robinson cubic equation of state (EOS) modelling was also applied to predict the MMC and MMP using the Computer Modelling Group (CMG PROP) software.

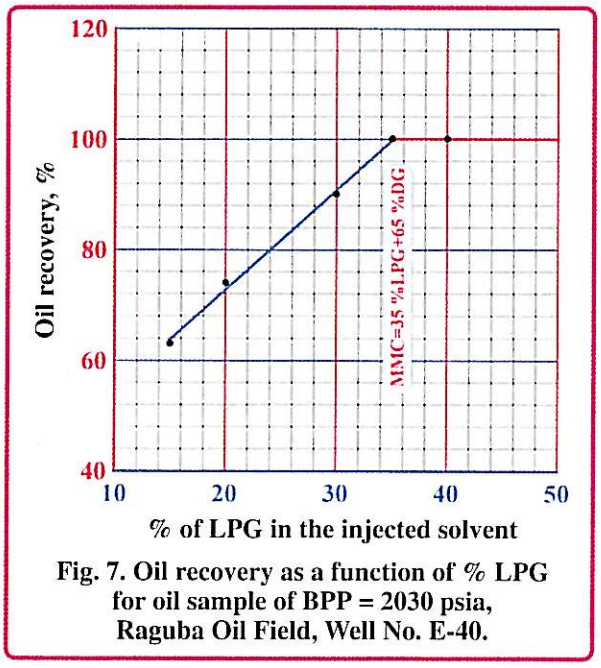


Fig. 7. Oil recovery as a function of % LPG for oil sample of BPP = 2030 psia, Raguba Oil Field, Well No. E-40.

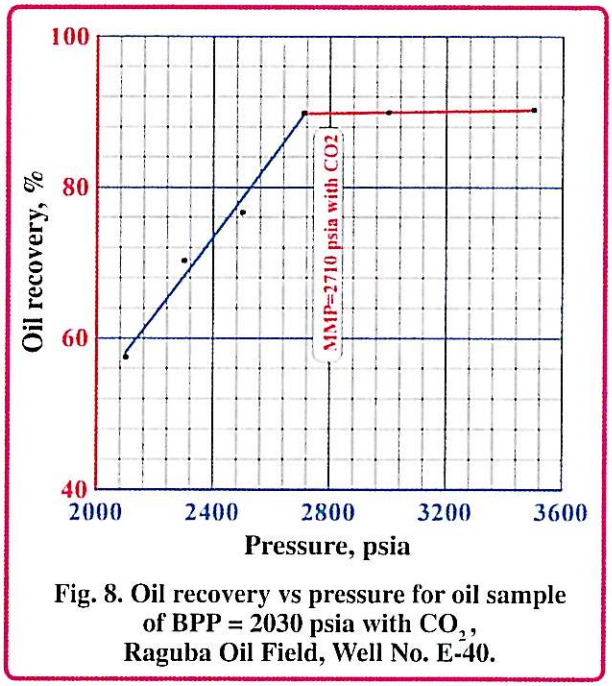


Fig. 8. Oil recovery vs pressure for oil sample of BPP = 2030 psia with CO_2, Raguba Oil Field, Well No. E-40.

Thermal Recovery Methods

Thermal recovery methods such as *in-situ* combustion, hot water and steam are used to increase the reservoir oil temperature and hence reduce appreciably the oil viscosity, reduce the interfacial tension, increase oil relative permeability, decrease the water relative permeability, increase irreducible water saturation and decrease residual oil saturation. Effects of heat on the above mentioned parameters improve the mobility ratio and increase the oil recovery factor. On the contrary to other fluid injection methods, heat has the ability to transfer throughout the reservoir by conduction and convection, hence subjected most of the oil reservoir portions to the heat effect. This is an additional advantage of thermal recovery methods compared to other EOR methods. In the in-situ combustion, air or oxygen

is injected in to the reservoir that reacts with the oil and generates heat and in turn increase the reservoir temperature until a spontaneous ignition occurs and the combustion front moves toward the production wells. Forward in-situ combustion takes place when the combustion front flows in the same direction of the reservoir fluid flow, while in the inverse combustion, the combustion front flow opposite the reservoir fluid flow.

Steam injection is of two kinds: the first kind is the steam drive processes, in which steam (about 80% steam quality) is injected into a well and the oil is produced at another. The second kind is the steam soak processes, in which steam is injected into an oil well for a period of time ranges from few days to few weeks, then, oil production will be resumed from the same well. Steam injection is one of the most famous thermal recovery methods applied to enhance oil recovery from petroleum reservoirs containing heavy and intermediate oil of higher viscosity. Figure 9 shows a schematic diagram for hot water and steam flooding apparatus[8]. Figure 10 represents oil recovery versus hot fluids injected in pore volumes. In a hot water (at reservoir temperature -30 °C) displacement experiment, oil recovery is found to be 15% of the OOIP. When this experiment is followed by injection of steam at temperature of 170 °C, oil recovery is increased to 60%. About (28%) oil recovery is obtained by injection of hot water at 120 °C. A highest oil recovery (71%) was achieved by steam injection at 170 °C. It appears that when steam injection is initially applied for heavy oil recovery processes, a higher oil recovery will be achieved as illustrated in figure 10.

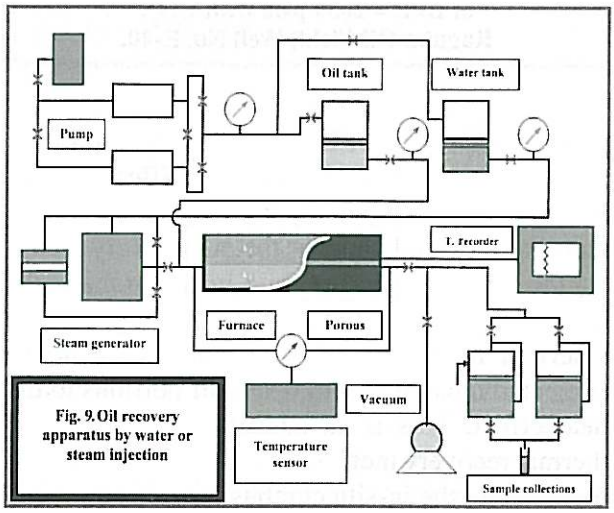


Fig. 9. Oil recovery apparatus by water or steam injection

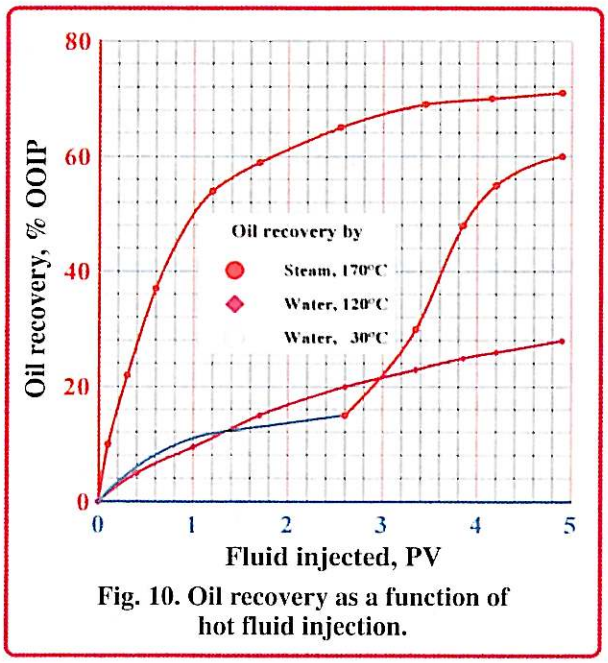


Fig. 10. Oil recovery as a function of hot fluid injection.

In-situ Foam Generation

One of the most important problems of steam injection is the override due to the high differences in the steam and oil densities and channeling through high permeable zones because of the very low steam viscosity compared to that of oil. Accordingly, steam will break through early at the producing wells resulting in poor sweep efficiency. To avoid these problems, surfactant solution was injected prior to steam injection. When steam is encountered with the surfactant solution, foam will be generated. Foam is a dispersion of a large volume of gas in a small volume of liquid phase in such away that the gas is the discontinuous phase and the liquid is the continuous phase. Simply, foam is a soap bubble filled with gas and bounded by a thin film of liquid in which gas volume is greater than 94% of the total volume of the system. Foams apparent viscosities are higher than either the liquid or the gas of which they are composed. Therefore, steam flow will be hindered instantaneously due to foam generation in the portions of the reservoir where over ride and/or thief zones exist.

Surfactants used in steam flooding should be able to tolerate the high temperature of steam. Consequently, a surfactant having thermal stability is required. Much of commercial surfactants failed the thermal stability test at 200 °C and pressure of 500 psia[9,10]. Suntech Group manufactured several

surfactants to be used in steam processes. Among nine surfactants, Suntech IV was found superior to fulfill the thermal stability requirement in addition to its ability to generate foam and reasonable phase partitioning with reservoir oil. The half-life time of Suntech IV was about two years[9,10].

Surfactant adsorption on sand grains surfaces with and without clay (Kaolinite) and phase partitioning with heavy oleic phase was thoroughly studied. The isothermal adsorption exhibited a Langmuirian model (Fig.11). Schematic diagram of oil displacement apparatus by foam and steam was designed (Fig. 12). An appreciable increase in oil recovery would be obtained when foam was generated ahead of the injected steam front in the porous medium[10].

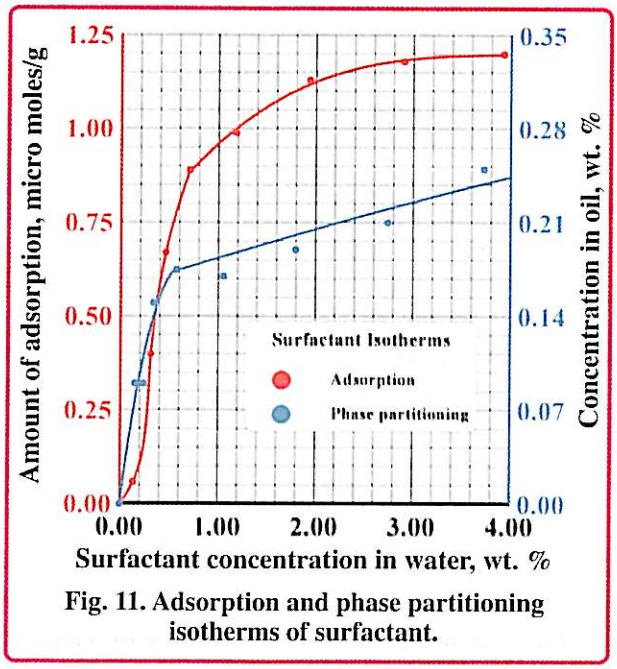


Fig. 11. Adsorption and phase partitioning isotherms of surfactant.

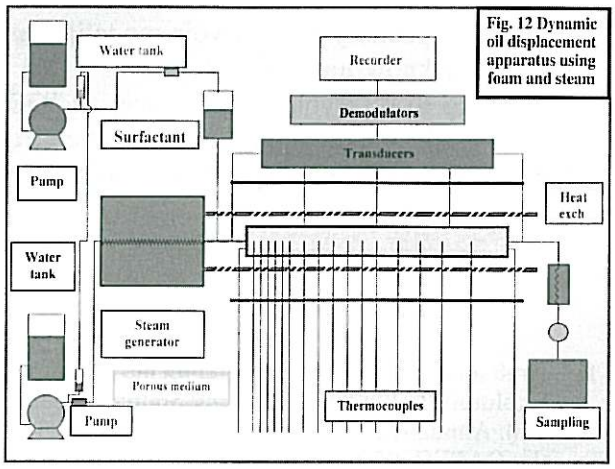


Fig. 12 Dynamic oil displacement apparatus using foam and steam

ENHANCED OIL RECOVERY IN THE ARAB WORLD

Most of the produced oil in the arab world depends on the natural energy. Pressure maintenance by gas and/or water injection is applied to some oil fields. Implementations of EOR are stile in the beginning except the miscible projects in Intisar "D" oil field in Al-Jamahiriya and Hassi-Masood oil field in Algeria. Intisar "D" oil field is one of the largest miscible gas injections in the arab world and internationally. Intisar "D" oil field project is a good example of an EOR miscible method implementation. About 70% of the original oil in place is recovered in this field by miscible gas injection. Accordingly, a first priority and a high attention should be given to EOR implementations, since about 1500 milliard barrels of oil will be left unrecoverable after applying primary and secondary oil recovery methods. A higher percentage of the unrecoverable oil is expected to be produced by implementation of the EOR technology.

PLANING FOR ENHANCED OIL RECOVERY PROJECT

Implementation of an IOR and/or EOR project to an oil reservoir requires programs of preparation for reservoir studies, and providing necessary data that are needed to enable selection of a proper method for increasing oil recovery. Figure 13 represents a general flow chart for this purpose. First, one should consider the reservoir and injection conditions of pressure, temperature, injection and production rates, number of wells, well pattern, pay zone thickness, formation geology and method of well completion. Second, provides experimental data pertained to physical and chemical properties of the reservoir fluids such as viscosity, density, interfacial tension, compressibility, and thermodynamic properties-PVT for the reservoir fluids. Also, provides data concerning physical and chemical properties of the reservoir rock, such as porosity, permeability, rock compressibility, wettability, fluid saturation, capillary pressure, resistivity and geological evaluation of the formation rock. In addition, provides thermal properties of reservoir fluids and reservoir rock should be studied, i.e. thermal expansion, conductivity, and specific heat determination.

In light of the above and any other necessary information, and using a proper screening criterion, a recovery method may be recommended to the reservoir of interest. A screening guide usually contains basic information of reservoir fluids and reservoir properties as viscosity and API gravity of the oil, formation water salinity, depth and thickness of the pay zone, reservoir temperature, rock porosity, permeability and transmissibility and the type of the reservoir rock. Accordingly, immiscible gas and/or water injection methods may be applied for pressure maintenance (secondary recovery) and improving oil recovery, or an appropriate miscible, thermal, and/or chemical method may be recommended to enhance oil recovery (tertiary recovery). The following studies have become necessary: study the petro-physical properties of the reservoir fluids and rocks, conduct experimental work pertains to the selected or proposed EOR method, apply the available geological and reservoir simulators, and predict the future reservoir performance after the history matching is done. Then, a pilot test should be applied in the field of interest, to examine the success or failure of the project in order to decide a full-scale application of the project. Enhance oil recovery is a heavy task which needs a great deal of efforts and time to accomplish. Planning to start such program as early as possible becomes very essential.

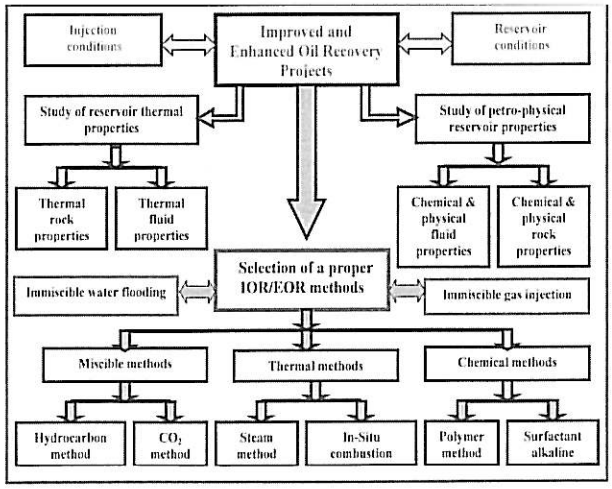


Fig. 13. Flow-chart for selection of an improved oil recovery and/or an enhanced oil recovery project.

CONCLUSIONS

In this investigation, oil recovery laboratory experimental work carried out, using different EOR methods demonstrate the following conclusions:

1. Oil recovery is significantly increased (about 70% of the OOIP) by injection of surfactant aqueous solution composed of 50% anionic and 50% nonionic with 0.6% by weight concentration.
2. Miscible displacement experiments show that 100% oil recovery using LPG/dry gas mixtures, and about 90% using CO_2 solvent could be achieved.
3. A higher oil recovery (about 71% of the OOIP) is obtained when steam injection is initially applied for a thermal oil recovery as compared to (60%) oil recovery obtained when steam is applied after water flooding.

RECOMMENDATIONS

Because of the huge amount of reservoir oil that will remain (about 1500 milliard barrels) after conventional production method application, it becomes necessary to give the IOR and/or EOR methods a high priority and consideration for the research and development. Chemical, thermal and miscible methods should be thoroughly investigated to determine the most effective method that may be applied to enhance oil recovery in the oilfields of the Arab World. Therefore, the following crucial recommendations are suggested for future planning to activate EOR technology in the Arab World.

1. Document all information, and develop programs for exchange experience.
2. Collaborate with the existing petroleum research centres in the Arab World and avoid research duplication. Also, co-operate with the international petroleum research centers for exchange of experience, scientific visits and training, especially in reservoir modeling as well as the know-how technology.
3. According to reservoir performance, an IOR and/or EOR method should be recommended for early or lately implementation in the life of a reservoir.

REFERENCES

[1] Arab and International Developments in Exploration, Reserve of Energy Sources, 1980. 25th Annual Report of the Secretary General of the OAPEC, 95–101 (in Arabic).

[2] *Oil and Gas Journal*, 28 Dec. 1998.
[3] *OPEC Annual Statistical Bulletin*, 1997.
[4] Lake, W. L., 1989. *Enhanced Oil Recovery*, Printce Hall, Inc., Englewood Cliffs, New Jersey.
[5] Herbeck, E.F., Heiztz, R.C., and Hastigs, J.R., Jan. 1976 through Feb. 1977. Fundamental of Tertiary Oil Recovery. *Petroleum Engineering International.*
[6] Al-Khafaji, A. H., Alswieh, Abuzbeda, S.T. and Alabani, S.O., Jan. 1996. Equation of state application to predict MMC and MMP for Raguba Oilfield, Libya, *Petroleum Res. Journal.* **8,** 1-11
[7] Enhance Oil Recovery Project, Raguba Oilfield, Phase-1 PVT Studies, Phase-2 Equation of state modeling, Phase-3 Miscibility Studies, Phase-4 Swelling Studies. 1996. *Prepared by PRC for Sirte Oil Company*, Tripoli, Libya
[8] Al-Khafaji, A. H., Zolotuhin, A.B., and Khromovitchev, M.N., 1988. Comparison of heavy oil recovery with water flooding and steam flooding techniques. *Fifth Scientific Conference*, Scientific Research Council, Baghdad, Iraq.
[9] Al-Khafaji, A. H., 1983. E*ffect of Temperature on Degradation, Adsorption and Phase Partitioning of Surfactants used in Steam Injection Oil Recovery*. Ph.D. Dissertation in Petroleum Engineering, Stanford University, Stanford, USA.
[10] Al-Khafaji, A. H., 1982. Steam-surfactant system at reservoir conditions. *Paper SPE 10777* presented at California Regional Meeting of SPE, San Francisco, California.

Petroleum Res. J. Vol. 12 (2000); P. 19–24, 8 Figs.

Seismic Interpretation of Gargaf Group Palaeostructures, NW of Concession 6, Sirt Basin, Libya

Senusi M. Harsha* and Falah H. Owaina*

التفسيرات السيزمية للتراكيب القديمة لمجموعة القرقاف في شمال غرب عقد الامتياز رقم 6، وسط حوض سرت، ليبيا

السنوسي محمد حرشة وفلاح حسن عوينة

تم تفسير تتابع مجموعة القرقاف ذات العمر (الكامبرو - أوردوفيشي)، وأعدت هذه التفاسير على هيئة خرائط زمن وسرعة وعمق.

أمكن التعرف على وجود منطقتين مهمتين من الناحية النفطية، الأولى تعد منطقة مكمن غازي حيث تم حفر معظم الآبار الغازية المنتجة منها والواقعة بالجزء الشرقي من منطقة الدراسة، أما المنطقة الثانية فهي واقعة في الجزء الغربي، وتعد منطقة مؤملة على الرغم من أنها بحاجة إلى دراسات تأكيدية إضافية.

توضح خريطة السمك لتكوين الباهي وجود توافق جيد بين منطقة المرتفع القديم المتمثلة بمنطقة عدم الترسيب ومنطقة المكمن الغازي في الجزء الشرقي، كما أظهرت مطابقة جيدة بين موقع المرتفع ومواقع الآبار المنتجة.

Abstract: *The top sequence of the Cambro-Ordovician Gargaf Group in NW of Concession 6 is interpreted. Time, velocity and depth contour maps were constructed.*

Two prospects were mapped in the studied area, one is well defined with many gas producing wells located to the east, the other, which was newly defined, is located to the west of the area. The second prospect appears to be an attractive one, but needs to be confirmed by further seismic survey.

The isopach map of the Bahi Formation shows a good coincidence between the structural closure and the Cretaceous palaeohigh structure of the area. Similar coincidence exists between produced well locations and the palaeohigh.

INTRODUCTION

The Sirt Basin is located in the north central part of Libya. It is a young-rifted intracratonic basin. An active subsidence and block faulting as a result of the collapse of the Sirt Arch in late Early Cretaceous time developed this basin. Marine sediments accumulated following the initial arching and rifting of the Sirt Basin. They unconformably overlie the igneous and metamorphic rocks of Precambrian basement, Cambro-Ordovician Gargaf group and/or Nubian Sandstone (Gumati, 1985).

The study area is located between the Hagfa and Wadayat troughs in the northwest of

* Department of Geophysics, Faculty of Science, Al-Fateh University, P.O. Box. 13379, Tripoli, Libya.

Concession 6 (Fig. 1), and is represented by a gas field. Three of the thirteen drilled wells were dry. The important structural element in the area of study is the major northwest-southeast trending normal fault, which extends along the southern flank of the area.

The objective of this study is to evaluate the field through mapping of the subsurface structures.

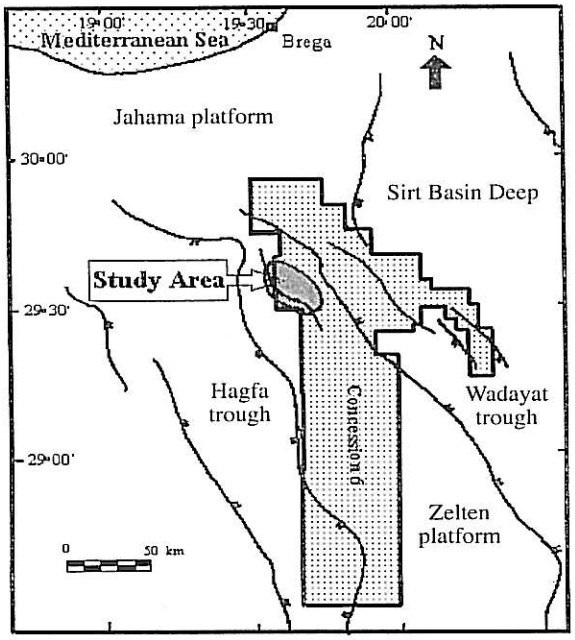


Fig.1. Location map of the study area.

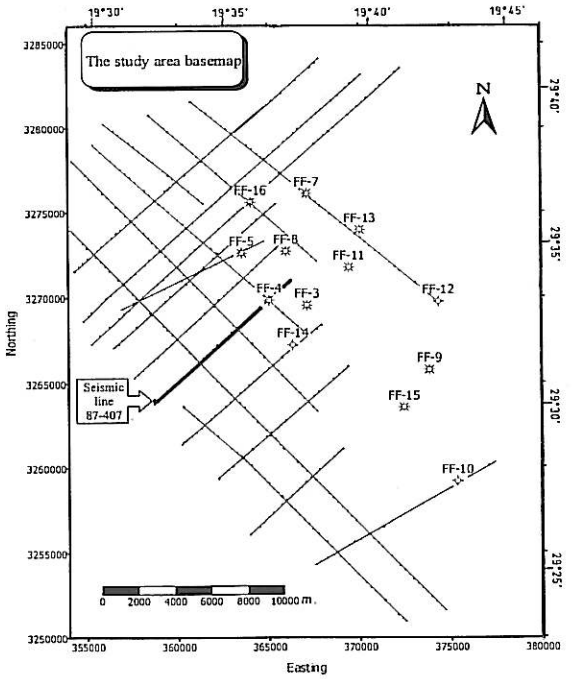


Fig. 2. The base map of the study area, the bold seismic line is the line 87-407, its interpretation is illustrated in Fig. 4.

All of the well logs and eighteen seismic lines were used to examine the tectonics and subsurface geology of the study area (Fig. 2). The top of the Gargaf sequence was chosen to be the interpreted seismic event. It was picked on the seismic sections and mapped in time and depth. Depth conversion was preformed using an average velocity function.

The available data provide a background information for the present geophysical interpretation. The analysis has resulted in the construction of time and depth contour maps for the top of Cambro-Ordovician Gargaf quartzites, which are identified as the principal reservoir.

GEOLOGICAL AND STRUCTURAL SETTING

The graben effects in the Sirt Basin started in the Late Cretaceous and ended with the downwarping of the interior sag in the middle Late Eocene (Parsons *et.al.*, 1979).

A number of transgressive and regressive cycles occurred during the Phanerozioc. The sedimentary sequences are dominated by marine shale, carbonates and evaporites in the Sirt Basin (Gumati *et.al.*, 1996).

The Sirt Basin within the vicinity of the area under study underwent regional uplift and tensional faulting, this has resulted in a northwest (NW) trending horst and graben structural style of considerable relief. The horsts were weathered and eroded with accumulation of sediments in the graben.

SEISMIC INTERPRETATION

The Sirt Oil Company (SOC) has provided us with the essential data for this study. It includes eighteen final stacked seismic sections obtained in 1987 and two synthetic seismograms for wells FF7-6 and FF12-6. The quality of the seismic data ranges from poor to good with low seismic resolution especially for deep reflectors. The data was non-migrated 2-D seismic sections. The mapping was conducted without any support of seismic interpretation workstation.

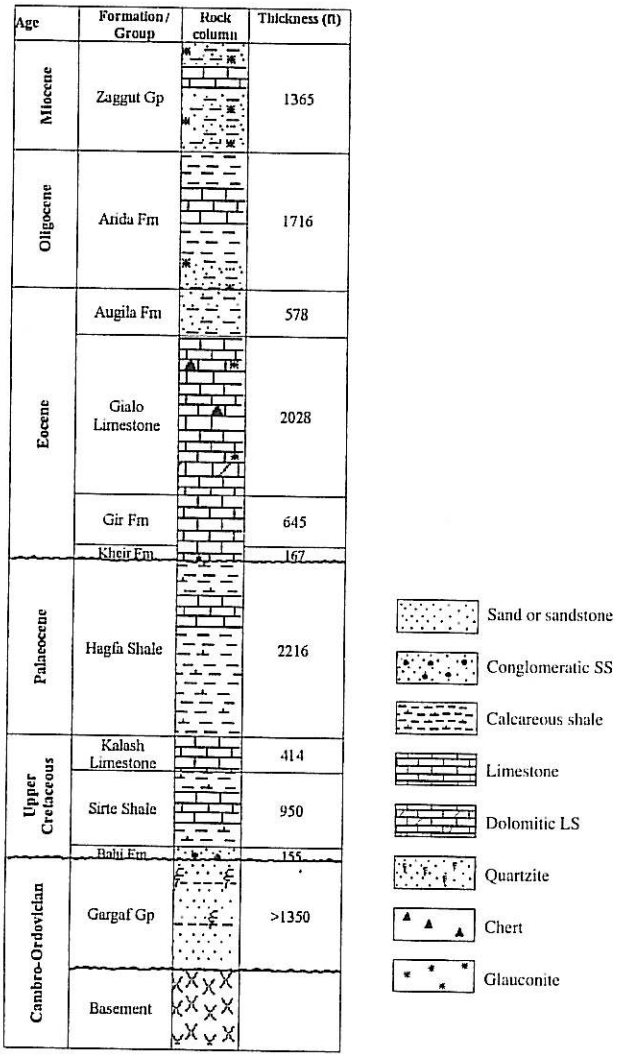


Fig. 3. A composite stratigraphic column of the study area.

Since the Bahi sandstone is overlying the Gargaf quartzites, the seismic event of the top of Gargaf Formation is marked by a weak amplitude peak on the synthetic seismograms of the available wells in the study area, this weak amplitude is an indication of poor reflection coefficient.

The top of the Gargaf horizon has fair to good continuity. It was difficult to pick, in many places, on the seismic and no mistie was recognized on the cross lines (Harsha, 1997). This horizon is overlain by different Upper Cretaceous sequences in the study area. The Kalash Limestone unconformably overlies it in wells FF8-6 and FF3-6. On the other hand, the horizon is overlain by the Sirte Shale as indicated in wells, FF10-6, FF9-6, FF11-6, FF5-6, FF16-6, and by the Bahi Formation in wells FF15-6, FF14-6, FF12-6, FF13-6, FF7-6, and FF4-6. The Gargaf horizon has reflection time of about 2.532 seconds in well FF12-6.

Only normal faults, were recognized on the seismic sections. They represent the rifting criteria that have taken place during the Sirt Basin building episode. They represent the dip line direction and are very clear in the SW-NE lines. Figure 4 is part of the interpreted seismic section ((87-407) which illustrates these structures. It shows the picked horizon, the graben and the horst structures that are existing in the area. Varying thickness on two sides of normal faults indicates growth fault mechanism.

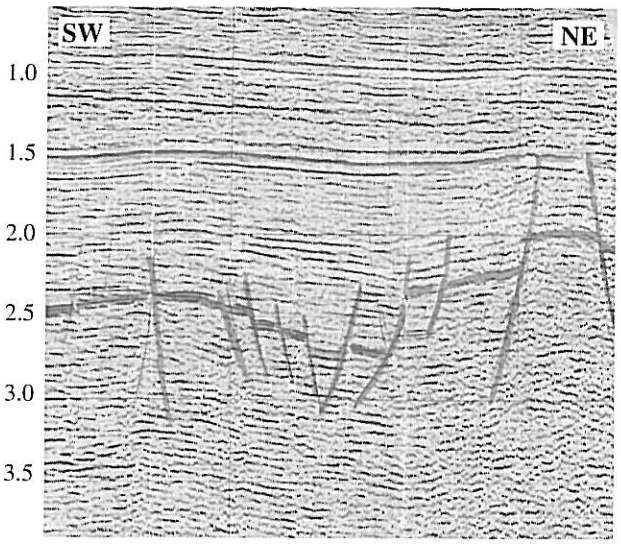


Fig. 4. Part of the seismic section (87-407) showing the normal fault system of the area, the horst, the graben and the picked seismic event of top Gargaf quartzites.

The major and minor faults, shown on the contour maps, follows the major NW-SE trending faults in the Sirt Basin. The faulting separated the area into three blocks. The first is a horst located on the east side of the area, the second is a graben located in the middle of the area and the third is another horst located on the west side. The south flank of the area is comparatively steep.

The time contour map shows a structural high in the centre of the area, with a contour range from 2450 to 2000 milliseconds (Fig. 5). The other structural high is in the west of the study area.

The average velocity map, which was constructed from the available well data, shows small lateral variations in the top of Gargaf velocity. The contour patterns on the average velocity map are sufficiently similar, and the contours show that the velocities differ by 150 m/sec. from one side of the area to the other (Fig. 6). Generally the velocity is increasing towards the southwest. The lowest velocity region (northeast) is 2800 m/sec, and the highest region (southwest) is 2950 m/sec. This gentle variation of the average velocity is very normal and accepted for depth conversion.

Gargaf depth below sea level. The closure contours vary from 3000 to 3500 m in the middle of the area, in particular over the structure. They show clearly the trend and the shape of the structure, which is a northeast – southwest trend. The area becomes slightly deeper away from the closuring contours, especially in the southwest where depth reaches 4000 m.

Most of the producing gas wells were drilled in the east block. However, an attractive structure appears west of the area. Even with the limited amount of information available it is easily shown that the structure in that part of the area will be very interesting.

The Bahi Formation isopach map was constructed based on information from thirteen wells (Fig. 8). It lies unconformably over the lower Palaeozoic sandstone from which it seems to have been derived. At wells within a Palaeozoic structural high, the Bahi Formation is missing, and in this area the Sirte Shale unconformably overlies the Lower Palaeozoic rocks. From the isopach map, it was recognized that the Gargaf Formation blankets the two sides of the study area, and is separated by NW-SE trending local post- Cretaceous high (Fig. 8). Thickness varies considerably within a short distance. It indicates thinning and non-deposition over the high. There is a good correlation between the eastern horst of Gargaf depth map and the palaeohigh as indicated by the Bahi isopach map. This result supports the conclusion of the relation between palaeohigh and the oil entrapment at the Gargaf reservoir level.

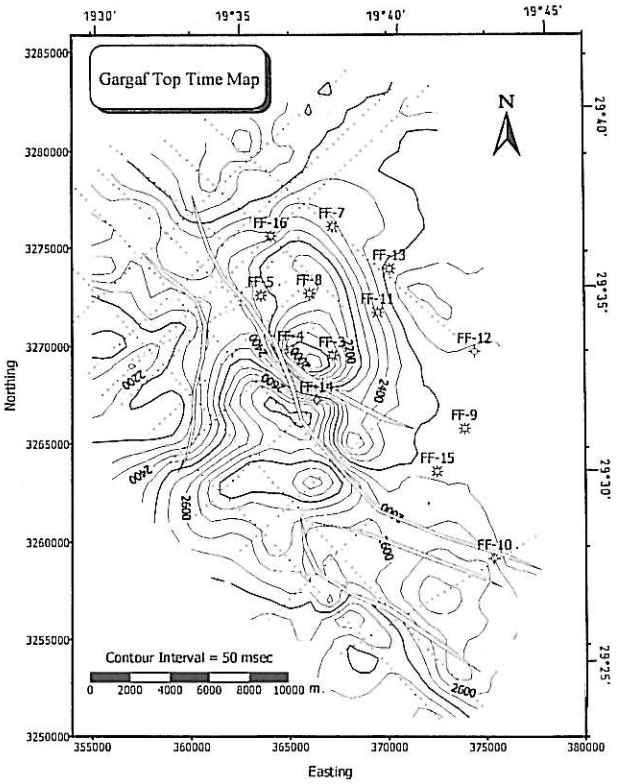


Fig. 5: Gargaf time contour map represents the interpretation of the picked horizon with the interpreted normal fault system of the area. The map was constructed using Surfer software.

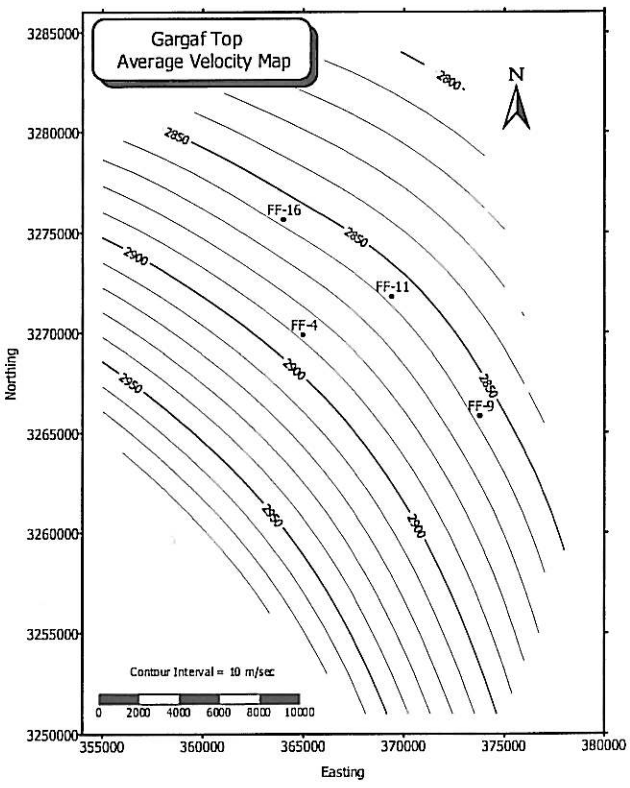


Fig. 6. Top Gargaf average velocity map. The velocity surface was constructed using four wells located in the middle part of the area.

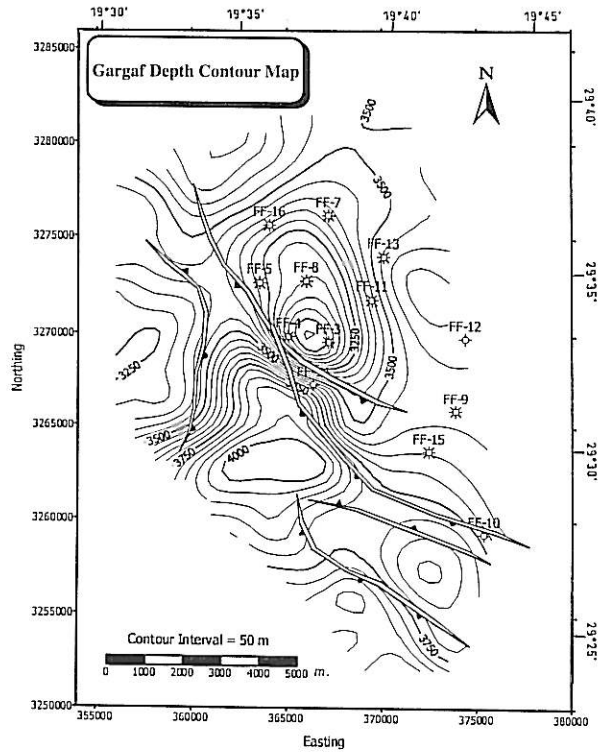


Fig. 7. Top Gargaf depth contour map. The fault system was not migrated in the spacial domain. The map covers the main horst structure, and shows all of the producing wells in the field.

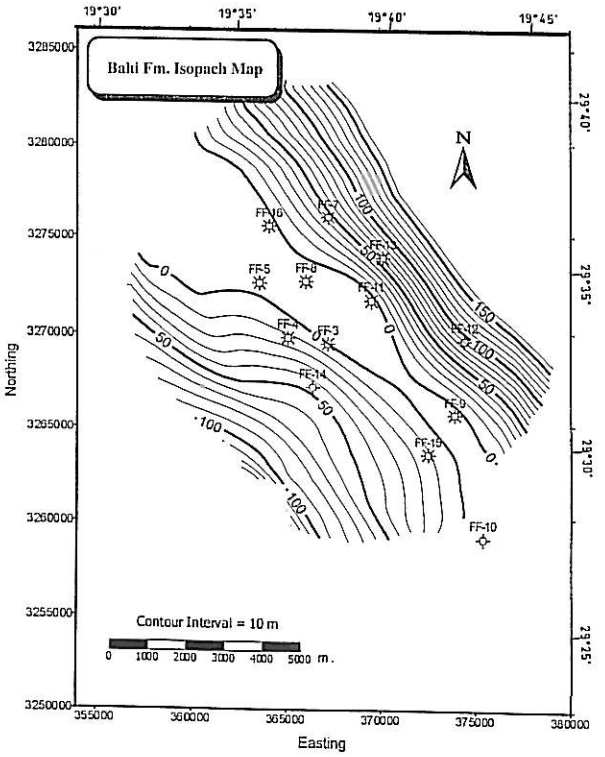


Fig. 8. Bahi isopach map. The Gargaf Formation blankets the two sides of the study area. NW-SE trending post-Cretaceous high separates them.

CONCLUSIONS

Major northwest-southeast trending normal faults are, an important structural element in the area, separating the area into three blocks. The most important structure in the study area is represented by a palaeohigh structure (Pre-Cretaceous high). All of the producing wells are located on the palaeohigh structure, while the three dry wells are located away from it.

The agreement between depth contour map and Bahi isopach map is represented by this palaeohigh.

There is an attractive structure in the west of the gas field, its dimension may exceed 5x5 km with more than 200 m of relief. This closure, may have the same reservoir characteristics of the productive field. Even from the limited available amount of information it is easily shown that this structure could be an important prospect.

The Cambro-Ordovician Gargaf sandstone and the Upper Cretaceous Bahi Formation represent the principal gas reservoir of the area. The Upper Cretaceous Sirte Shale is regarded as the main hydrocarbon source rock of the Cretaceous reservoirs and the underlying Gargaf sandstone.

ACKNOWLEDGEMENTS

The authors wish to thank Sirt Oil Company, Libya for providing the essential data for this paper. Thanks are also extended to Mr. Ross McCullough for his English language reviewing.

REFERENCES

Gumati, Y. D., 1985. *Crustal Extension, Subsidence, and Thermal History of the Sirte Basin, Libya*, Unpublished Ph.D. thesis, Earth Sciences and Resources Institute University of South Carolina, USA.

Gumati, Y. D., Kanes, W.H. and Schamel, S., 1996. An evolution of the hydrocarbon potential of the sedimentary basins of Libya. *J. Petrol. Geol.* **19**(1), 92-112.

Harsha, S. M., 1997. *Stratigraphic Correlation and Seismic Interpretation of Attahaddy Field, Sirt*

Basin, Libya, Unpublished Ph.D. thesis, Faculty of Physical and Applied Sciences, University Kebangsaan, Malaysia, Bangi-Malaysia.

Parsons, M. G., Zagaar, A. M. and Curry, J. J., 1979. Hydrocarbon occurrences in the Sirte Basin, Libya, In: *Facts and Principles of World Petroleum Occurrence. Mem. Can. Soc. Petrol. Geol.* **6**, 1-15.

Petroleum Res. J. Vol. 12 (2000); P. 25–38, 12 Figs.

Estimated Generation Time and Migration Trends of Upper Cretaceous Source Rocks, Sirt Basin

A. M. Ben-Ashour*

تقييم زمن تكوين وهجرة المواد الهيدروكربونية لصخور المصدر، التابعة للكريتاسي العلوي بحوض سرت الرسوبي

عبد الرحيم بن عاشور

تتناول هذه الدراسة الأوجه الجيوكيميائية وتطور الكيروجينات الموجودة في صخور المنشأ الكريتاسية العليا وتوزيعها الأفقي (حوض سرت الرسوبي). نوقش تطور الكيروجينات من الناحية الزمنية والعمق.

تشير التحاليل الجيوكيميائية أن صخور المَصدر الفاعلة ونضوج الكيروجينات يقتصر وجودهما على المناطق الوسطى لمنخفضي زلة واجدابيا وكذلك المناطق الجنوبية من منخفض مرادة. ونتيجة لعدم الثقة، وبالتالي الاعتماد على درجات الحرارة المقاسة بالسرود، فقد استعمل عامل تصحيح بسيط لتعديل الأخطاء عند كل درجة حرارة مقاسة عند 13° ف، وتم إعداد خريطة توضح توزيع الحرارة الأرضية للحوض.

تم دمج درجات الحرارة المصححة وعمق الدفن بهدف التنبؤ بمستويات النضوج وزمنه بمنطقة الدراسة حيث يعتقد أن أوان النضوج الأصلي كان ما بين العصر الأيوسيني المتأخر إلى الميوسيني المتقدم والذي تم باستمرار عملية الترسيب والهبوط المصاحب بمنطقة تكوين المواد الهيدروكربونية. إن نطاق نافذة النفط قد اعتبر نطاقاً (حركياً متجاوباً) للتباين في معدلات الدفن والتعرية، ويعتقد بأن هجرة المواد الهيدروكربونية إلى التراكيب داخل المنخفض وإلى المرتفعات (المسطحات) المجاورة، كان إلى مسافات ليست بعيدة عن النشأة وأن الصدوع من أهم العوامل الموصلة بين المكامن وطبقات المنشأ.

Abstract: *Owing to a lack of confidence and reliability in measured log temperatures a simplified temperature correction was applied to compensate for the error at every measured temperature of about 13° F. Corrected temperatures and corrected burial depth were used to predict generation time for various locations and sites in Sirt Basin. Evaluation of collected data indicates that source rocks and maturation of the kerogens are restricted to central parts of Zallah, Al Kotlah, Hameimat, Ajdabiya and southern Al Hagfa troughs. Generation time is estimated to be late Eocene to early Miocene and progressed forward as subsidence and sedimentation continued. Generation and migration are closely related time-wise and faults are the main element that connected reservoirs to the source beds under consideration. Migration of hydrocarbon to the reservoirs within trough systems and to the adjacent platform is thought to be of short distance. Hydrocarbon accumulations prior to the late tilting (southeast) of the platforms of Sirt Basin reacted to the resulted structural configuration and formed the present accumulations.*

* The Geology Dept. The University of Al-Fateh, P.O. Box 13258, Tripoli, Libya.

INTRODUCTION

This study discusses the geochemical aspects and evolution of Upper Cretaceous source rocks present in the sedimentary section of Sirt Basin. It is based on geochemical data collected from the National Oil Corporation combined with geological background gained in the past century. Evolutions of Sirt Basin Upper Cretaceous source rocks are dealt with in time and depth that are directly related to temperature and duration of heat. Previous published studies, most related to this work are, those of Gumati and Kanes (1985) and El-Alami, *etal* (1989).

As is cited in the geochemical literature, maturation of kerogene in source Rocks are controlled primarily by temperature and duration of heat. Direct measurement of maturation is based on analysis of vitrinite reflectance and other kerogen and hydrocarbon constituents in samples of exploration wells that are mostly drilled on structural highs. On the other hand, presumably, more maturation of the organic constituents contained in the source rock is at lower structural levels in the basin, where drilling is not recommended by exploration geologists. Therefore, carrying out interpretation based on purely analytical data is most probably, misleading especially in Zallah-Ajdabiya troughs. Here, lack of dependence of maturation levels on depth position of source rock is encountered, which strongly suggest that elevated temperatures were maintained during the kerogen evolution.

To quantify the effect of time and temperature on the conversion of kerogen into petroleum and gas, the burial history of the basin should be established.

The proposed method by Magara (1976) for estimating maximum depth of burial for a given sedimentary section as well as a simplified method to correct bottom hole temperatures were employed to account for generation time and the dynamics of the oil windows of the Upper Cretaceous source rocks present in the sedimentary section of Sirt Basin.

GEOLOGY

A long list of investigators contributed to the description of the geology and structural evolution of Sirt Basin, including, Conant and Goudarzi (1967), Selley (1968), Barr and Weegar (1972), Van Houten (1980), Goudarzi (1980), and many others.

Two major hypotheses to the tectonic mechanism of forming the Sirt Basin were formulated. Van Houten (1980) attributed the opening of the Sirt Basin to the drift of north central Libya over a fixed mantle hot spot during early Cretaceous, whereas the second hypothesis suggests that the Sirt Basin formed in a failed spreading arm that extended southeast from the Tethyan spreading system to the north.

Following the Hercynian deformation, which ended Palaeozoic deposition, the Sirt Basin region underwent prolonged erosion before the beginning of sedimentation in the late Mesozoic. The floor of the basin is formed mainly of Precambrian rocks and the basin thus developed on the site of a deeply eroded high.

The general epierogenesis of the basin began late in the Mesozoic and continued well into the Holocene, (Selley, 1968). The subsidence kept pace with sedimentation and was locally fault controlled, with the result that considerable variation in thickness and facies exists in the contained sediments. The sediments are predominantly marine, mainly carbonates and shales, but with local thick developments of evaporates. Sandstones also occur, notably at the bottom and the top of succession. Stratigraphic variations within the individual units are largely regional in character and are controlled by position within the basin.

Sharp local variations also occur and these are most directly related to contemporaneous faulting. Most of the faults are normal faults and were active early in the development of the basin. Smaller numbers of normal faults are regional, and were generally active intermittently throughout the history of the basin and these had an important influence on the development of the basin into a series of horst and graben structural style with a NW-SE orientation, except the Al Kotlah trough that has a NE-SW alignment (Fig. 1). The oil producing structures of the basins are due to these faults and to the sedimentary drape over them. Hydrocarbons occur in commercial quantities at several stratigraphic levels within the basin.

1. In sandstones and quartizites of the pre-Upper Cretaceous units;
2. In sandstones and carbonates of the Upper Cretaceous;
3. In limestones, chalk and dolomites at various levels in the Palaeocene;
4. In sandstones of the Upper Eocene – Oligocene.

The overall distribution of oil in these reservoirs seems to be controlled by the regional facies variations within the major stratigraphic interval concerned.

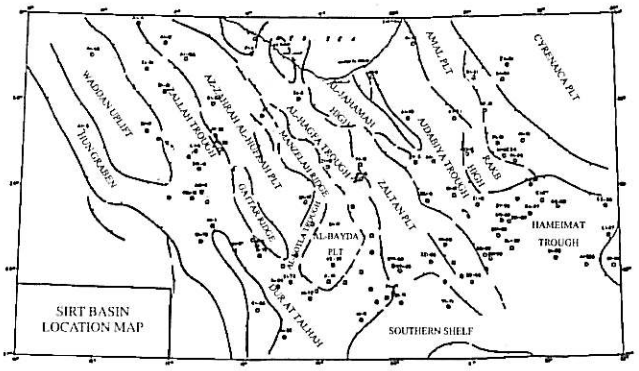


Fig. 1. Sirt Basin location map with well locations included in this study.

SOURCE ROCK

In Sirt Basin, geochemical analyses have indicated several stratigraphic units to be rich in organic content. However, maturity is restricted to sediments of middle Nubian shales and Upper Cretaceous (Rakb Group) Sirte, Rachmat and Tagrifet Limestone. Targrifet Limestone is restricted to the Ajdabiya and Hameimat troughs, which with Sirte Shale give a combined thickness of average 1,500 ft, while Rachmat Formation (shale) has a widespread distribution in the other troughs of the basin with Sirte Shale both make an average thickness of about 1,300 ft in Al Hagfa, 1.200 ft in Zallah and 800 ft in Al Kotlah areas. Total organic content ranges from 0.5% to 5% and heigher and the amorphous kerogen types derived from land plant materials were detected from the Upper Cretaceous source rock.

Delineation of the areas of Upper Cretaceous source rocks in Sirt Basin was based on S_1, S_2, P.I. and T.O.C. data classification (Fig. 2). The scarcity of data in the northern parts of Al Hagfa and Ajdabiya troughs hinders satisfactory rating of source rock potentiality in those parts of the basin, although early exploration has indicated mostly disappointing results of hydrocarbon accumulation discoveries.

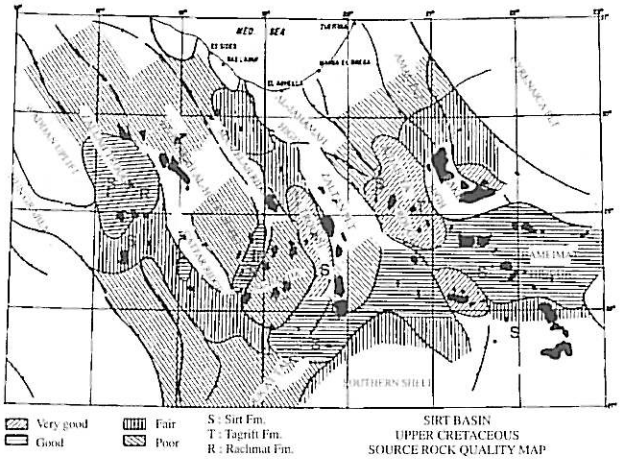


Fig. 2. Source rock quality map, Upper Cretaceous Sirt Basin.

ESTIMATED REMOVED STRATIGRAPHIC SECTIONS

Geologic evidence indicates that considerable parts of the stratigraphic section are missing from the exposed outcrops in the Sirt Basin. Lower Eocene rocks are exposed at the surface in some western parts of the basin, Oligocene outcrops in the central areas of the basin, while east central and eastern regions include Miocene and younger outcrops. The missing stratigraphic cover in the western Sirt Basin (Zallah trough) must have been comparable with those preserved in the eastern Sirt Basin. This large difference in removed stratigraphic section will have a major influence

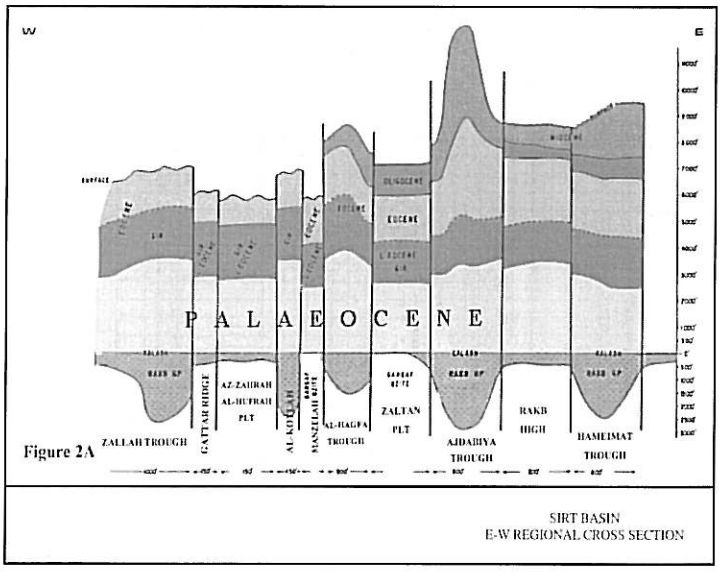


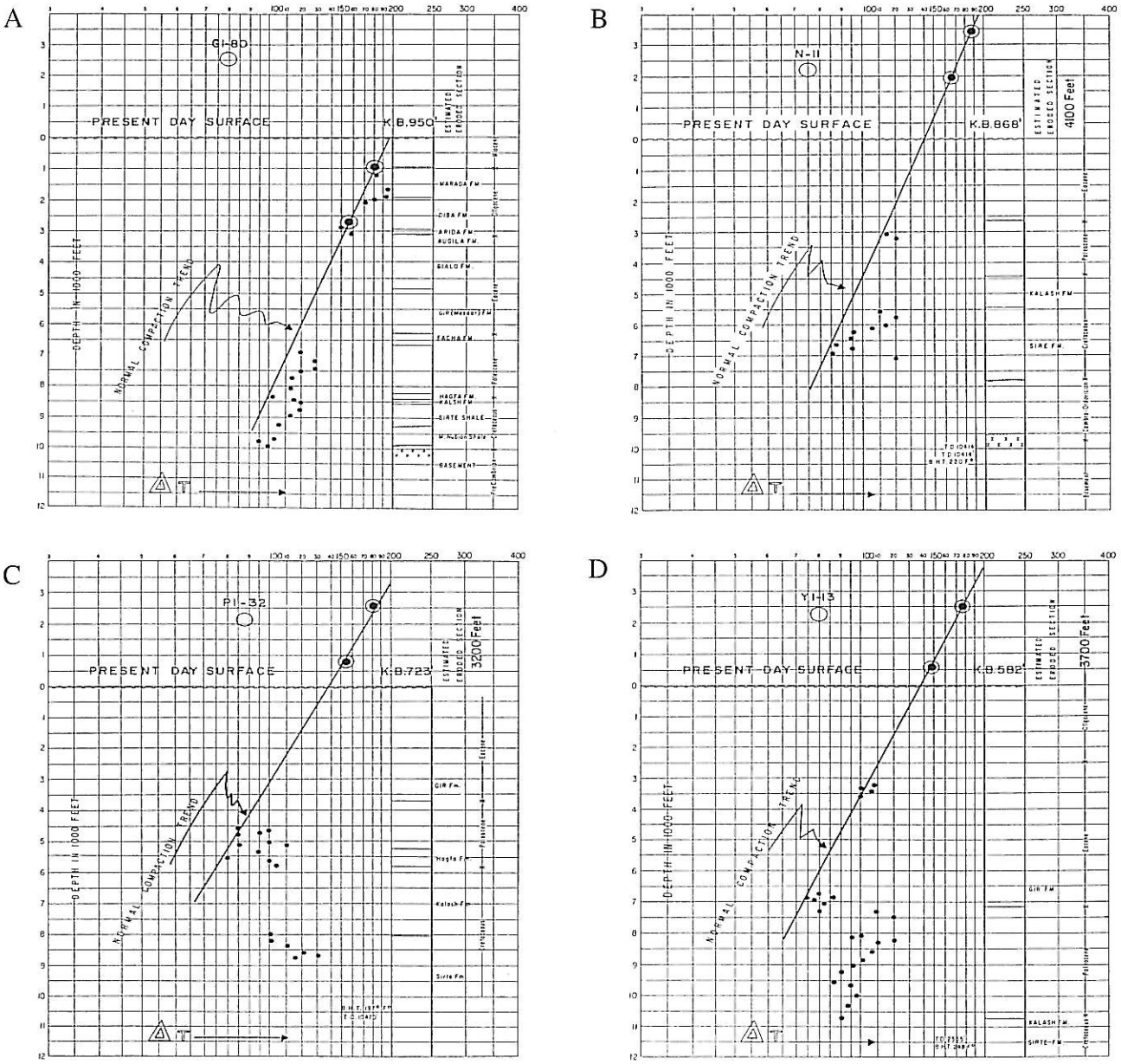
Figure 2A

Fig. 2 (a). East–west regional cross-section.

on estimates of the maximum temperature attained by kerogen-bearing rocks mainly in the Zallah trough. (Fig. 2A)

Magara (1976) established a method for estimating the maximum depth of burial for a given sedimentary section. His method was based on the fact that porosity in shales decreases exponentially with increasing depth because porosity is linearly related to sonic transit time. Therefore the transit time through a shale section should decrease exponentially with depth of burial. If transit time (ΔT) of a shale section is plotted on a logarithmic scale against depth plotted on a linear scale, the plot should be a straight line. Since clay on the modern day sea floor has a transit time of approximately 200 m sec/ft, a straight-line extrapolation to the 200 m sec/ft point should give an estimate of the maximum depth of burial. Magara's technique was employed here to estimate the thickness of the eroded overburden and hence maximum burial depth of Upper Cretaceous source rocks of Sirt Basin.

For the calculation of eroded stratigraphic sections estimates, well G1-80, where it is believed that not much erosion of overburden has occurred, was used as a standard normal compaction trend for areas in Sirt Basin where subsequent removal of stratigraphic sections is believed to have taken place. (Fig.3, A, B, C. and D). The average



Fig, 3. A, B, C, and D normal compaction trends, G1-80, N1-11, P1-32, Y1- 13.

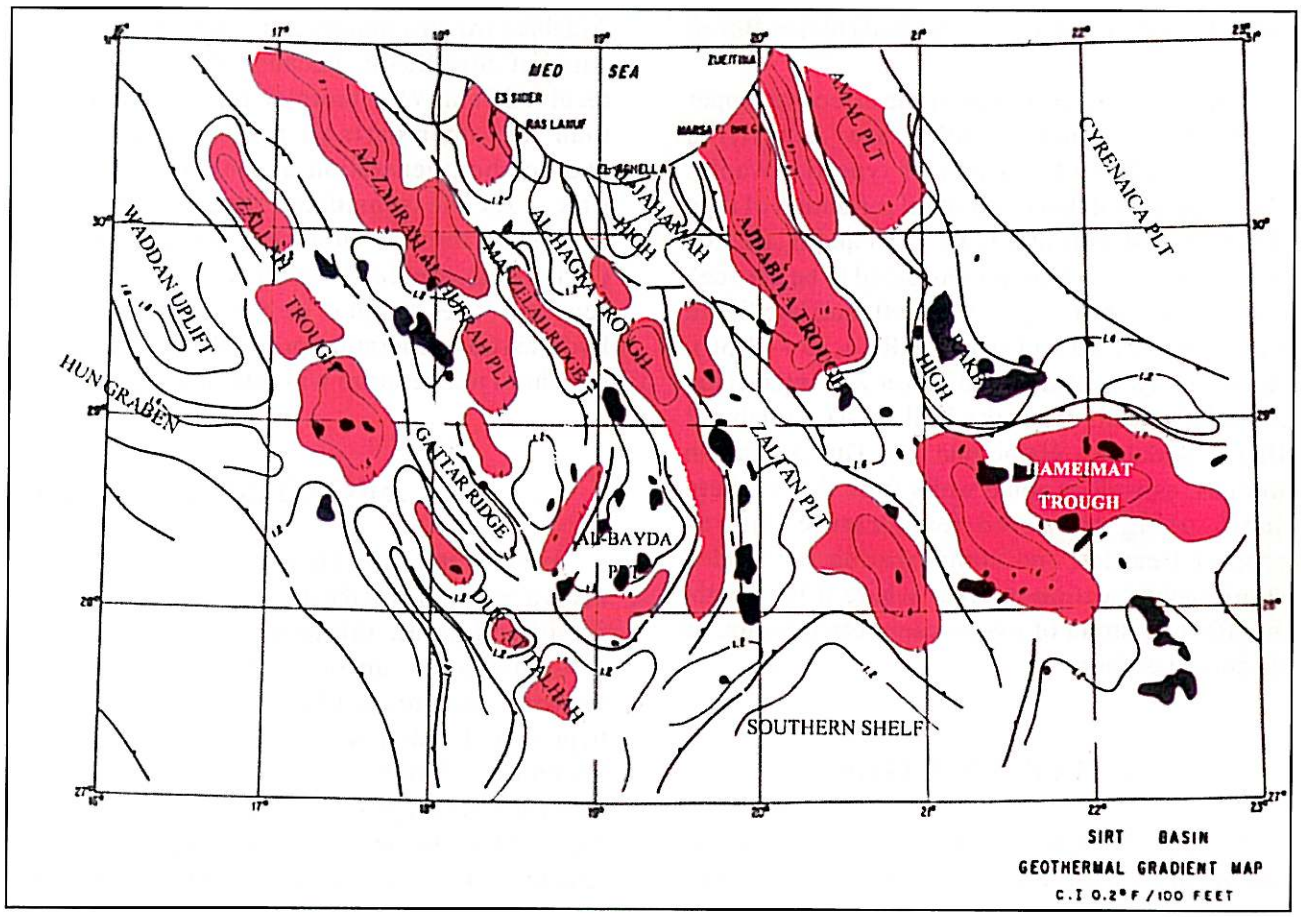
estimated missing thickness of overburden in the indicated areas that has affected the present geothermal gradient is calculated in the order of 3,200 to 4,000 ft of sediments.

TEMPERATURE AND MATURATION HISTORIES

The measured log temperatures are systematically lower than stabilised subsurface temperatures. They are inaccurate for analysis of geothermal gradients owing to insufficient knowledge of mud circulation time prior to logging, difference in borehole size, friction and compression during DST's and time needed to reach formation temperature equilibrium during shut-in periods. Scarcity of accurate measured temperatures limits the use of many proposed bottom hole temperatures correction methods and the Horner plot, in particular, requires at least two accurate temperature measurements at the same depth for any correction to be made. Since it is almost impossible to meet the requirement set for correction of measured log temperatures, it is assumed that the error in equilibrium thermal temperature estimates is unlikely to be more than 10°C and certainly greater than 1°C (Denning and Chapman, 1988). The error involved in surface temperature is in the order of 2°C to 3°C. Accordingly, the error of any one equilibrium temperature is estimated to be in the order of 7°C (13°F) which is used as correction value added to measured temperature data involved in this study.

The calculated geothermal gradients, on the basis set forth earlier (Fig. 4), are superimposed on a tectonic map compiled by Mouzughi and Taleb (1981). High geothermal gradients occur over the platform whereas lower geothermal gradients exist over the trough regions. As the geothermal gradient is the rate of increase of temperature with depth, so the high geothermal gradients are not necessarily obtained from wells of high temperature but possibly of shallow depth.

The geothermal gradient map patterns also indicate that high geothermal gradient values are



Fig, 4. Geothermal gradient map, Sirt Basin.

to the north (1.8°F/100 ft) whereas the southern region is characterized by relatively lower geothermal gradient with an average of 1.2° F/100 ft, with some local anomalies. The Palaeocene producing horizons in the central and eastern oil fields are within the range of 5,000 ft below sea level. Converting geothermal gradients to temperatures at a common depth of 5,000 ft in much of the Sirt Basin gives a figure of 150 ° F. While in the western Sirt Basin 150 ° F is reached at a shallower depth.

During the course of this study, it was recognized that the depth of burial seems to be the controlling element for maturation of kerogens in the Upper Cretaceous source rock based on the discrepancies among the maturity levels reported and stratigraphic position of source rock samples. Therefore, interpretations based on purely analytical data are most probably misleading, especially in Zallah trough. Here lack of dependence of maturation levels and depth position of source rock is encountered, which strongly suggests that elevated temperatures were maintained during the kerogen evolution present in the Upper Cretaceous source beds of Sirt Basin.

The identified kerogens of the effective Upper Cretaceous source rocks are classified geochemically to be mainly of type II. Waples (1985) proposed that onset of oil formation of type II kerogens begins at TTI (3 – 10) and R_0 (0.50 – 0.60), whereas its peak is considered to be between TTI (20) and (50), R_0 (0.70 – 0.90) and late liquid stage ends at TTI (180) and R_0(1.35 – 1.50). Accordingly, maturity evaluation was interpreted to include wells from the Zallah, Al Kotlah, Al Hagfa, Ajdabiya, Hameimat and Dur At Talhah troughs, as well as some wells from the southern shelf, using corrected temperature data as proposed earlier, and compensating for eroded stratigraphic section in areas where it is thought an effective strata of overburden was missing, as discussed earlier.

GENERATION TIME

Connan (1974) has stated that in a continuously subsiding basin the generation time at the threshold temperature is the time elapsed since source rocks reached the corresponding depth of burial, and it correlates with the age of the geologic formation, although chemical reaction of organic matter was in process at a much earlier state before the threshold temperature was reached. In Sirt Basin, where sedimentation and subsidence are believed to be uninterrupted since the deposition of the Upper Cretaceous sequences, and at least till the Miocene time. An average geothermal gradient of 1.4°F/100 ft and calculated estimated depth of 9,000 to 10,000 ft. was the required depth of burial to reach the threshold point for initial hydrocarbons generation. As sedimentation continues, obviously overburden thickness will increase and maturation levels proceed forward to reach peak and late maturation levels. A series of regional isopach maps were constructed (Figs. 5,6 and 7) to establish overburden thickness that affected the effective source rock sediments under consideration. A montage of those maps with the Upper Cretaceous source rock quality map (Fig. 8), and tracing the (10,000 feet) thickness of overburden, would result in the delineation of areas that attained the required burial depth for initial time of hydrocarbons generation (Fig. 9). Generation of hydrocarbons in the center of Ajdabiya trough commenced earlier than the other parts of Sirt Basin, because this region has received relatively more sediments, time-wise, than the other parts of the basin that led to hydrocarbon generation at the close of Eocene time. As the subsidence and sedimentation continued, through Oligocene time, other Upper Cretaceous source rocks in Sirt Basin troughs reached the proper depth of burial, and hydrocarbon generation proceeded as soon as the threshold temperature was attained.

MIGRATION

Avenues and paths are a product of rock fatigue and deformation, and the movement of hydrocarbons is either lateral, through bedding plains and permeable layers, and/or vertical, through faults and the hairy fractures resulting from rock fatigue due to pressure build-up in the walls of the hydrocarbon generating chambers, Meissner (1978). These passage ways for gas and oil generated from source rocks led to the accumulation of hydrocarbons in structural and stratigraphic reservoirs present at the time, within the troughs and the adjacent platforms in Sirt Basin.

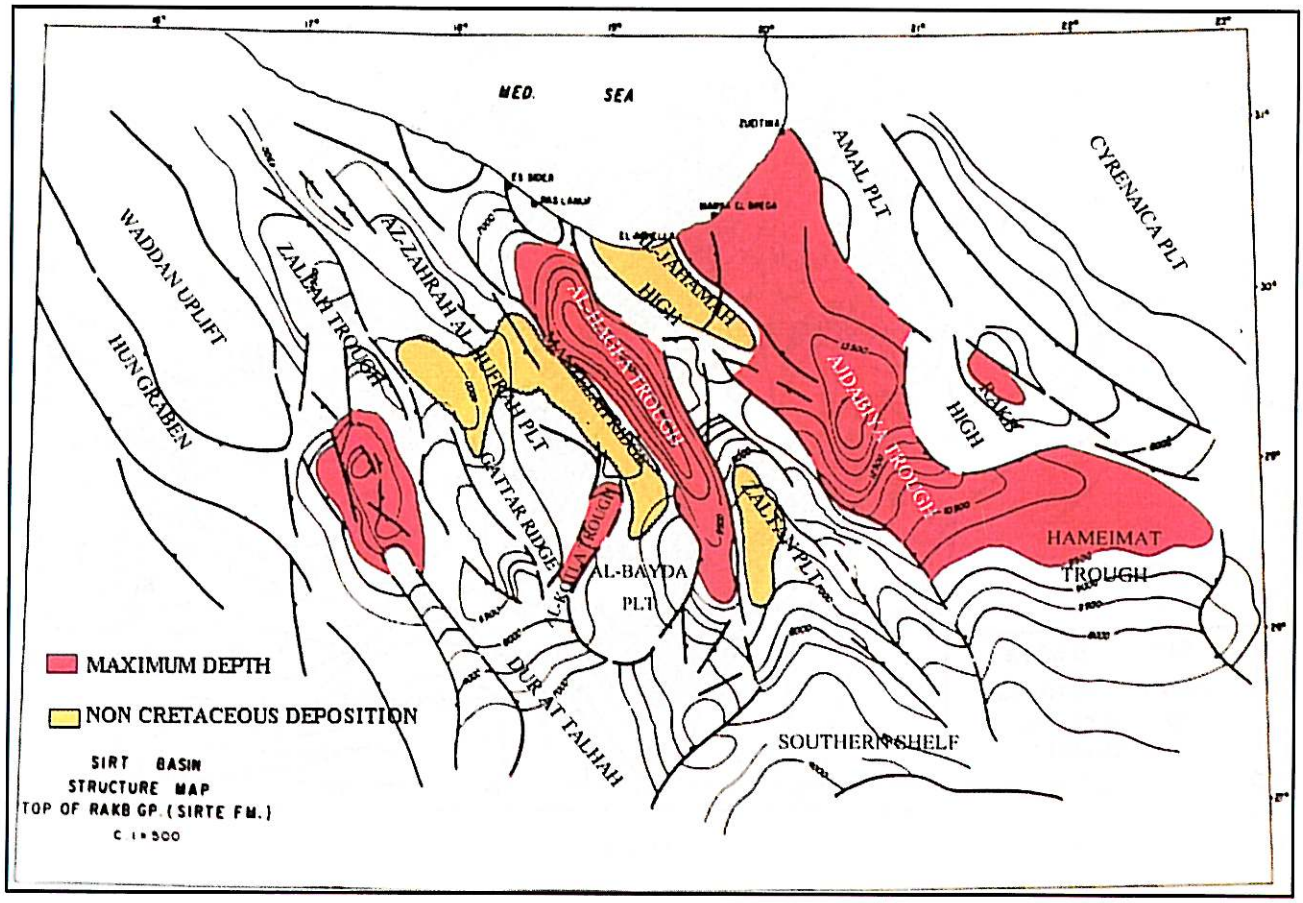


Fig. 5. Structure map top of Rakb Group (Sirte Formation).

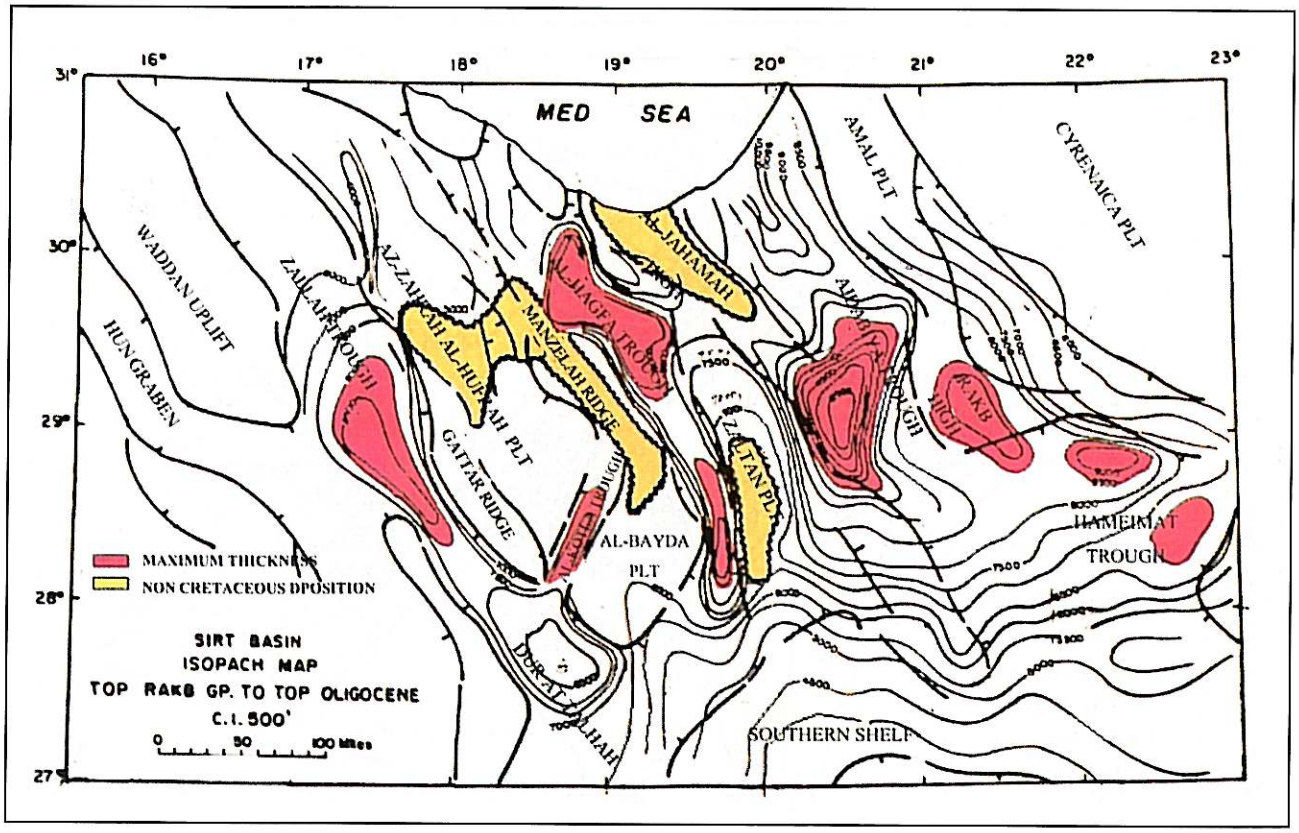


Fig. 6. Regional isopach map – top of Rakb Group – top of Eocene.

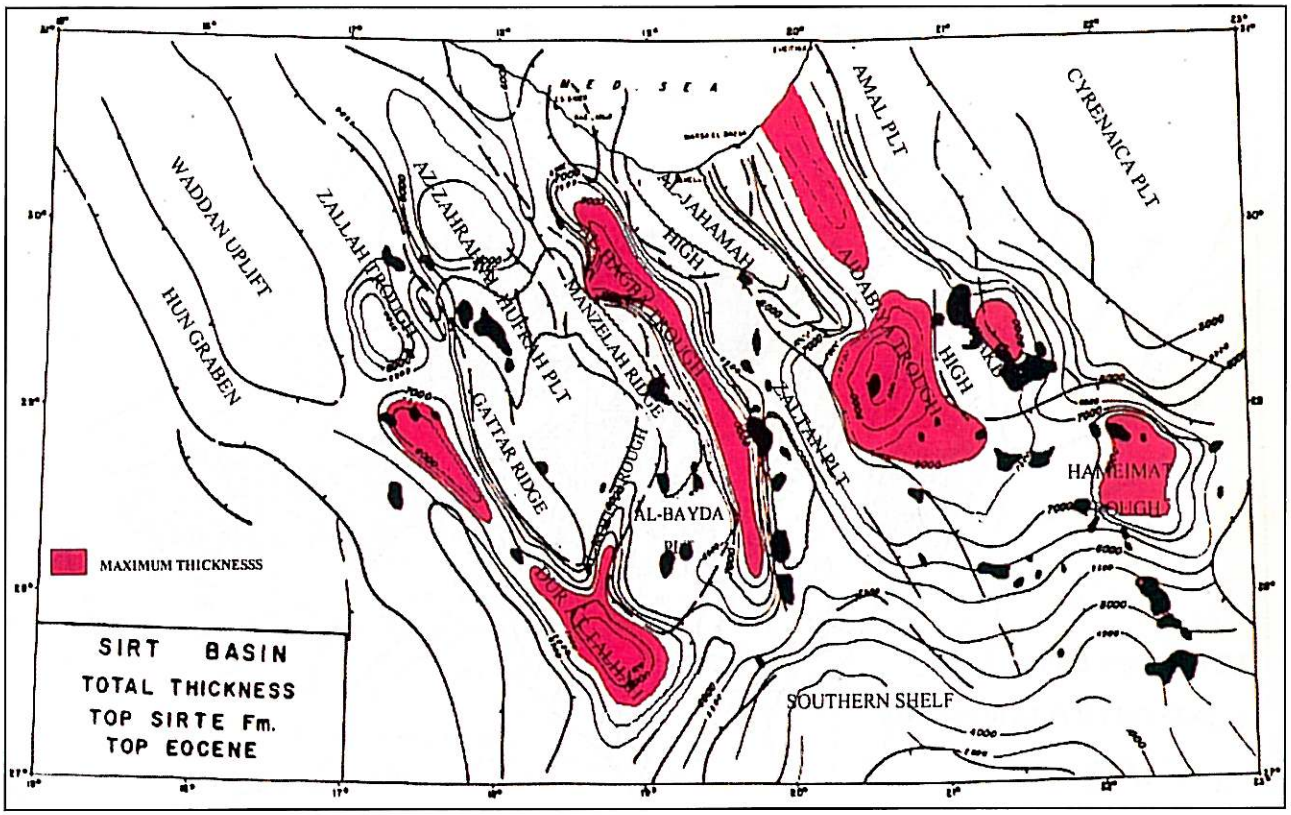


Fig. 7. Regional isopach map – top of Rakb Group – top of Oligocene.

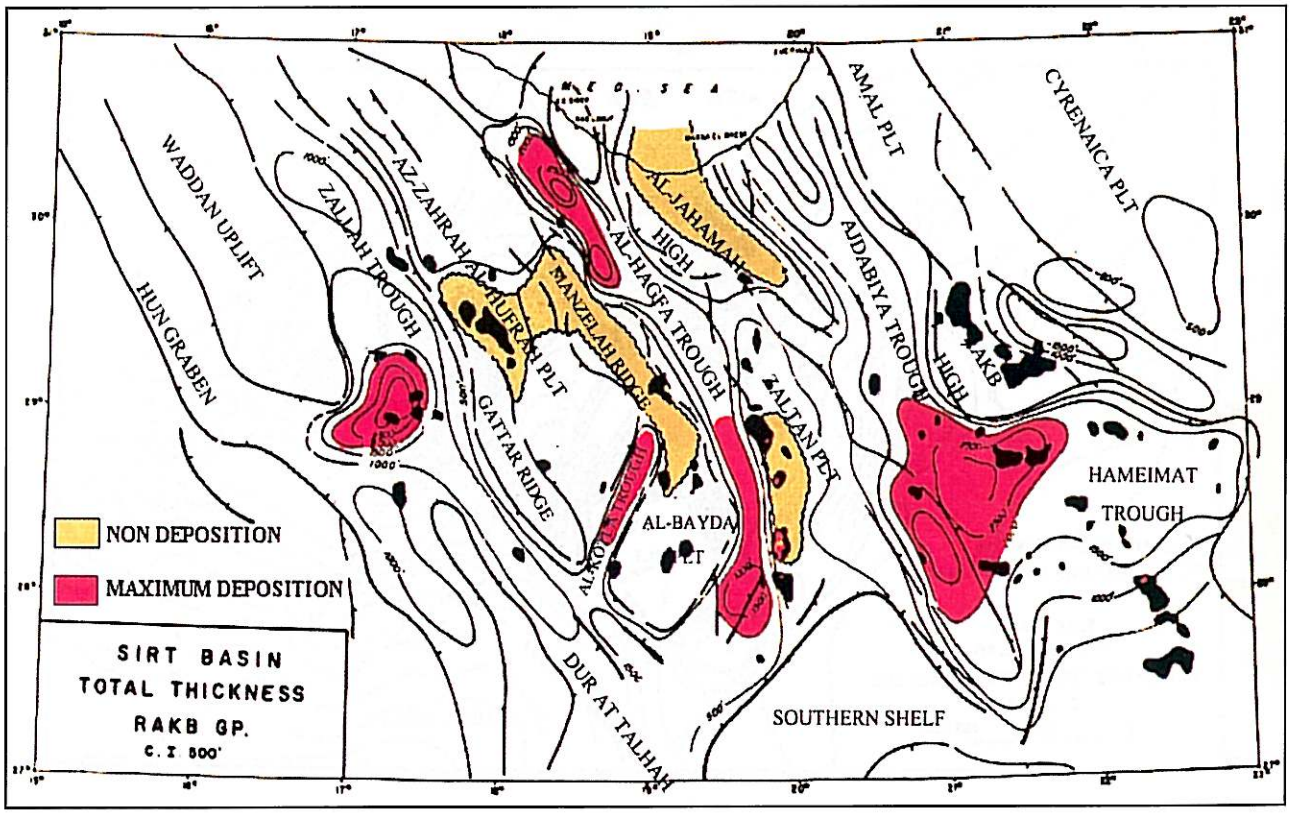


Fig. 8. Isopach map total thickness of Rakb Group.

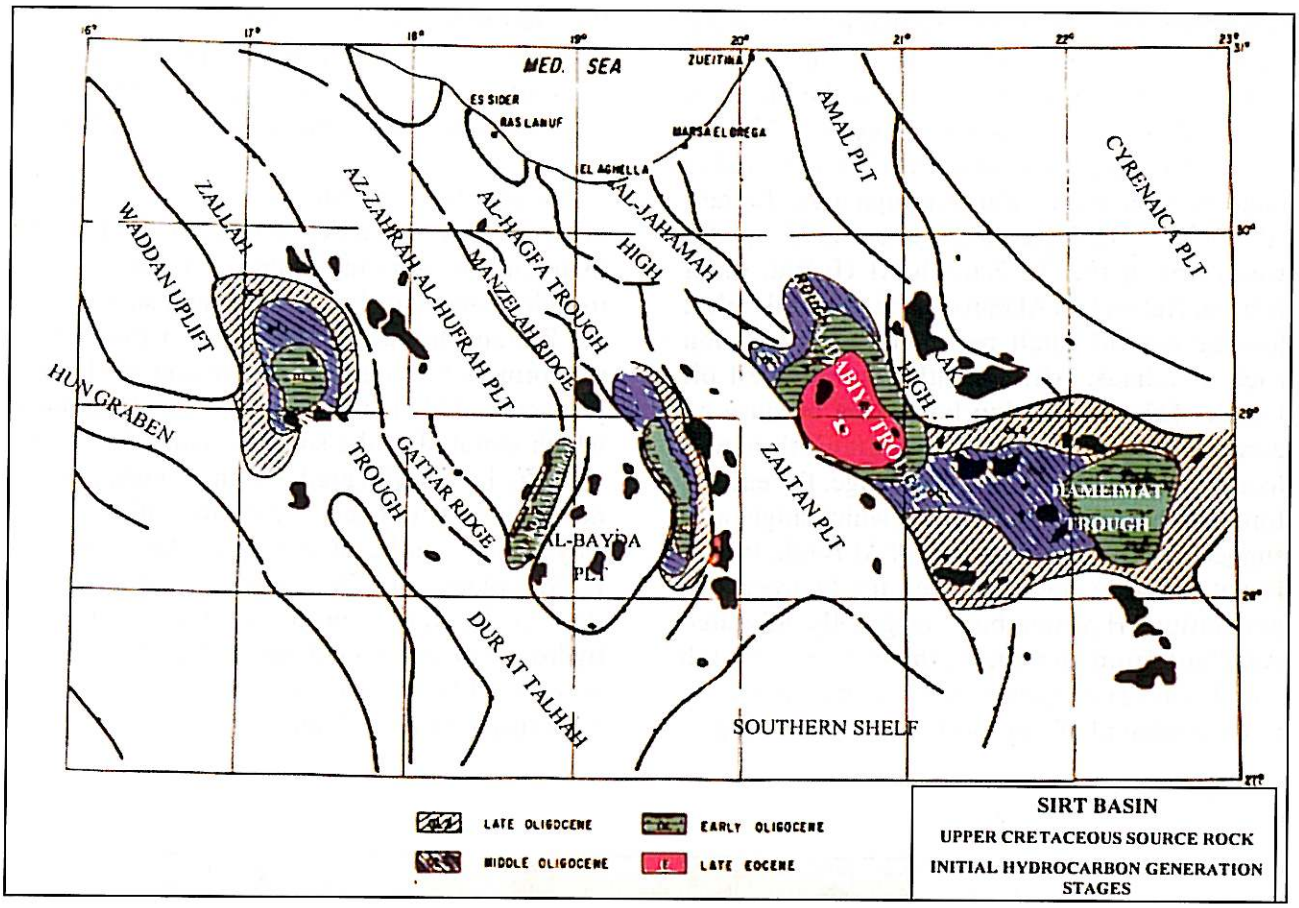


Fig. 9. Initial hydrocarbon generation stages map (Upper Cretaceous source rocks).

The migration of hydrocarbons in Sirt Basin is closely related to the progressive rate of generation, as subsidence and sedimentation progressed, since the close of the Eocene times. As it was indicated earlier, generation of oil and gas in Sirt Basin from Upper Cretaceous source rock initially started in the epi-centre of Ajdabiya trough and continued to include the surrounding potential areas. The yielded hydrocarbons moved to fill reservoirs within the trough and the adjacent Amal platform. As the generation proceeded in Ajdabiya trough, kerogens in the southern Al Hagfa trough reached the required depth of burial and threshold temperature, and the generated petroleum migrated to accumulate within the trough reservoirs and in the bordering reservoir rocks (Al Bayda, Zaltan, Az Zahrah-Al Hufrah platforms). Simultaneously, relative to other troughs of Sirt Basin, the generated petroleum in depo-centre of Zallah trough was migrating to fill the reservoirs within the trough proper and reservoir in the western Az Zahrah-Al Hufrah platforms. Also, probably hydrocarbons generated in the central Zallah trough have found their way through faults to the Waddan uplift, that were not preserved, most likely because it was eroded as a result of the intense period of erosion.

Oil fields that are located on the western flanks of Az Zahrah-Al Hufrah platforms would not have taken their source from Zallah trough, if the present day structural configuration of north-north east dipping of strata had prevailed since Eocene times. (Fig. 10). However, synthesis of the structural development of these platforms using several east-west cross-sections perpendicular to the strike (Fig. 11) indicated almost unified thickness distribution of sediments, continuous sedimentation and south-southwest dipping of strata since Eocene through Miocene times. Therefore, generated hydrocarbons in central Zallah trough have migrated eastward up dip to Az Zahrah-Al Hufrah platform during Oligocene and Miocene times, as soon as maturation levels of kerogens in this trough were reached. The migrated hydrocarbons

probably reached distances further east in the Az Zahrah-Al Hufrah platform to fill the existed reservoirs. When the NE tilting of the platform occurred and as a response to the new NE dip direction, hydrocarbons, which originally migrated from central Zallah trough to Az Zahrah-Al Hufrah platform, were regrouped up dip westward in the Az Zahrah-Al Hufrah giant (Dahra, Hufra) Um Al Faroud and other oil fields, leaving behind small petroleum accumulation such as Almas, Ali, and other single-well oil fields. This explanation holds true because no commercial hydrocarbon accumulation was located so far in the Menzellah ridge, the eastern limits of the platform, (Fig. 12) which might also suggest that the northern half of Al Hagfa trough is not a highly potential area for hydrocarbon generation. Hydrocarbons originally migrated eastward from the southern Al Hagfa trough (south Z1-13) to occupy the existing reservoirs in the Zaltan platform, prior to the NE tilting of the platform reacting to the adjustment in the regional NE dip direction that prevailed to the present, forming large hydrocarbon accumulations at the western edge of the platform.

In addition to the migration condition proposed and discussed previously, a possible hydrocarbon sourcing occurred from Ajdabiya trough to areas at the far north and southeast of the Zaltan platform after the NE tilting of the platform as the regional adjustment of the area proceeded. Other large volumes of hydrocarbons, which matured in the southern half of Al Hagfa trough, have migrated south, southeast and northeastward to charge reservoirs of eastern Al Bayda and southeast corner of Az Zahrah-Al Hufrah platforms. The matured source rocks of the Al Kotlah trough are the source for hydrocarbon accumulations in the reservoirs of western Al Bayda and southeastern flanks of the Az Zahrah-Al Hufrah platforms.

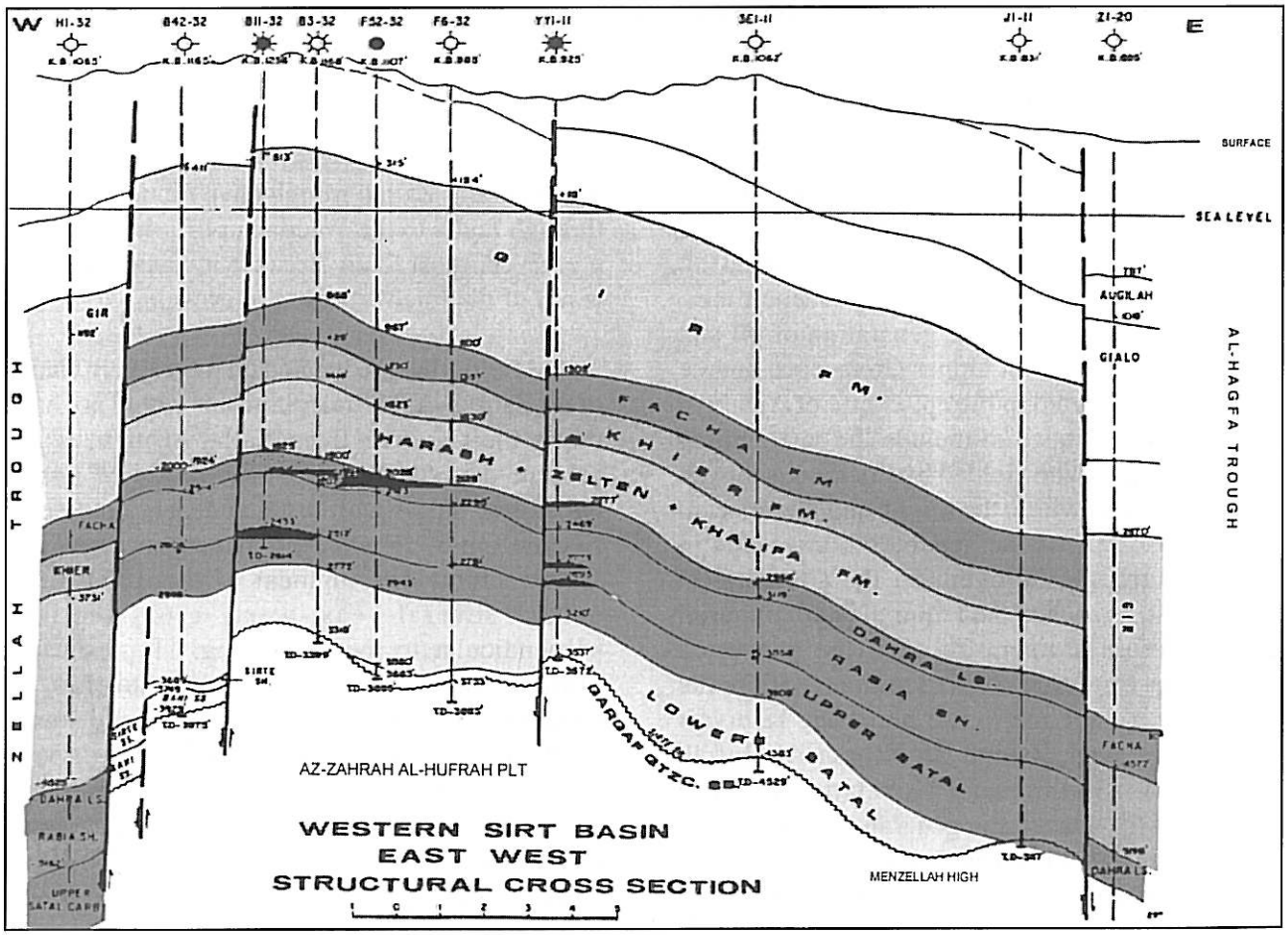
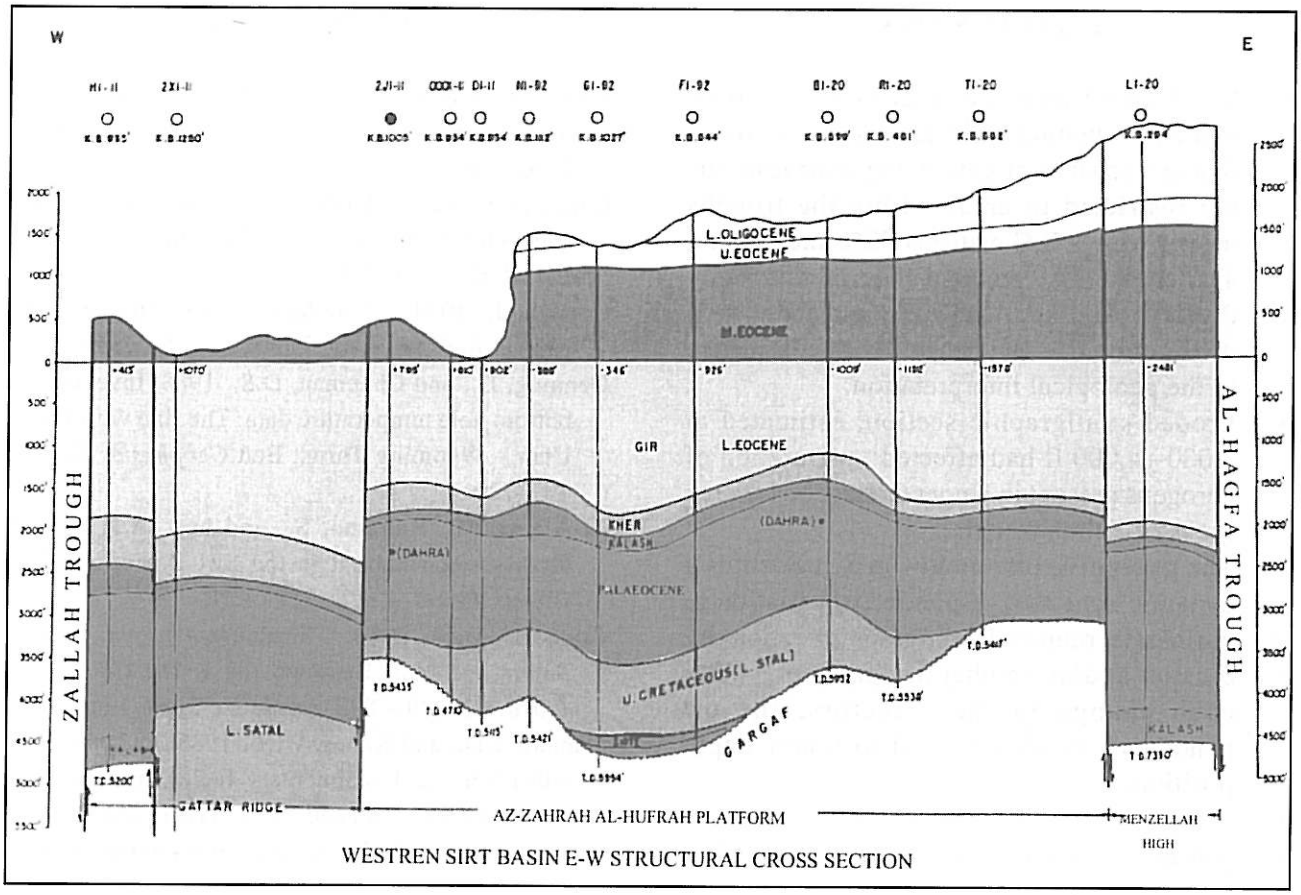
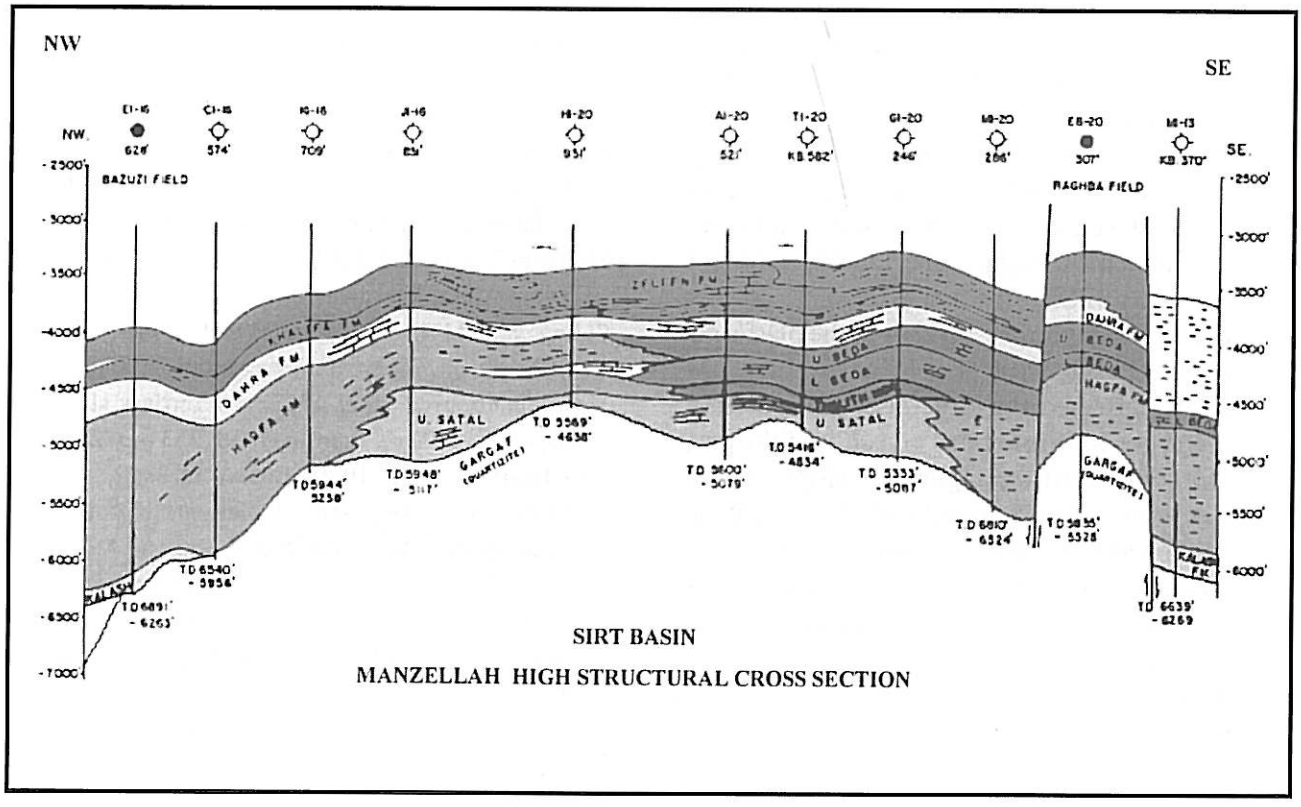


Fig. 10. Western Sirt Basin east –west structural cross – section.



WESTREN SIRT BASIN E-W STRUCTURAL CROSS SECTION

Fig. 11. Western Sirt Basin east – west structural cross section using top of Gir Formation datum line.



SIRT BASIN

MANZELLAH HIGH STRUCTURAL CROSS SECTION

Fig. 12. Northwest –southeast structural cross-section along western Al Hagfa trough (Menzellah ridge).

CONCLUSIONS

- Sirt Basin Upper Cretaceous source rock quality evaluation indicates that source rocks that are capable of generating hydrocarbons are restricted to areas within the troughs proper with T.O.C. values of 2% and greater.
- The geothermal gradient map of this study displays first-hand information about heat distribution that can be used with confidence in the geological interpretation.
- Eroded stratigraphic section, estimated at 3,000– 4,000 ft had affected maturation of kerogens present in Upper Cretaceous source rocks of Zallah trough.
- The generative oil window in Sirt Basin is a dynamic zone that responded to variation in burial rate, removed stratigraphic sections by erosion and/or geothermal gradient. With each change in these factors, the oil generative window moved to a new depth position.
- The initial time of hydrocarbon generation in Sirt Basin Upper Cretaceous is estimated to be late Eocene-Oligocene, and continued as generation stages proceeded to cover the outer flanks of the generating sites of the troughs.
- The northern parts of Al Hagfa, trough probably did not contribute hydrocarbons to the reservoirs of Sirt Basin owing to the lack of proper source rocks in its sediments.
- Hydrocarbon migration was principally through the fault systems that connect matured source beds with the reservoirs present in the troughs proper, and the adjacent platforms of Sirt Basin.
- The regional northeast tilting of the platforms of Sirt Basin since post-Miocene time has greatly affected the structural configuration of the pre-Miocene traps and shifted the pre-Miocene southwest general slope of the platforms to the east-southeast slope, until the structural conditions of present day were reached. Simultaneously, hydrocarbons occupying the pre-Miocene traps responded to the new structural conditions and migrated up-dip westward to accumulate in the newly formed traps.

REFERENCES

Barr, F.T. and Weegar, A.A., 1972. *Stratigraphic Nomenclature of the Sirt Basin, Libya.* Petrol. Explor. Soc. Libya, 179 p.

Conant, L.C., and Goudarzi, G.H., 1967. Stratigraphic and tectonic framework of Libya. *Bull. Am. Assoc. Petrol. Geol.* **61**, 719 – 730.

Connan, J., 1974. Time-temperature relation in oil genesis. *Bull. Am. Assoc. Petrol. Geol.* **58**, 2516–2521.

Denning, D., and Chapman, D.S., 1988. Inversion of bottom hole temperature data: The fine view Field, Utah – Wyoming Thrust Belt.*Geophysics* **53**, (5), 707–720.

El-Alami, M., Rahuma, S., and butt, A.A., 1989. Hydrocarbon habitat in the Sirt Basin, northern Libya. *Petrol. Res.* J. **1**, 17 – 28

Goudarzi, G.H., 1980. Structure – Libya. In M.J. Salem and M.T. Busrewil (eds). *The Geology of Libya*, III, 879 – 892. Academic Press, London.

Gumati, Y.D., and Kanes, W.H., 1985. Early Tertiary subsidence and sedimentary facies, northern Sirt Basin, Libya. *J. Petrol. Geol.* **11**(2) . 205-218.

Lapotin, N.V, 1971. Temperature and geologic time as factors in goalification. *Acad. Nauk SSSR.* **17**, Ser Geol., No. 3, 95 – 106. English translation by N.B. Bostick. *Illinois Geol. Surv.* 1972.

Magara, K., 1976. Thickness of removed sedimentary rocks, pale pore pressure and pale temperature, southwestern part of Western Canada Basin. *Bull. Am. Assoc. Petrol. Geol.* **60**, 554 – 565.

Meissner, F.F., 1978 *Petroleum Geology of the Bakker Formation*, Williston Basin. Williston Basin Symposium. *Montana Geol.* Surv. 207– 227.

Mouzughi, A.J., and Taleb, T. M., 1981. OAPEC 2nd Symposium, Kuwait.

Selley, R.C.M 1968. Facies Profile and other new methods of graphic data presentation, application in quantitative study of Libyan Tertiary shoreline deposits. *J. Sed.. Petrology*, **38**, 353 – 372.

Van Houton, F.B., 1980. Latest Jurassic – Early Cretaceous – regressive facies, northwest Africa creation. *Bull. Am. Assoc. Petrol. Geol.* **64**, 857 – 867.

Waples, D.W., 1980. Time and temperature in petroleum formation application of Laotian's method to petroleum exploration. *Bull. Am. Assoc. Petrol. Geol.* **64**, 916 – 926.

Waples, D.W., 1985. *Geochemistry in Petroleum Exploration.* D. Reidel Publishing Company.

NATIONAL OIL CORPORATION (Reports).

Regional Geochemical Evaluation of Gialo High. Area, East-Central Libya. January 1977.

Regional Geochemical Evaluation of the Eastern Concession 59 and 71 Area, Libya. August 1979.

Regional Geochemical Evaluation of the Western Concession 59 and 71 Area. Libya. January 1979 and May 1979.

Regional Geochemical Evaluation of the Concession 31 Area, Libya September 1980.

Regional Geochemical Evaluation of the Concession 32 Area, Libya. February 1982.

Geochemical Evaluation by Deminix of Libya's Al-NC 107 well. February 1983.

Five-well Regional Geochemical Evaluation of Concessions 65 and 80. March 1984.

Geochemical Evaluation of the Section Below 7,55′ in D1-32. March 1984.

Petroleum Res. J. Vol. 12 (2000); P. 39–46, 10 Figs.

Groundwater Recharge in Jabal al Haruj and Vicinity, Central Libya

M.T. Busrewil*

تغذية المياه الجوفية بجبل الهروج والمناطق المجاورة، وسط ليبيا

المبروك أبوسريويل

تفيد الدراسات الحقلية أن منطقة جبل الهروج تعرضت حديثاً إلى عدة رخات قوية من الأمطار وأن جزءاً منها قد وجد طريقه للخزان الجوفي العلوي، ونظراً لنمو الأعشاب والأشجار ببطون الوديان بالهروج وتواجد بعض الحيوانات الثدية آكلة الحشائش به فإنه بالإمكان القول وبدرجة عالية من الثقة أن منطقة الهروج تلعب دوراً هاماً في تغذية الخزانات العلوية بالمنطقة المجاورة له، إلا أن هذه التغذية لا تكفي بالضرورة لمتطلبات الزراعة المروية على نطاق واسع. كما أن تعرض مناطق غات والسرير وشرقي جبل الحساونة إلى هطول أمطار غزيرة أحياناً، توحي بأن الخزان الجوفي العلوي، لتلك المناطق قد لا يعتبر بالضرورة غير متجدد.

تحوي الهروج أدلة على تساكن الإنسان القديم به ووجود بحيرات قديمة بالمناطق المجاورة له ترجع نشأتها إلى جريان المياه من مرتفعات الهروج إبان تعرض هذه المنطقة وشرقي الصحراء الكبرى إلى مناخ مطير ورطب. كما يعتقد أن الهروج يمثل أحد منابع نهر قديم موجود أثاره بالسرير حالياً، كما يستدل من تواجد صخور البيوميس الموجود حالياً بالسرير أن هذه المنطقة قد عبرها نهر قديم نبع أحد فروعه من جبل تيبيستي المصدر الوحيد لتلك الصخور البركانية.

Abstract: *Field observations suggest that Al Haruj area is subjected recently to periodic heavy showers and parts of the surface water are diverted from surface to underground routes. The presence of herbivores animals and the wide spread of vegetations in wadi beds, is suggestive, with a high degree of confidence, that Al Haruj region is certainly acting as a recharge zone to the local basal aquifer and subsequently to the interconnected aquifers. The present recharge in Al Haruj and adjacent areas will always be essentially smaller than major extraction demand for irrigation purposes. Periodic heavy showers on Ghat Oasis, As Sarir and East Al Hassawinah areas can tentatively suggest that the groundwater of the upper aquifer of these areas cannot be considered as a fossil water.*

The area contains evidence of in-situ prehistoric sites and eviron palaeolakes. It is thought that surface water was formed locally in the surrounding of the present discharge areas, mostly during a time when a more humid climate prevailed all over the Al Haruj, and the East Sahara. The palaeoriver in As Sarir is thought to have been originated mostly from the eastern slopes of Al Haruj. Pumice rock fragments, found in As Sarir area, are taken to indicate that these rock fragments, were associated with discharge areas from Tibisti massif, the source of this type of volcanic rocks.

*Department of Geology, Faculty of Science, University of Al-Fateh, P.O.Box 13258, Tripoli – Libya, G.S.P.L.A.J.

INTRODUCTION

Jabal Al Haruj al Aswad is situated in central Libya. The highest elevation lies approximately 700 m above the surrounding terrain. The catchments consist largely of Tertiary and Quaternary basaltic lava flows. These flows cover an area of approximately 42,500 km^2. Scattered outcrops of Tertiary sediments occur mostly in the southern parts of Al Haruj area. Climatic records and hydrogeological data of the area do not exist (Pallas, 1980) and the palaeoclimatology of al Haruj area has not been studied. The northern and central parts of the area were dealt with by Woller (1984), Vesely (1985) and Busrewill and Swaisi (1993) as part of the programme of regional mapping of Libya.

The winter is typically Saharan: warm in winter (very cold at night with occasional frost, and warm during the day), and hot in summer, with a few gheblis (sand storms). Perennial shrublets are *Rus tripertata, Acacia tortillas* and *Ziziphus lotus*. The annuals (herbs and grasses) provide a ground cover over the pre-existing landscape of lava flows, but barren ground is widespread when the area was cursed by droughts.

RECENT SURFACE DRAINAGE

Drainage developed on lava flow surfaces shows systematic change with increasing flow age. Field and remote sensing data show drainage frequency increases as flows become progressively older. The most common type of drainage pattern in the older lava flows is dendritic. This type of drainage pattern is very well developed on phase two lava flows (Busrewil and Swaisi, 1993). The other type of drainage is the radial drainage pattern. It consists of wadis flowing away from the central area of Al Haruj to the north, east and south directions. The drainage in the more recent lava flows is entirely internal and no system is recognizable. Here, rainfall usually finds its way to underground routes through existing lava ridges (Fig. 1) and joints. The most important drainage channels in the area are Wadis Bu al Hidan, Sayyad, Maayder, al Had, Bil Qaraf, Aj Jidari, al Baqar, Bu Shubayrim, al Mrar, Waddan and al Atheb

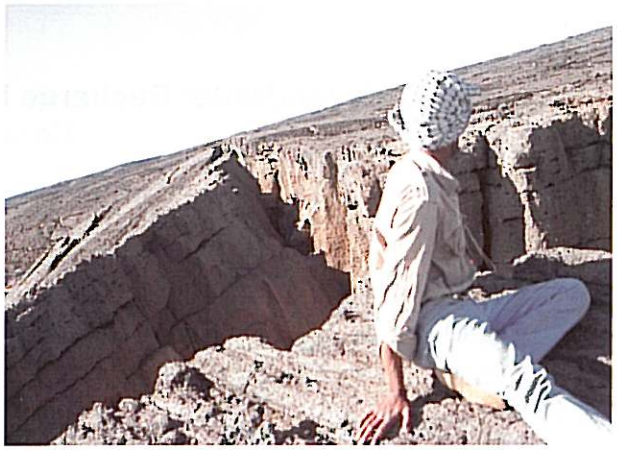


Fig. 1. This photograph, taken in Al Mashaqaq, exhibits a typical lava ridge in phase six lava field, east of Al Fuqaha. Similar features are common in phase five lava flows.

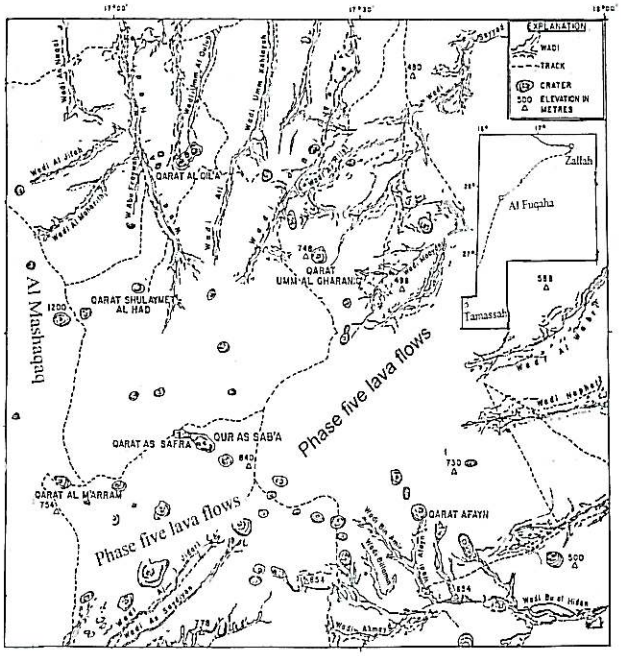


Fig. 2. Drainage pattern in central jabal Al Haruj al Aswad.

(Fig. 2). The present day Sebchas in Tamassah and Hatiyat Meduin in Zallah Oasis may constitute discharge areas.

The arrangement and distribution of the above mentioned wadis suggest that rainfall increases with increasing in elevation from the periphery to the upper Jabal area, decreasing outwards towards low areas. The lack of any prominent drainage system along the west side of Al Haruj is related to topographic relief which might have been related to a basement high and the outpouring of the more recent lava flows.

PALAEODRAINAGE

Interpretation of Landsat images revealed the presence of streams originating at the surface of lava flows on the north, east, south-east and south-western side of Al Haruj. It also points to the existence of margins of possibly huge palaeolakes NE of Tamassah and SE of Waw al Kabir. Traces of the shoreline can still be recognized east of Tamassah (Fig. 3), but sand sheet had obliterated traces of wadi lines in much of the area SE of Waw al Kabir. The presence of ash within the latter

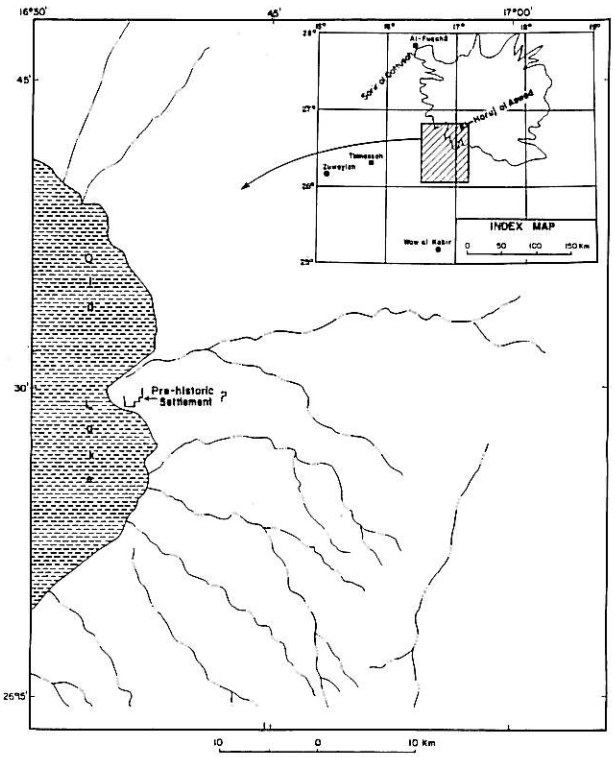


Fig. 3. Landsat interpretation of a margin of a palaeolake SW of Al Haruj (Londsat 5 TH. Band 6, 17 July, 1984).

palaeolake deposits may suggest that Waw an Namus volcano was possibly active during humid periods in late Pleistocene times. The stream at As Sarir (Ahmed, 1978), is thought to have been originated in part from the eastern slopes of Al Haruj during the pluvial time, with the present day Wadi Bu al Hidan and Wadi Bu Shobayrim representing remnants of old drainage tributaries of the streams. The surface expression of the uppermost of the prior streams died out in the sand dunes and part of the ancestral streams appear as discontinuous traces which meander across the plains toward Jalu Oasis. The proof that water courses flowed over east of Al Haruj at As Sarir and the entire length of the Libyan desert from NE Tibisti massif to the north is given by the composition of gravels at As Sarir pipe manufacture for the Great Man-made River Project. In this locality, the old drainage system is totally defunct and can be deduced only from alluvial deposits it left behind.

East of the ancestral stream and at about 3 m higher a spread of quartz pebbles and rock fragments is being quarried for aggregates. Pumice was found among other rock fragments and were interpreted to have been associated with very high discharge from the NE Tibisti massif, the source area of this type of rocks to the present day As Sarir area. The old drainage system from Al Haruj and Tibisti, may form the large scale water courses from mountainous recharge areas in Al Haruj and Tibisti to discharge areas in the Sirt Basin and finally to the Mediterranean Sea (Busrewil, 1993). Silimar conclusion was suggested by Pachur, (1996). The distribution of palaeolakes in the vincinity of Al Haruj may suggest that groundwater was collected locally in these areas during a time when a more humid climate prevailed all over the present area.

FIELD OBSERVATIONS

Meteorological records of Al Haruj *sensu strictu* do not exist. Climatic records of historical periods depend equally on indications of change rather than direct instrumental measurements. Bearing this in mind, field work coupled with intensive enquiries, were carried out for all available unpublished information, pertaining not only to Al Haruj, but also for the surrounding areas, in order to develop the regional distribution of surface waters that might afford better understanding of local conditions. These observations revealed the presence of at least two generations of perennial shrubs.

A large desiccated thorn trees and a subsequent young generation of grown plants. Ponded water in a broad shallow depression (called locally baltas, Fig. 4) was also observed. It may require several weeks or even months for these temporary water ponds to dry (Fig. 5). However, when the water has evaporated a great flat of recent mudcracks can be seen on the floors of these baltas. In addition, straw and/or mud marking the



Fig. 4. Photograph of a ponded water in Al Haruj. Ponded water in broad similar depressions is a common feature in many places of the study area (e.g. Wadi Bu Al Hidan, Qarât Shalesh, Al Badari, Qararat Sayyad ...)



Fig. 5. Photograph of a dry water pond (Grarat Alya, looking NW).

height of water can also be observed along the banks of many depressions (Fig. 6), indicating that such depressions were recently flooded by water. Elongate-shaped, interconnected, large depressions (Qararat) lying within old wadi channels are common (Fig. 7) and represent areas for herds of livestock pastoralism.



Fig. 6. This photograph was taken in the periphery of Al Mashaqaq east of Al Fuqaha. It marks the height of water in that locality.



Fig. 7. Photograph of interconnected large depression lying within Wadi an Naqai, looking north.

Enquiries to accompanist guides revealed that local rainfall, though irregular, is common. Some parts of Al Haruj, however, are either receiving very little or no rain at all in some years. Heavy showers of rain producing runoff are not uncommon. During the period December 1981 to June 1982, the south and south central parts of Al Haruj areas were subjected to three storms. One of these storms lasted for nine hours and caused runoff and hazardous driving conditions (J. Humprey of Brown and Root, London, Pers. Comm.). Widespread sheet-flooding on the plains of northern Jabal as Sawda, central Libya were reported, (Nov. 1989), to have lead to rapid groundwater recharge. Similar flooding occurred in As Sarir in Feb. 1989 (As Sarir Project Authority. Pers. Comm.). Diversion of surface water to underground routes was observed in Qararat Umm ash Shih (27° 21' N 17° 17' E), Qarat Shalesh (27° 48' 20" N 17° 15' 10" E) and al Badari (27° 39' 30" N 17° 46' E). A sinkhole along a wadi bank (Graret Umm Atheilah, 28° 03' 11" N 16° 58' 15" E) in the SW part of Sheet Zallah was visited during the fieldwork (Fig. 8). The



Fig. 8. Photograph of a sinkhole along a Wadi bank (Grarat Umm Atheilah), looking east.

guide (Hag Ruffah) mentioned that this sinkhole and Al Badari are so effective in collecting surface runoff that the water of the wadis are rarely able to cross the sinkholes. Similar sinkholes can be seen NE of Al Haruj (e.g. Al Battah, Fig. 9)

Elders in the surrounding villages retain the memory of an earlier time in which Al Haruj was heavily wooded, possibly until sixty years ago.

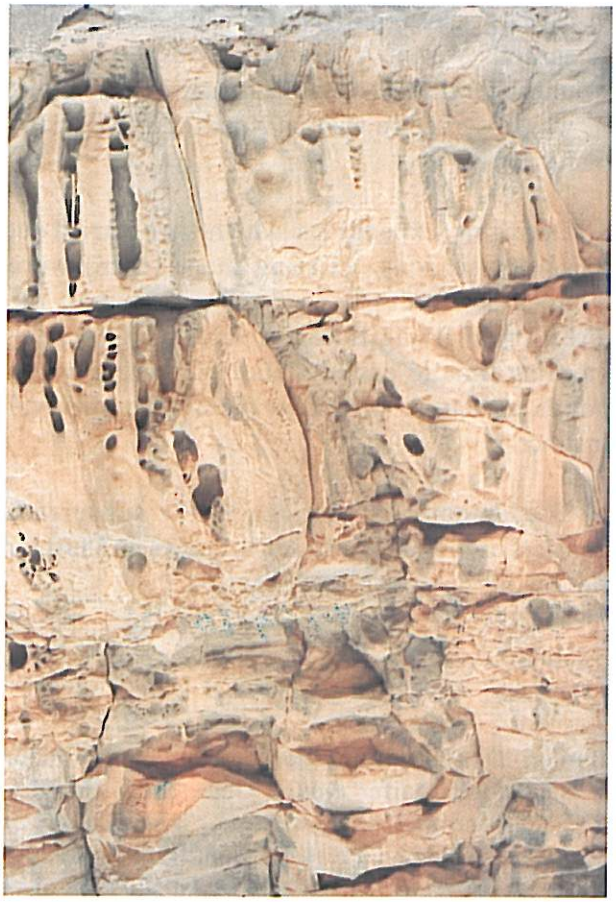


Fig. 9. Side view of the wall of one of few sinkholes along The Zallah – Tazirbu track, NE of Al Haruj. Traces of downfall water seepage (vertical groves) can still be observed and was possibly active during the pluvial time. The guide mentioned that palm trees are growing inside a near-by sinkhole. In all, drainage, around this sink hole today, is total defunct (Hammer, top left, is used for scale).

PREHISTORY SITES

Sites with inscriptions and artifacts left by prehistoric inhabitants of the area were found, including engraved figures and Neolithic stone weapons, (arrow heads). The animals depicted in the engravings are similar to mammals now living south of the Sahara, such as lions, elephants, giraffes, bubales, antelopes (Fig. 10) and deer. There are also some unidentifiable birds. Sites of



Fig. 10. Close-up view of engraved mammal taken in Ghadir ad Duwaylaa, Wadi al Had.

engraving were found in Wadi al Had (Ghadir al Duwaylaa, 27° 50' 67" N – 17° 00' 47" E; Klitzsch, 1968; Busrewil and Swaisi, 1993). Wadi an Naqai (An Naqaa al fawqiyah, 27° 58' N – 16° 57' 30" E) Qarat ar Ruwais (27° N – 17° 43' E) and Ghadir Bu Attusawir (Wadi al Mrar).

The arrow heads are widely distributed over much older and more accessible lavas and can also be found near the water pools and places where wadis broaden out. An ancient habitation site of unknown age was observed a few kilometers south of Waw al Kabir along scarp edges in the range of few hundred metres across. In addition, an ostrich's egg shell was found in a nearby wadi terrace. These observations suggest that climatic conditions allowed palaeolithic bands to roam over most of Al Haruj area and other parts of Libya. Similar occurrences of prehistoric sites have also been described from south-western Libya and northern Tibisti (Ziegert, 2000, and references cited in). The extension in time and space of these cultures over this desert area, cannot yet be concluded from the data available, and is beyond the scope of this work.

DISCUSSION

Research work on the Libyan Sahara during the past three decades by numerous geologists and geographers furnished data that this area had been subjected to heavy rains and witnessed prosperous palaeolakes during the pluvial time (El Ramly, 1980; Pachur and Braun, 1980, 1986; Petit-Maire, *et al.*, 1980). In the meantime, numerous ^{14}C measurements were carried out on carbonates or

organic matter. The ages fall mostly between 5 and 35 ka BP and on the basis of these dates several authors (Pachur, 1980; Pachur and Braun, 1986; Wright, 1986) deduced the occurrence of one or several humid episodes during Late Pleistocene and Holocene times. Similar work suggested that groundwater should be considered as a non-renewable source and should be treated as a fossil water (Burden, 1980; Klitzsch, *et al.*, 1976).

This study, based on field observations and remote sensing data supports previous conclusions that groundwater was formed locally in the surrounding of Al Haruj during a time when more humid climate prevailed all over the present desert. The area contains evidence of *in situ* prehistoric sites and environ palaeolakes. Some dendritic and meandering morphologic pattern, having on the whole, the characteristic of an extinct hydrographic system, was observed east, south-east and south-west of Al Haruj, implying the existence of palaeodrainage.

Meteorological records within Al Haruj are lacking, and striking discrepancies were observed between ^{14}C ages and Th/U ages for several Saharan localities (Szabó *et al.*, 1989; Fontes and Gasse, 1991). Enquiries from local inhabitants and field observations suggest the reconstruction of the climate over the past two hundred years in Al Haruj as follows.

1. A period from the nineteenth century until some time before 1917 in which the area experienced substantial rainfall with respect to the beginning of the present century. Ostriches, now living south in the equator, are thought to have been common in the area during the early time of this century. Remnants of their egg shells were observed west and south of Al Haruj (Kanter, 1967).

2. A marked change toward famine and droughts along the margins of Al Haruj during most of this century. It is characterized by the 1917 famine in Fezzan (Kanter, 1967) and a decrease and impoverishment of flora in surrounding areas. The last of a tame ostrich in Tobga (south of Mizdah) disappeared at the beginning of this century (Kanter, 1967). Within Al Haruj limited rainfall is envisaged, as old and preliminary topographic maps of Zallah and Tamassah (The Italian Geographic Military Institute, (1932-33)) show names and locations of a still existing Thameds, Ghodran (single Ghadir) and Geltas (places of water accumulation and ponding).

3. It is suggested that the area has experienced increased rainfall during the last two decades. This is supported by the presence of almost of a new generation of thorn bushes. Some current recharge via runoff is occurring during rainy seasons within Al Haruj. Evidence of very unusual rainfalls causing damages to livestock was observed in wadi al Atheb (26° 37' N 16° 58' E).

During my expeditions, which were carried out in spring seasons, existing maps (then) were utilized successfully in conjunction with the direction of flying flocks of sand grouse during morning time to explore place of existing water ponds as nature provided them with survival instinct.

The amount of recharge to the subsurface aquifers around Al Haruj is not known and further field work is, therefore, suggested.

REFERENCES

Burdon, D. 1980. Infiltration conditions of a major sandstone aquifer around Ghat, Libya. In M.J. Salem and M.T. Busrewil (eds.). *The Geology of Libya*. Academic Press, London, **II**, 595–609.

Busrewil, M.T., 1993. The role of Jabal Al Haruj al Aswad in groundwater recharge. Geoscientific Research in NE Africa, Berlin.

Busrewil, M.T. & Swasi K.S. 1993. Geological map of Libya, 1:250,000. *Sheet: Al Haruj al Aswad. Explanatory Booklet*, Ind.Res.Cent.Tripoli.

Clarke, J.I. 1960. The Siaan: Patoralists of the jefara. In: S.G. Willimott and J.I. Clarke(eds.). *Field Studies in Libya*. Durham Univ. Dept. of Geogr. Res Pap ser. 4, 52–59.

El Ramly, I.M. 1980. Al Kufra Pleistocene lake – Its evolution and role in present-day land reclamation. In: M. J. Salem and M.T. Busrewil (eds.). *The Geology of Libya*. Academic Press, London, II, 659–670.

Fontes, J,Ch. & Gasse, F. 1991. PALHYDAF (Pahoehydrology in Africa) programme: objectives, methods, major results. *Palaeogeography, Palaeoclimatology, Palaeoecology*, **84**, 191–215.

Kanter, H. 1967. *Libya – Geomedical Monograph Series*, Springler-Verlag Berlin, Heidelberg New York, 163 p.

Klitzsch, E. 1968. Der Basaltvulkanismus des Djebel Haroudj, Osrfezzan, Libyen. *Geol. Rundsch.*, **57**, 585–601.

Klitzsch, E. & Pesce, A. 1966. Remarks about prehistorical sites in southern Libya and Tibisti. In: J.J. Williams (eds.). *South Central Libya and Northern Chad*. Petrol. Explor. Soc. Libya: 8th Annu.Field. Conf.

Klitzsch, E., Sonntag, C., Weistroffer, K. & El Shazly, E.M. 1976. Grunwazzer des Zentralsahara; Fossile Verrate. *Geol. Rundsch.*, **65**, 1, 264–287.

Pachur, H.,J., 1996. Reconstruction of Palaeodrainage systems in Sirt Basin and the area surrounding the Tibisti Mountains: Implications for the hydrological history of the region. In: Salem, M.J.; Mouzughi, A.J. and Hammuda, O.S. (eds). *The Geology of Sirt Basin*, 157–166, Elsevier.

Pachur, H.,J, & Braun, G. 1980. The paleoclimate of the central Sahara, Libya and the Libyan desert. Palaeoecology of Africa and the surrounding islands, 12, 351–363.

Pachur, H,J. & Braun, G. 1986. Drainage systems, lakes and ergs in Eastern Sahara as indicators of Quaternary climatic dynamics. *Berliner geowiss Abh.* (A) **72**, 3–16.

Pallas, P. 1980. Water resources of the Socialist People's Libyan Arab Jamahiriya. In: M.J. Salem and M.T. Busrewil (eds.). *The Geology of Libya*. Academic Press, London, II. 539–594.

Petit-Maire, N., L. Casta, G. Delibrias & Ch. Gaven, 1980. Preliminary data on Quaternary Palaeolacustrine depostis in Wadi ash Shati area, Libya. In: M.J. Salem and M.T. Busrewil (eds.). *The Geology of Libya*. Academic Press, London, III, 797–808.

Szabó, B.J., Mchugh, W.P. Schaber, G.G. Hayner, C.V. Jr. & Breed, C.S. 1989. Uranium series dated authigenic carbonates and acheulian sites in southern Egypt. *Science*, **243**, 1053–1056.

Vesely, J. 1985. Geological map of Libya 1:250.000. *Sheet: Zallah NH 33–16. Explanatory Booklet.* Ind Res. Cent., Tripoli, 125 p.

Woller, F. 1984. Geological map of Libya 1:250.000. *Sheet: Al Fuqaha NG 33–3. Explanatory Booklet.* Ind Res. Cent., Tripoli, 123 p.

Wright, E.P. 1986. Review of the hydrogeology of the Kufra Basin, North Africa. *Berliner geowiss Abh.*, (A) **72**, 76–86.

Ziegert, H., 2000. Prehistoric environments and settlements in eastern Fezzan. In Klitzsch, E. and Ziegert, H., *Short Notes and Guidebook on the Geology of the Dar el Gussa-Jabal Bin Ghanimah Area.*, 39-52. Earth Sc., Soc., Libya

Petroleum Res. J. Vol. 12 (2000); P. 47–56, 4 Figs.

The Effect of Hydrogen, some Hydrocarbons, Carbon monoxide and Sulphur Treatments on the Structure of Platinum Supported Catalysts

Ezziddin A. Arafa*

تأثير المعالجة بالهيدروجين وبعض الهيدروكربونات وأول أكسيد الكربون والكبريت على حفازات البلاتين المدعم

عز الدين أحمد عرفة

تم استخدام تقنيات الإختزال الحراري المبرمج والتقفي بالأثر الأشعاعي والمجهر الألكتروني في دراسة تأثير معالجة عدد من حفازات البلاتين المدعم على السيليكا (Pt/SiO_2) والألومينا ($Pt/A|_2O_3$) بالمواد: الهيدروجين (H_2) والايثين (C_2H_2) وأول أكسيد الكربون (CO) والكبريت (S).

نتائج الاختزال الحراري المبرمج بينت أن معالجة هذه الحفازات بالهيدروجين عند درجات حرارة تصل إلى 4K± 773 ليس لها أي تأثير على الشكل الخارجي لهذه الحفازات وكذلك على انتقائيتها في هدرجنة الإيثين والبيوتاديين.

إمتزاز المواد المستخدمة في المعالجة يتم على مرحلتين متتاليتين، أولية على ذرات البلاتين وثانوية على مواقع تم تشكيلها على اسطح الحفازات كنتيجة للامتزاز الأولي وهذه المسؤولة على تفاعلات هدرجنة الإيثين والبيوتاديين.

سبب امتزاز الكبريت وهدرجنة الإيثين تغييراً طفيفاً للشكل الخارجي للحفازات المدعمة على السيليكا بينما لم يؤثر في إنتقائية نواتج الهدرجنة.

المواقع الحامضية المتواجدة على سطح الألومينا استقطبت تكون خيوط كربونية على الحفازات المدعمة على الألومينا.

بصفة عامة، جميع الحفازات التي تم دراستها بينت نفس الخواص من حيث امتزاز المواد المستخدمة في المعالجة وثباتها وانتقائيتها في تفاعلات هدرجنة الايثين والبيوتاديين لتؤكد بأن هذه التفاعلات غير حساسة لشكل الحفازات.

Abstract: *The effect of various treatments such as, hydrogen, hydrocarbon, carbon monoxide and sulphur adsorption on the structure of supported platinum catalysts and upon the selectivities of ethyne and buta-1,3-diene hydrogenations were studied, using temperature programmed reduction (TPR), radiotracer and electron microscopy techniques. The TPR results show that hydrogen treatment at temperatures up to 773 K ±4K have no effect upon the selectivity and morphology of the studied Pt-catalysts. The adsorption of these materials on the studied catalysts surfaces occur in two stages, as primary and secondary processes. Catalytic hydrogenation is associated with the sites of the secondary process. Ethyne*

* Tajoura Nuclear Research Centre, P. O. Box 30878, Tajoura, Libya.

hydrogenation and sulphur adsorption resulted in some morphological changes to the Pt-particles of the silica-supported catalyst (Europt-1), though such changes have no influence on the selectivity. The acidic sites of the alumina-support induced carbon filament formation on Europt-3 catalyst. Generally, the examined catalysts displayed similar behaviour and low selectivities towards ethyne and buta-1,3-diene hydrogenations demonstrating that such reactions are insensitive to catalysts morphology.

INTRODUCTION

Supported catalysts are frequently found to exhibit activities and selectivities which depend on catalyst preparation and pretreatment conditions. This behavior could have many causes including variation of particle size[1], metal interaction with the support[2] and the existence of poisoning molecules such as carbon and sulphur[3].

This work is undertaken with the aim to look at the effects of hydrogen activation, adsorbed hydrocarbons, hydrogenation reactions and sulphur poisoning on the reactivity and morphology of platinum catalysts supported on various materials using different preparation methods.

EXPERIMENTAL

Apparatus

The apparatus which was used for the deactivation of the catalysts with adsorbed hydrocarbons, reaction mixtures or sulphur adsorption, consisted of a conventional vacuum system, maintained at a pressure of ~ 0.01 pa by means of a mercury diffusion pump backed by an oil rotary pump. The system incorporated a number of glass bulbs for the storage of the required gases and a reaction vessel similar to that described previously[8,12,13].

Materials and Catalysts

All chemicals used were of analytical purity grade and were used without any further treatment.

Three catalysts of platinum supported on silica (Cab-O-Sil), μ-alumina (Dequsa Ltd.) and molybdenum trioxide (Koch-Light Ltd.) of 99.9% purity, were prepared by the impregnation method by adding the aqueous solution of the metal chloride (H_2PtCl_{16}) containing the required weight of the metal, to an aqueous suspension of the support. The excess water was evaporated using a rotary evaporator and the materials were then dried in an air oven at 423 K. These catalysts were characterized as (w/w), 0.8% Pt/SiO_2, 0.8% Pt/Al_2O_3 and 0.5% Pt/MoO_3. Another two supported catalysts designed by the Council of Europe Catalysis group as standard reference catalysts namely, Europt-1 (6% (w/w) Pt/SiO_2) prepared by Johnson Matthey Chemicals, plc., by an ion exchange method of $Pt(NH_3)_4Cl_2$ solution on Sorbosil grade AQ U30 silica gel. The mixture was filtered and the silica material was washed with demineralised water and dried in circulating-air oven at 378 K[4]. Europt-3 (0.3% (w/w) Pt/Al_2O_3-0.82% Cl) which is prepared by alumina (Al_2O_3 CK 300, from Cyanamid Ketjen, Amsterdam) impregnation with an aqueous solution of H_2PtCl_6-HCl. This catalyst is currently being employed as a commercial industrial catalyst under the code KETJEN-CK303[5].

Experimental Procedures

For catalysts reduction typically 0.1g catalyst was placed in the boat of the reaction vessel which was controlled via a 4 mm three-way stopcock to the vacuum system. The vessel was evacuated for ~ 30 minutes, isolated from the vacuum system via the 4 mm tap and the catalyst boat was moved by the aid of a magnet to furnace part of the vessel. H_2 gas stream (flow rate = 30 ml min-1) was introduced on the catalyst and gradually heated to 523 K. After 2 hours the catalyst was evacuated for 30 minutes at 523 K and then cooled in vacuo to room temperature (293±2K).

Deactivation of the catalysts by reaction mixtures was performed by carrying a number of reactions in a static system at room temerature using 6.67 Kpa either of the reaction mixture (3:1, H_2:ethyne) or (3:1, H_2:1,3-butadiene). Deactivation by hydrocarbons or sulphur was carried out by pulsing the catalysts with ~ 2 Kpa of the respected hydrocarbon or hydrogen sulphide. These treatments were followed by

evacuation of the reaction vessel for 30 minutes to remove gas phase materials.

In the temperature programmed reduction (TPR) experiments, using a set-up similar to that developed by McNicol *et al.*[7], the catalyst was contained in a Pyrex glass cell and then flushed with a stream of helium gas at a flow rate of 30 ml min^{-1} to remove the physically adsorbed impurities. The gas stream over the sample was then changed to 6% H_2N_2 (flow rate, 30 ml min^{-1}) and the sample temperature ramped at a linear rate of 10 K min^{-1} up to 773 K, with the hydrogen concentration in the effluent gas stream being recorded as a function of sample temperature.

Samples of catalysts pre-deactivated by hydrocarbon adsorption, hydrogenation reactions or sulphur adsorption, were examined by Transmission and Scanning Electron Microscopy (TEM) and (SEM) respectively, to investigate the effects of these processes on the catalyst's morphology. The TEM employed was a JEOL 1200 EX, operated at accelerating voltage of 120 kV and ground catalyst samples were added to H_2O and mounted onto standard 3 mm copper grids, covered with carbon films and then fired. When the catalysts were investigated by SEM (Philips EM420), they were embedded in methylmethacrylate-butyl methacrylate mixture, followed by an ultra thin sectioning using a diamond knife.

RESULTS AND DISCUSSION

Adsorption of Hydrocarbons, Carbon Monoxide and Hydrogen Sulphide

Using the ^{14}C-radiotracer technique the adsorption of ^{14}C-ethyne on these catalysts was studied on freshly reduced catalysts. As shown in figure 1, with the exception of the 0.5%Pt/MoO_3 catalyst, the adsorption of ethyne on Europt-catalysts, Pt/SiO_2 and Pt/Al_2O_3 catalysts occurred in two stages, a non-linear "primary" process followed by a linear "secondary" process. This is in agreement with the results reported on supported Rh, Pd, Ir and Ni catalysts[8], in which the primary adsorption process was suggested for ethyne adsorption on metal sites, whereas the secondary adsorption process was ascribed to ethyne adsorption on the adlayer formed as a

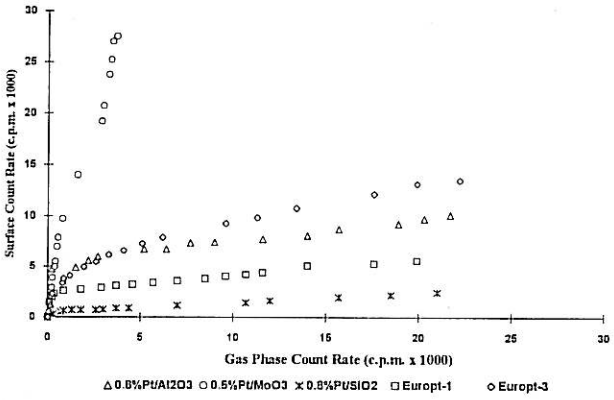


Fig. 1. Adsorption of ^{14}C-ethyne on Pt-catalysts at 293±2K.

result of surface restructuring. The extent of ethyne adsorption on 0.5%Pt/MoO_3 catalyst showed distinctly different behavior: a steep primary region followed by a non-linear secondary region with a sharp slope rising rapidly as the pressure of ^{14}C-ethyne was increased. Even though no specific studies using MoO_3 supported-Pt catalysts have been reported, it is worthwhile considering the possibilities involved in ethyne adsorption on this catalyst. Yashu *et al.*[9] studied the difference in surface properties between Pt/MoO_3/SiO_2 catalysts prepared by different

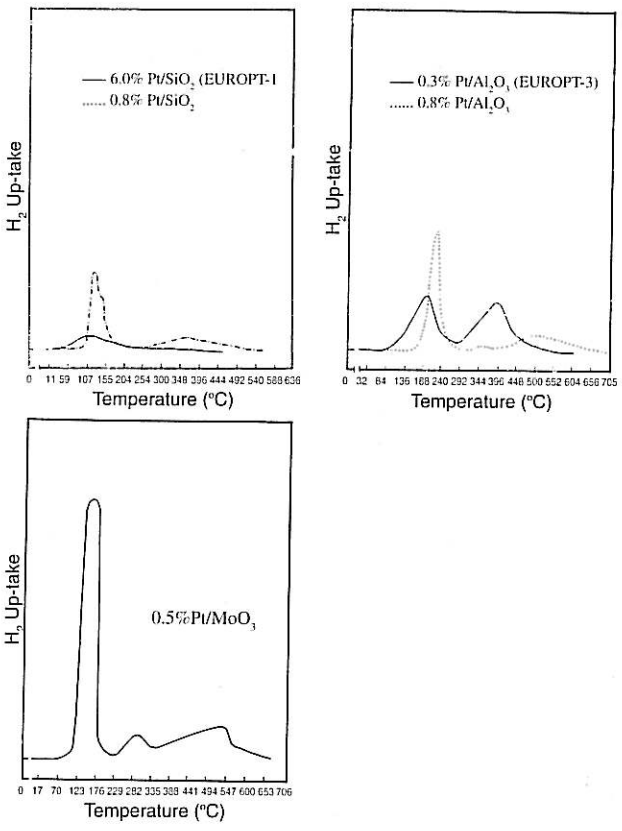


Fig. 2. TPR profiles of Pt-catalysts.

methods. Their results using TPR, electron spin resonance, ESR, and TEM techniques showed that the impregnated catalysts consisted of mixed oxygenated Pt-particles, various molybdenum oxides and a Pt-Mo alloy. The TPR measurements conducted in this work (Fig. 2) showed that, on this catalyst, a large peak appeared at ~ 417 K, accompanied by two broad peaks at 576 and 820 K. It is likely that the low temperature peak corresponds to the reduction of the precursor $H_2(PtC1_6)$ as reported by McNicol *et al.*[7] and the high temperature peak may be assigned to the reduction of the molybdenum oxide species [10]. Thus, it is plausible that the primary adsorption process corresponds to the adsorption of ethyne on the Pt-component and that, the secondary adsorption process is attributable to adsorption on the molybdenum oxide support. No plateau region was observed on these catalysts although gas pressures in excess of 0.67 Kpa were used.

Table 1 shows the effects of evacuation and molecular exchange on ^{14}C-ethyne adsorbed species. Approximately 21-46% of the adsorbed ethyne was removed by evacuation for 30 minutes, with further *ca.* 18% on Europt-1, 3.6% on Europt-3, 5.6% on Pt/MoO_3, 4.0% on Pt/SiO_2 and 3.9% on $Pt/A1_2O_3$ being displaced by $^{12}C\text{-}C_2H_2$ with about 2.0-10.0% of the adsorbed hydrocarbon species being removed by treatment with hydrogen. It is interesting to note that a large fraction, ca. 54.5% on Europt-1, 39.7% on Europt-3, 63.6% on Pt/MoO_3, 54.4% on Pt/SiO_2 and 56.5% on Pt/Al_2O_3 of the adsorbed ethyne was retained by the catalysts as strongly bound species. These observations suggest that the adsorbed species in the secondary adsorption region are reactive, which is in accordance with the conclusions of Webb and co-workers[8,11] made on ethyne adsorption on various Group IIIV supported catalysts, that these species are associatively adsorbed on the surface and represent the catalyticaly active species in the hydrogenation reactions.

Adsorption of ^{14}CO on freshly reduced 0.8% Pt/SiO_2 and 0.8% $Pt/A1_2O_3$ showed isotherms similar to those reported on Europt-1 and Europt-3[12,13]. They showed a primary adsorption region followed by a secondary region which displayed a progressively increasing ^{14}CO uptake as the gas pressure was increased. No plateau region was observed up to a pressure of 0.67 Kpa. ^{14}CO adsorption on 0.5% Pt/MoO_3 showed a Langmuir-type isotherm, i.e. the surface count rate increased slowly as the pressure of ^{14}CO was increased until a saturation plateau was reached. Evacuation of these catalysts for 30 minutes resulted in the removal of ca. 47.4% (Pt/SiO_2), 26.4% ($Pt/A1_2O_3$) and 68% (Pt/MoO_3) of the adsorbed CO species compared with the removable 2.5% (Europt-1)[12] and 23.1% (Europt-3)[13]. Subsequent treatments of these catalysts with 0.67 Kpa 12CO for 15 hours displaced approximately 1% (Pt/MoO_3), 90% (Pt/SiO_2) and 84% ($Pt/A1_2O_3$) of the species which could not be removed by evacuation. Collectively, these results provide an evidence that on these catalysts, adsorbed CO exists in two states. One is weakly bound and can be removed by evacuation or molecular exchange with ^{12}CO. The other form of CO (~15-30%) is more strongly bound to the surface and could not be removed with such treatments from either catalyst.

Table 1. The effects of evacuation and molecular exchange on ^{14}C-ethyne adsorption species at 293±2K

Catalyst / treatment	Catalyst / treatment (counts min-1)	Total change (%)
Europt-1 = 0.080 g	5560*	-
(A)	4381	-21.2
(B)	3336	-40.0
(A')	3280	-41.0
(C)	3030	-45.5
Europt-3 = 0.268 g	9950*	-
(A)	5293	-46.8
(B)	4935	-50.4
(A')	4900	-50.7
(C)	3950	-60.3
$Pt/Mo0_3$ = 3.710 g	28157*	-
(A)	19907	-29.3
(B)	18330	-34.9
(A')	18290	-35.0
(C)	17920	-36.4
Pt/SiO_2 = 2.050 g	2513*	-
(A)	1633	-35.0
(B)	1532	-39.0
(A')	1480	-41.1
(C)	1368	-45.6
$Pt/A1_2O_3$ = 3.710 g	10300*	-
(A)	6488	-37.0
(B)	6084	-40.9
(A')	6010	-41.6
(C)	5815	43.5

*Count rates on freshly reduced catalysts; (A) evacuation of adsorbed ^{14}C-ethyne (0.67 Kpa) on freshly reduced catalyst for 30 minutes; (B) treatment of (A) with 0.67 Kpa ^{12}C-ethyne for 15 hours; (A') evacuation for 30 minutes; (C) treatment of (A') with 13.3 Kpa H_2 for 15 hours.

Table 2, compares the number of adsorbed CO, C_2H_2 and C_2H_4 molecules and the effect of adsorbed hydrogen sulphide on the studied catalysts under identical conditions. Although the radiotracer technique does not permit an absolute comparision of the amounts of CO adsorbed on the different catalysts used, nevertheless, it is possible to draw some comparisions regarding the relative number of adsorbed CO molecules and the CO:Pt ratios. From the results of Table 2, the ratio of the number of CO molecules adsorbed on the freshly reduced catalysts to the total number of Pt atoms present, CO:Pt, was *ca.* 1.9 (Europt-1), 4.0 (Europt-3), 0.60 (0.8% Pt/SiO_2), 1.3 (0.8% Pt/Al_2O_3) and 0.3 (0.5% Pt/MoO_3). These values are higher than the reported ratios of 0.60 with Europt-1[4] and of 0.20 for Pt/Al_2O_3 and 0.07 for Pt/SiO_2 reported by Bain *et al.*[16]. From these values, it is clear there is an overall excess uptake of CO compared with that expected for a Pt:CO ratio of unity. Three possible reasons for this can be considered: (i) spillover or adsorption of carbon monoxide on the support; (ii) an enhanced adsorption of CO in the presence of hydrogen or other species, such as, oxygen, and (iii) a surface reconstruction as the CO adsorption reaches a semi-saturation.

The effect of spillover or adsorption of CO molecules on to the support is unlikely, as has been reported by Kinnaird *et al.*[14] and as claimed by Levy and Boudart[15], such a phenomenon requires suitable sites on the support.

In studies of co-adsorption of H_2 and CO on Pd and Pt[16,17] a considerable interaction between the two molecules has been observed to occur, resulting in a shift of the C-O stretching frequencies to higher regions. It has also been reported[18] that Pt-supported catalysts retain considerable quantities of hydrogen which can act as a promotor for carbon monoxide decomposition. However, with regard to Europt-1, it has been shown[4] that this catalyst exists in a hydrogen-deficient state under the experimental conditions used in this work and hence such a possibilty can be eliminated. Even though Europt-1 is of a Pt-O character, rather than as a metallic Pt, the possibility of interaction of CO with oxygen has been investigated[4] and found to have no effect on the Infrared (IR) spectra of adsorbed CO.

The other explanation of the high uptake of CO could be as a result of perturbation of the metal atoms leading to surface reconstruction, probably through migration of the metal atoms in the CO-adlayer. This, indeed, could be the case, since, as observed in this work, (Table 2) pre-adsorption of sulphur appears to reduce the amount of CO adsorption to give Pt:CO of ~ 1.0. This may be due to the fact that the presence of sulphur stabilises the metal surface to any restructuring similar to that suggested above under the influence of CO alone.

The results of Table 2, also shows that the relative amounts of adsorbed CO and those of C_2H_2 and C_2H_4 are in the approximate ratios, CO:C_2H_2, 1.0:1.0 (Europt-1), 1.5:1.0 (Europt-3), 15:1.0 (0.8% Pt/SiO_2), 4.7:1.0 (0.8% Pt/Al_2O_3) and 0.6:1.0 (0.5% Pt/MoO^3) with

Table 2. The number of adsorbed CO,C_2H_2 and C_2H_4 molecules on clean and sulphur poisoned Pt-catalysts at 293±2K

Catalyst	H_2S	CO molecules x10^{20}g-1	C_2H_2 molecules x 10^{20}g-1	C_2H_4 molecules x 10^{20}g-1	Condition
Uropt-1	0.00	3.50	3.98	0.49	F
	0.00	0.70	0.40	0.07	S
	0.10	–	1.64	–	P
	0.13	–	0.66	–	P
	0.20	–	–	080	P
	0.28	4.45	–	–	P
	0.32	–	–	0.49	P
	0.40	3.20	–	–	P
	0.46	–	–	0.37	P
	0.54	2.10	–	0.71	P
	0.60	–	1.11	0.98	P
Europt-3	0.00	0.36	0.25	0.05	F
	0.00	0.06	0.04	0.01	S
	0.25	0.00	0.00	0.00	P
0.8%Pt/SiO_2	0.00	0.15	0.01	–	F
0.8%Pt/Al_2O_3	0.00	0.33	0.07	–	F
0.5%Pt/MoO_3	0.00	0.05	0.09	–	F

F=freshly reduced; S=steady state (C_2H_2/H_2-deactivated), P=sulphur poisoned; – =not derermined.

the CO:C_2H_4 ratio being 1.8:1.0 (Europt-1) and 7.1 (Europt-3). These ratios suggest that the primary adsorption region of these hydrocarbons (Fig. 1) occur directly on the metal surfaces and the turning point observed in the adsorption isotherms corresponds to monolayer coverage.

The effect of sulphur poisoning on the adsorption of hydrocarbons and carbon monoxide and on the selectivity of mono-olefin formation from ethyne and buta-1,3-diene hydrogenation has been investigated[19,22] and the results were interpreted in terms of a site blocking mechanism.

Hydrogenation Reactions

The reaction of ethyne with hydrogen has been used as a test reaction to compare the activities and selectivity of these catalysts. The selectivity of Europt-1 and Europt-3 to yield ethene as opposed to ethane has been found to be equal to 0.3 and 0.6 respectively[12,13]. The observed initial selectivity on 0.8%Pt/SiO_2 and 0.8%Pt/$A1_2O_3$ were found to be 0.85 and 0.40 respectively. No appreciable reaction between ethyne and hydrogen was observed to occur on the 0.5% Pt/MoO_3 catalyst, only traces of unmeasurable amounts of ethene and ethane were detected.

It was decided to perform a series of buta-1,3-diene hydrogenation reaction on Europt-1 and Europt-3 with the aim to compare their reactivity and selectivity behaviur with those observed in ethyne hydrogenation. The kinetic and product distribution results are reported elsewhere[19] and the initial selectivity for both catalysts was found to be 0.6. The kinetics and product distribution results of ethyne and buta-1,3-diene hydrogenations on 0.8% Pt/SiO_2 and 0.8% Pt/$A1_2O_3$ catalysts showed similar characteristics to those of Europt-1 and Europt-3[12,13,19] which indicated that the major route to paraffin formation is via a route involving the direct hydrogenation of di-unsaturated hydrocarbons rather than via mono-olefin as an intermediate. The results of TPR indicate that sintering of the Pt-particles is likely to be the cause of the inertness of the (0.5% Pt/MoO_3) catalyst for ethyne hydrogenation.

Temperature Programmed Reduction

Samples from the catalysts used in the present work were subjected to TPR investigation to look at the extent of their reduction. The TPR spectra of these catalysts are shown in figure 2. H_2-consumption by Europt-1 was observed to start at room temperature 293±2K with the TPR spectra showing a broad band with its maximal at 383 K. This is in accordance with the findings of Bond and Gelsthorpe[20] who reported a reduction temperature between 200 and 423 K for this catalyst. Similar H_2 uptake behavior was observed with Europt-3, it displayed two large peaks with their maximal at 465 and 668 K. The TPR profiles of the impregnated catalysts, (0.5% Pt/MoO_3), (0.8% Pt/SiO_2) and (0.8% Pt/$A1_2O_3$) showed intense single peaks in the low temperature region, with their maximal at 417, 458 and 487 K respectively, together with broad bands at the high temperature region 573-823 K. The 417 K peak of the (Pt/MoO_3) catalyst is an indication that this catalyst is likely to exist in the form of the bulk $H_2(PtC_{16})$[7]. The high temperature bands at < 573 K are characteristic of the reduction of support materials[1,2,7]. The consumption of H_2 over Europt-1 at ambient temperature and the appearance of a reduction peak at 383 K is characteristic of PtO_2[20]. This is consistent with the results of extended X-ray absorption fine structure (EXAFS), which indicated that Europt-1 contains a disordered platinum oxide phase[4]. The other catalysts (Europt-3, 0.8% Pt/SiO_2 and Pt/$A1_2O_3$) showed main reduction peaks at ~ 473 K representative of an interaction between the Pt-particle and the supports.

Electron Microscopy Profiles

Samples of Europt-1 and Europt-3 have been chosen as model catalysts and were investigated by TEM and SEM to examine the platinum particle size and distribution and the effect of hydrocarbon and sulphur adsorptions and hydrogenation reactions on the catalysts morphology. The Pt-containing particles were imaged on the micrographs as small dark spherical or semi-spherical spots. Ten measurements of ten counts each were used to estimate the average Pt-particle size.

Figure 3 (a-d) shows the TEM micrographs of Europt-1. Plate a is a typical micrograph of the catalyst after it had been reduced in H_2 at 523 K for 2 h. From this it can be seen that the Pt-particles

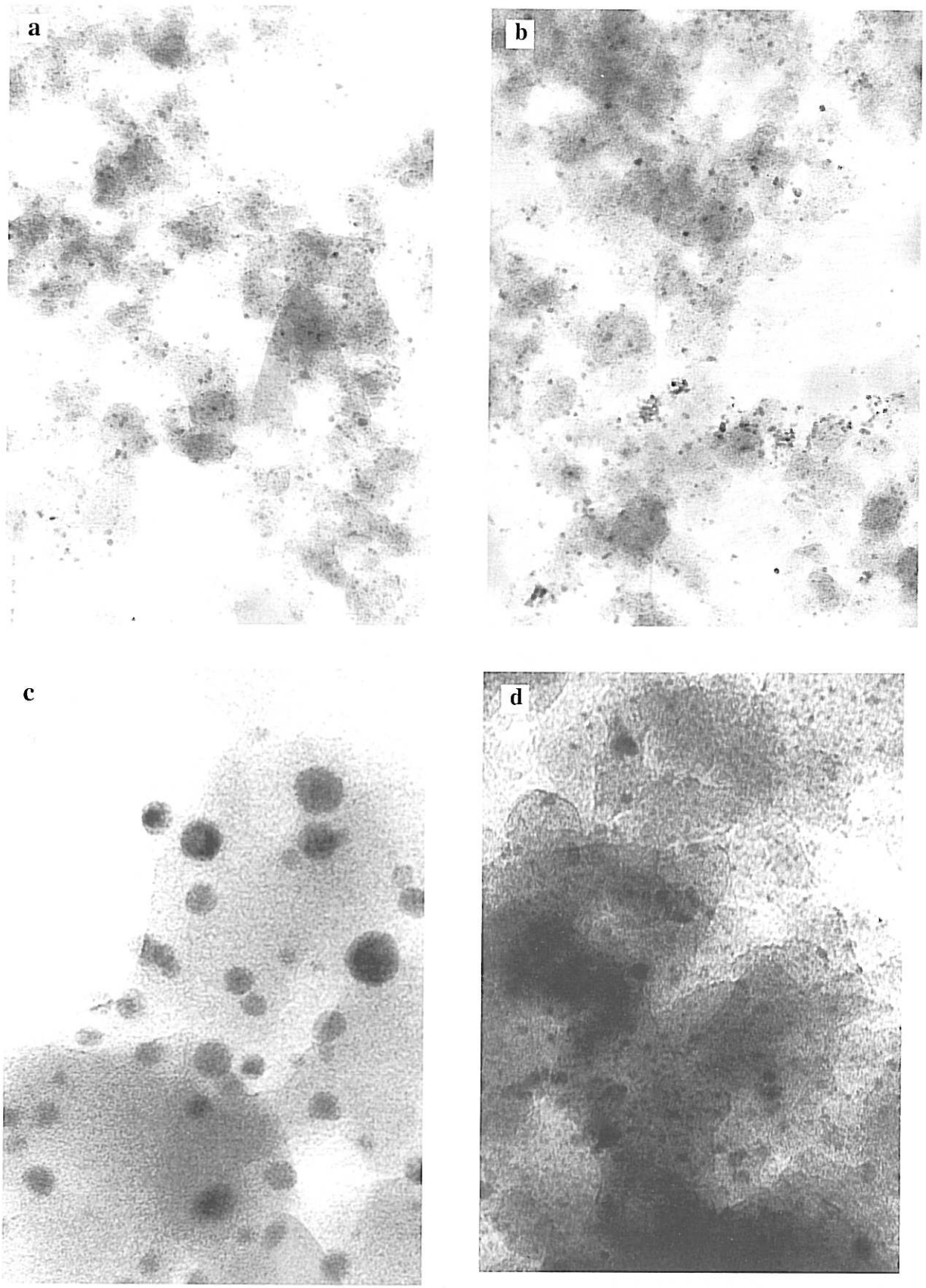


Fig. 3: (a) TEM micrograph of Europt-1 reduced at 523±3K/H_2/2h(x100K);
(b) TEM micrograph of Europt-1 deactivated with C_2H_2/H2 at 293±2K (x100K);
(c) TEM micrograph of Europt-1 deactivated with C_4H_6/H2 at 293±2K (x200K);
(d) TEM micrograph of europt-1 deactivated with H_2S at 293±2K (x200K).

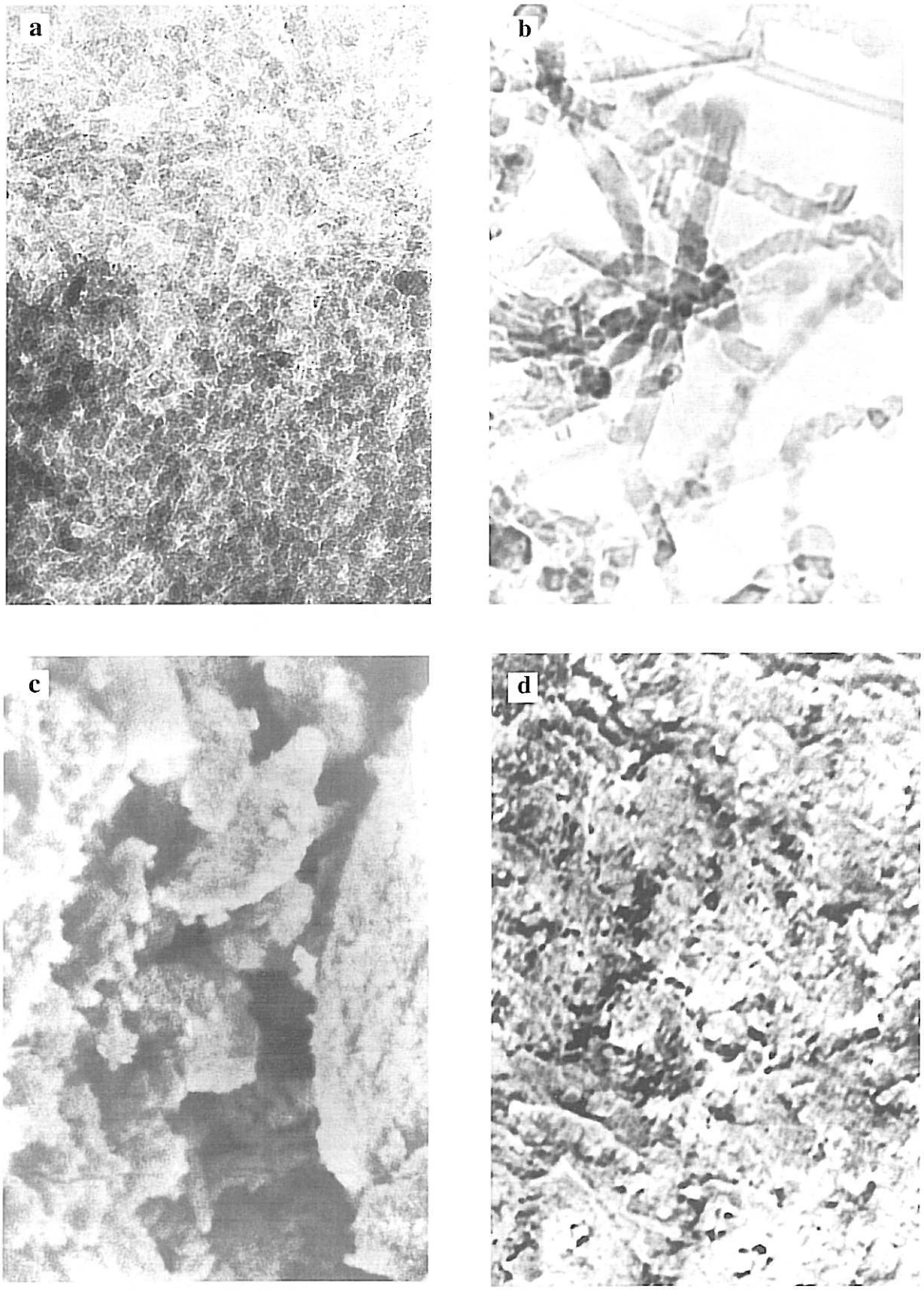


Fig. 4. (a) TEM micrograph of Europt-3 reduced at 523±3K/H_2/2h (x320K);
(b) TEM micrograph of Europt-3 deactivated with C_2H_2/H_2 at 293±2K (x120K);
(c) SEM micrograph of Europt-1 (x320K);
(d) SEM micrograph of Europt-3 (x640).

are homogeneously dispersed, though, in some micrographs, fractions of the Pt-particles are clustered together in the form of aggregates. The particles sizes were calculated as 2.00 ± 0.06 nm, which is consistent with the size range 0.9-3.5 nm, reported by the Council of Europe Catalysis Group[4]. Plate b is the TEM of the catalyst after being employed for ethyne hydrogenation. It showed a similar particle size distribution to that of freshly reduced catalyst (~2 nm), indicating that the catalyst is resistant to sintering under the experimental conditions used in this study. However, when Europt-1 was used for buta-1,3-diene hydrogenation a growth to the particle size ranging between 2 and 10 nm was induced. Furthermore, these particles displayed different shapes, vis, spheres, hemi-spheres, squares and hexagons (plate c). It is possible that buta-1,3-diene and/or the products, butanes, in the presence of hydrogen created a carbon induced faceting to the Pt-particles, similar to that reported to occur with $Pt/A1_2O_3$ catalysts in the presence of various hydrocarbons at elevated temperatures[3,21]. The samples of Europt-1, which were poisoned with H_2S, showed a slight growth in the average particle size from 2.0 to 2.5 nm (plate d). This demonstrates the remarkable stability of Europt-1, even under treatment with sulphur, which is known to severely disturb the morphology of the metal particles[3].

The SEM micrographs of the catalyst (Fig. 4, plate c) show the granular morphology of the silica support. No carbon filaments were observed in these or other micrographs of the catalyst in its working condition.

Europt-3 also showed an even distribution of Pt-particles after the catalyst had been reduced in H_2 at 523 K for 2 h as determined by the TEM. Its particle size was between 3 and 6 nm (Fig. 4, plate a). Interestingly, catalyst samples which had been deactivated by a series of ethyne hydrogenation, displayed carbon filaments in the micrograph (Fig. 4, plate b). Although the mechanism of carbon-filament formation is not well documented in the literature, it is possible that the chlorinated sites located on the alumina of Europt-3 acted as a promoter for carbon deposition on the support, which in turn diffused progressively to the Pt-particles, forming such carbon tubes.

The SEM micrograph of Europt-3 catalyst, which had been deactivated to the steady state activity by C_2H_2/H_2 mixtures, is shown in (Fig.4, plate d). From this it can be seen that the morphological texture of the alumina of Europt-3 is much softer and more amorphous than the silica of Europt-1.

CONCLUSIONS

The results obtained showed that the adsorption of hydrocarbons, carbon monoxide and sulphur takes place primarily on the exposed metal atoms and secondarily on the metal adlayer to the primary adsorbed species formed as a result of a surface restructuring. The adlayer contains the catalytical centers for hydrogenation reactions. Platinum catalysts supported on silica or alumina and prepared by different methods showed almost similar and low selectivity for ethyne and buta-1.3-diene hydrogenations.

The TPR profiles indicate that treatment of the studied catalysts with hydrogen and heat (up to 773K) has no effect on the catalyst morphology and the observed metal support interaction under such treatment has no role on the selectivity of these catalysts for di-unsaturated hydrocarbon hydrogenation.

Hydrocarbon and sulphur adsorption induced morphological changes to the particles of silica-supported Pt-catalyst (Europt-1). The acidic sites of the alumina support on Europt-3 have enhanced carbon filament formation. However, these structural changes have no effect on the selectivity of ethyne and buta-1,3-diene hydrogenation which are known as structure-insensitive reactions[23].

ACKNOWLEDGEMENTS

The author wishes to thank Dr. F. Hunedy, Chemistry Department, Al-Fateh University, for his encouragement and support and Dr M. Elleed, TNRC, for reading the manuscript.

REFERENCES

[1] Paal, Z. and Menon, P. G., 1983. Hydrogen effects in metal catalysis. *Catal. Rev.-Sci. Eng.*, **25**, 229–324.

[2] Bond, G. C. and Burch, R., 1983. Strong metal-support interactions. In: G. C. Bond and G. Webb (eds.), *"Catalysis", Specialist Periodical Reports*, **6**, 27–60. The Chemical Society, London.

[3] Harris, P. J. F., 1987. The morphology of platinum catalyst particles studied by transmission electron microscopy. *Surface Sci*, **185**, 459–466.

[4] Bond, G.C. and Wells, P.B., 1985. Characterization of the standard platinum/ silica catalyst Europt–1. *Appl. Catal.*, **18**, 221–259.

[5] Musso, J. C. and Parera, J. M., 1987. Adsorption and spillover of hydrogen on Al_2O_3 and Pt/Al_2O_3. *Appl. Catal.*, **30**, 81–90.

[6] Bain, F. T., Jakson, S. D., Thomson, S. J., Webb, G. and Willocks, E., 1976. Interactions of carbon monoxide with platinum /alumina and platinum/ silica catalysts. *J. Chem. Soc. Faraday Trans.* **I**, 72, 2516–2525.

[7] McNicol, B. D., Hurst, N. W., Gentry, S. J. and Jones, A., 1982. Temperature programmed reduction. *Catal. Rev-Sci, Eng.*, **24**, 233-309.

[8] Al-Ammar, A. S. and Webb, G., 1978. Hydrogenation of acetylene over supported metal catalysts. *J. Chem. Soc., Faraday Trans.* **I**, 74, 195-205; 657–664.

[9] Yashu, Y., Xiexian, G., Huimin, L., Maicun, D. and Zhiyin, L., 1983. Surface properties of platinum supported catalysts. In: P. A. Jacobs and G. Poncelet (eds). *Preparation of Catalysts*, IV, 701–710. Elsevier, Amsterdam.

[10] Yao, H. C., Sieg, M. and Plumer Jr, H. K., 1979. Surface interactions in the Pt/Al_2O_3 system. *J. Catal.*, **59**, .365–374.

[11] Kuhnen, N. C., Thomson, S. J. and Webb, G., 1983. Rhodium-catalysed hydrogenation of allene. *J. Chem. Soc., Faraday Trans* **I**, 79, 2195–2210.

[12] Arafa, E. A. and Webb, G., 1993. A ^{14}C-radiotracer study of the hydrogenation of ethyne over EUROPT-1. *Catal. Today*, **17**, 411–418.

[13] Arafa, E. A., 1998. A ^{14}C-radiotracer study of the hydrogenation of ethyne on 0.3% Pt/Al_2O_3 (Europt-3). *Petroleum Res. J.*, **10**, 31–37.

[14] Kinnaird, S., Webb, G. and Chinchen, G. C., 1987. Radiotracer studies of chemisorption on copper-based catalysis. *J. Chem. Soc. Faraday Trans.* I, 83, 3399–3413.

[15] Levy, R. B. and Boudart, M., 1974. Adsorption of carbon monoxide on supported catalysts. *J. Catal.*, **32**, 304–320.

[16] Eischens, R. P. and Pliskin, W. A., 1958. Adsorption of H_2 and O_2 on Pd and Pt. catalysts. *Adv. Catal.*, **10**, 2–25.

[17] Kavtaradze, N. N. and Sokolova, N. P., 1970. Chemisorption of H_2 on supported catalysts. *Russ. J. Phys. Chem.*, **44**, 93–101.

[18] Altham, J. A. and Webb, G., 1970. Methanation of carbon monoxide. *J. Catal.*, **18**, 133–140.

[19] Arafa, E. A., 1998. ^{35}S-Radiotracer studies of sulphur poisoning of platinum supported catalysts: 1. Hydrogenation of Buta-1,3-diene, *Proceedings 4th Arab Conference on Peaceful Uses of Atomic Energy, Tunisia.*

[20] Bond, G. C. and Gelsthorpe, M. R., 1987. A study of Europt-1 by temperature programmed reduction. *Appl. Catal.*, **35**, 169–176.

[21] Harris, P. J. F., 1986. Sulphur-induced faceting of platinum catalyst particles. *Nature*, 323, 792–794.

[22] Arafa, E. A., 1999. ^{35}S-Radiotracer studies of sulphur poisoning of platinum supported catalysts: 2. Hydrogenation of ethyne. *Petroleum Res. J.*, **11**, 51–59.

[23] Somorjai, G. A., 1990. Modern concepts in surface science and heterogeneous catalysis. *J. Phys. Chem.*, **94**, 1013–1023.

Petroleum Res. J. Vol. 12 (2000): P. 57-60, 4 Figs.

The Influence of Edge Surface Finishing on the Fatigue Life of Low Carbon Steel Sheet

Muhsin M. Hamdoon *

تأثير نعومة سطح الحافة على عمر الكلال للصلب الصفائحي منخفض الكربون

محسن محمود حمدون

تحسين عمر الكلال للصلب الصفائحي SAE 1005 بواسطة التجليخ عالي الدقة والتلميع قد تم بحثه. النماذج المستوية حُمّلت دورياً بواسطة جهاز الكلال الانحنائي المستوى بنفس قيم الإجهادات المتوسطة والمتناوبة. حيث أدت عملية التجليخ إلى تحريك منحنى الإجهاد - العمر لجهة اليمين، وحسّنت من مقاومة الكلال للصلب قيد الدراسة.

تم الحصول على أفضل نتيجة في مقاومة الكلال من خلال عملية التلميع حيث ارتفع عمر الكلال بنسبة 150% عن نظيره للنماذج غير الملمعة.

Abstract: *The improvement of fatigue life of SAE 1005 steel sheet by high precision grinding and polishing has been investigated. The flat speciments were cyclically loaded by a plane bending fatigue testing machine, with similar levels of mean and alternating stresses. The relation between edge surface roughness and fatigue life has been studied. Grinding process gives a movement of S-N curve to the right, and improves the fatigue strength of the steel under study. The best improvement in fatigue resistance is obtained by polishing, where the fatigue life has been increased by 150% of the fatigue life of specimens prepared from the as-received steel sheet. The fatigue life is considered as the number of cycles to cause failure.*

INTRODUCTION

Fatigue failure had been considered an important problem that can produce sudden fracture of components and machine members, and causes financial and personal disasters. Therefore, the improvement of fatigue resistance of materials has taken a considerable importance (Weibull, 1961). [1]

The term "surface" , as used here, has the connection of a layer of finite depth, usually small compared with the thickness of the fatigue test sample. Each of the numerous surface treatments establishes a characteristic state of residual stress in subsurface layer. From a somewhat simplified viewpoint, the capacity of this stressed layer to affect the fatigue life of the part depends on the sign of the residual stress, and the fact that the applied tensile stress will be maximum on the surface, decreasing toward the centre.

The residual stress is always algebraically subtracted from the tensile strength of the material in arriving at an allowable fatigue strength, thus the benefit of residual compression is related to its minus sign.[2]

*Mechanical and Industrial Dept., Al Fateh University, Tripoli Libya.

In addition to the compressive residual stresses caused by grinding and polishing, there is a removing of surface irregularities, partially or completely. Some previous researchers[2,3,4&5] have studied the influence of surface finishing on the fatigue life of materials by means of surface roughness. In the present work, the edge roughness was the considerable point in fatigue results comparison.

Similar investigations were made by Lai & Nee[6] on the improved fatigue life of holed flat specimens made from medium carbon steel, using reaming, ballizing, and emery polishing processes. Polishing is, generally, found to give the longest fatigue life, while ballizing generates the shortest life.

EXPERIMENTAL TECHNIQUE

The material used in the present study was SAE 1005, a low carbon steel sheet that has wide applications in the industries, because of its suitable mechanical properties, which is used in manufacturing of 35–75 litres water boilers in one of the indudstrial factories. A typical chemical composition is 0.056 percent, C, 0.1 percent, Si, 0.236 percent, Mn, 0.007 percent P, and 0.009 percent S. The microstructure of the mentioned steel is viewed where the planes of figure and rolling are perpendicular to each other (Fig. 1).

Ninety rectangular specimens (170x29 mm) were cut from a single stock of 2 mm steel sheet in ordinary climate conditions, i.e., temperature of 25°c and humidityh of 30%. Difference in surface finish of

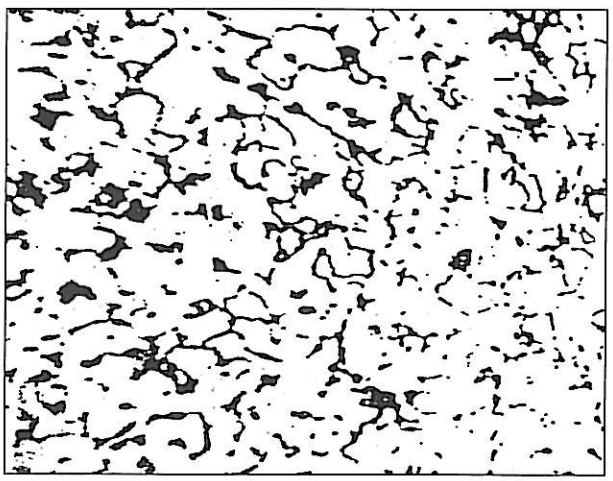


Fig. 1. The microstructure of SAE 1005 steel sheet. 2% nitric acid diluted in alcohol (x200).

speciments edges was achieved by grinding machine and elc. polisher. For each specimen tested by fatigue machine, the surface roughness of each edge was measured, where calculations involved the centre line average (Ra), average roughness depth (Rz), and maximum roughness depth (Rmax). Figure 2 represents the indication of one of the roughness tests which were carried out.

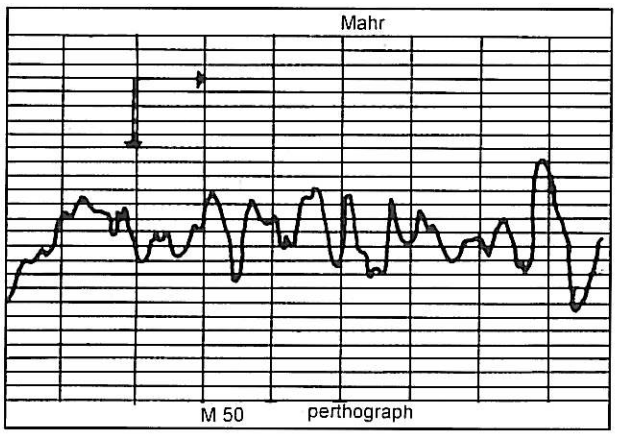


Fig. 2. Sample of roughness measurement indication.

RESULTS AND DISCUSSSION

The influence of edge surface roughness on the fatigue life of the steel under study is shown (Fig. 3).

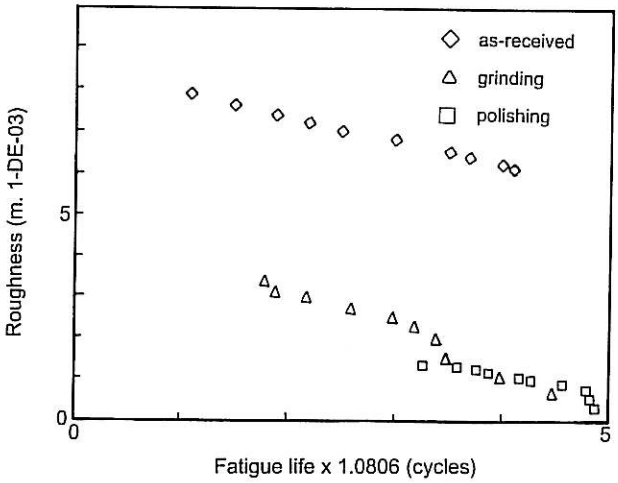


Fig. 3. Sample of roughness measurement indication.

The range of roughness of the polished specimens is between 0.5–1.5 μm and for the grinded specimens is about 0.8-3.5 μm, while the edge roughness of the as-received (unfinished) specimens is about 6.5–8.1 μm. There is an obvious effect of the surface roughness on the fatigue life where there is an adverse

relation between roughness and fatigue life. There is a small difference in fatigue life between the as-received and ground specimens, because of very close surface finish, so that the crack initiates after small difference of cyhcles life of the two types. In the present study, the polishing process gives a larger effect on the fatigue life than its effect in Lai & Nee's study.

In the present work, the fatigue life increased by polishing at a fatigue percentage approaching 150%, while that of the above mentioned investigators is about 120% of fatigue life of the as-recived specimens.

Figure 4 shows the effect of high-precision grinding and polishing processes on the S-N curve of the steel under study. In case of grinding, the curve is shifted to the right with higher magnitudes of fatigue strengths of the tested specimens under the same conditions. While in case of the tested specimens under the same conditions. While in case of the polished specimens there is an emphasis in shifting and fatigue strength improvement.

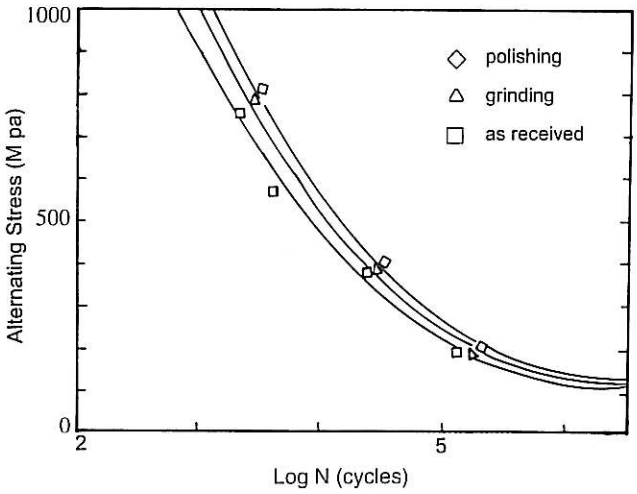


Fig. 4. The effect of grinding and polishing on the S-N curve.

Fatigue crack initiation has been superintended, for the fatigue tests which experienced by the plane bending fatigue testing machine. For the as-received specimens, the crack initiates after 30–50 percent of the number of cycles of crack initiation of the grinded specimens, and it initiated after 20–35 percent of that of polished specimens. The diversity of the obove notes of crack initiation is due to the removing of edge surface irregularities (which act as stress raisers) by surface finishing processes, where fatigue crack initiates at the surface and propagates at core region.[7]

CONCLUSIONS

1- The lowest values of edge surface roughness could be obtained in case of polished specimens, which had been approached 0.5 μm.
2- Polishing process improves the fatigue of SAE 1005 steel sheet by 150 percent of the as-received specimens fatigue life.
3- The S-N curve of the grinded specimens has been shifted to the right, and fatigue strength increased. These effects have appeared obviously in case of polished specimens.
4- The fatigue crack of the as-received specimens was initiated after 30–50 percent of the number of cycles of crack initation of the grinded specimens, while it initiated after 20–35 percent of the polished specimens crack initiation.

REFERENCES

[1] Weibull, W., 1961. *Fatigue Testing and the Analysis of Results*, Pergamon Press Ltd.
[2] Osgood, C.C., 1970. *Fatigue Design*, John Wiley & Sons, Inc.
[3] Forrest, P.C., 1962. *Fatigue of Materials*, Pergamon Press, Ltd.
[4] Kravchenko, P Ye., 1964. *Fatigue Resistance*, Pergamon Press Ltd.
[5] Harris, W.J., 1961. *Metallic Fatigue*, Pergamon Press Ltd.
[6] Lai, M.O. & Nee, A.Y.C., 1988. The effect of several finishing processes on the fatigue resistance of hole surfaces. *Journal of J. Engin. Mater. Tech.*, **111**/71.
[7] Grover, H., 1964. *Fatigue Crack Propagation in Sheet Specimens, Materials Research and Standards.*